# PASSIVE VARIABLE COMPLIANCE FOR DYNAMIC LEGGED ROBOTS

Kevin C. Galloway

A DISSERTATION

in

Mechanical Engineering and Applied Mechanics

Presented to the Faculties of the University of Pennsylvania in Partial Fulfillment of the Requirements for the Degree of Doctor of Philosophy

2010

Supervisor of Dissertation

---

Mark Yim
Associate Professor of Mechanical Engineering and Applied Mechanics

Graduate Group Chairperson

---

Jennifer R. Lukes
Professor of Mechanical Engineering and Applied Mechanics

Dissertation Committee

Jonathan E. Clark, Assistant Professor of Mechanical Engineering, Florida A&M–Florida State University

Daniel E. Koditschek, Professor of Electrical and Systems Engineering

Vijay Kumar, Professor of Mechanical Engineering and Applied Mechanics

Mark Yim, Associate Professor of Mechanical Engineering and Applied Mechanics

PASSIVE VARIABLE COMPLIANCE FOR DYNAMIC LEGGED ROBOTS

COPYRIGHT

2010

Kevin C. Galloway

# Acknowledgements

My stay at the University of Pennsylvania has been an exciting and life defining experience that would not have been possible without the support of friends, colleagues, and my advisors. I have benefited from their creativity and insights and take away a very important lesson that can only truly be appreciated through experience; research requires resilience.

There are many people to thank, and I would like begin by thanking Dr. Mark Yim for being my advisor and supporting my research interests over the years. Your encouragement to pursue ideas enabled me to explore interests in product development and entrepreneurship that I am certain under any other tutelage I would not have been as successful.

I must also thank members of my committee including, Dr. Dan Koditschek for his insightful guidance and willingness to support my research interests. Supporting legged locomotion research in his lab has been a wonderful learning experience in teamwork, interdisciplinary research, and project management. Additionally, Jonathan Clark receives my sincerest gratitude for his invaluable mentorship and encouragement. His positive attitude and creative energy have been a tremendous resource.

To my friends in Modlab most notably Thomas Mather, Mike Park, Jimmy Sastra, Chris Thorne, and Paul White, thank you for being a sounding board for a lot of bad ideas and some good ones. I fondly remember our lunchtime brainstorming sessions where we temporarily suspend reality and ask “What if...?”

To my friends in Kodlab most notably Dr. Galen C. Haynes, Dr. Haldun Komsuoglu, Berkay Deniz Ilhan, and Aaron Johnson, thank you for your help and technical support these last few years. EduBot has come a long way and I am grateful for the opportunity to have a played in significant role in its mechanical design.

Additional thanks goes to Maryeileen Griffith for her help in navigating graduation requirements and for putting things into perspective.

Finally, a very special thank you goes to my wife, Emily, who has endured my graduate student schedule all these years. You are the love of my life, and none of this would have been possible without your encouragement.

ABSTRACT

PASSIVE VARIABLE COMPLIANCE FOR DYNAMIC LEGGED ROBOTS

Kevin C. Galloway

Mark Yim

Recent developments in legged robotics have found that constant stiffness passive compliant legs are an effective mechanism for enabling dynamic locomotion. In spite of its success, one of the limitations of this approach is reduced adaptability. The final leg mechanism usually performs optimally for a small range of conditions such as the desired speed, payload, and terrain. For many situations in which a small locomotion system experiences a change in any of these conditions, it is desirable to have a tunable stiffness leg for effective gait control.

To date, the mechanical complexities of designing usefully robust tunable passive compliance into legs has precluded their implementation on practical running robots. In this thesis we present an overview of tunable stiffness legs, and introduce a simple leg model that captures the spatial compliance of our tunable leg. We present experimental evidence supporting the advantages of tunable stiffness legs, and implement what we believe is the first autonomous dynamic legged robot capable of automatic leg stiffness adjustment. Finally we discuss design objectives, material considerations, and manufacturing methods that lead to robust passive compliant legs.

# Contents

# List of Tables

# List of Figures

# Chapter 1

# Introduction

## 1.1 Motivation

As the cost of components used in robot production decrease and microprocessor capabilities increase, it seems logical that robots will gradually play a more central role in our daily activities. Yet, there are numerous barriers to the integration of robotic solutions into our lives. Most centrally our environment was not designed for robots. Consequently, we must design robots to respond to our environment. The mobility of robots, given the different terrains that they must traverse, has been a focus of robotic research and development. Most commercial robotic platforms rely on traditional wheeled or tracked means for mobility; however, the limitations of these systems have become increasingly evident. This has motivated considerable research into robotic legged locomotion which draws inspiration from nature.

In recent years, legged robotic systems have become more capable and sophisticated thanks in part to improved energy density of battery technology, smaller and more powerful processors, and increased access to light weight composite materials all of which improve the power-to-weight ratio of the final platform. However, in light of these advances there remains a significant performance gap in terms of speed, efficiency, and agility between legged animals and robots. Animals have a

sophisticated high degree-of-freedom musculoskeletal system that is impossible to duplicate with motors and gears. However, biomechanical studies have shown that in spite of this sophistication there are behaviors and responses that can be captured with simple mechanical models. One such response is that animals adjust their leg stiffness when confronted with changes in speed, payload, and terrain. We speculate that in order to close the performance gap between the two systems and thereby improve the utility of legged robots, tunable leg stiffness will play an integral part in future robotic systems.

To date, little experimental work has been done to understand the role of leg compliance especially tunable passive leg compliance. This is understandable as conducting research in this arena requires access to a robust, dynamic legged robot of which very few exist. Of those that do, most leg development innovations have produced fixed stiffness passive compliant mechanisms. As we have alluded, one of the limitations of fixed leg stiffness is a reduced adaptability of the final leg mechanism as it usually performs optimally for a small range of conditions such as a certain robot weight, terrain, speed, and gait. Part of the difficulty in designing a tunable stiffness leg lies in the competing constraints of size, strength, flexibility, weight and final integration of the robotic appendage. Novel designs are required to meet these heretofore unmet stringent design requirements and to give robotic structures the kind of adaptability and robustness found in nature. For without an experimental platform capable of running with variable passive stiffness, it is impossible to understand how to apply the lessons from simple models and animals to improve the performance of legged robotic systems.

## 1.2 Contribution

An overriding goal throughout this dissertation has been to create a variable passive compliant leg that extends the capabilities of any running robot, but more specifically

our RHex-like hexapedal platform, EduBot. The most notable contribution derived from this work is what we believe is the first autonomous dynamic legged robot capable of leg stiffness adjustment. This was achieved through innovations on the method of structure-controlled stiffness, which is a tunable stiffness approach that changes the active structure of an elastic element. Typically this means changing the active length of a spring or its second moment of intertia. The proposed final tunable leg configuration incorporates a self-locking actuation system that changes the second moment of inertia of a composite C-leg with a compliant tuning element that slides along the length of the leg. Furthermore, the proposed design strategy and resulting stiffness adjustment method is not limited to RHex-like robots. It is quite generic and can be implemented on other robot configurations including centipede robots. This, then, is a contribution to the larger field of legged robotics.

We also report empirical results which offer insights into the role that passive tunable leg compliance has on efficiency and speed. Thousands of running experiments were performed using a Nelder-Mead optimization scheme and a motion capture system to tune our hexapod's six gait parameters – stride period, stance phase angle, duty factor, offset angle, proportional gain, and derivative gain (see Chapter 2.6 for more detail)– for a range of leg stiffnesses. With our tunable leg we experimentally demonstrate that tuning the leg stiffness enables the robot span a range of speeds and efficiencies for a variety of terrains and payloads. For example, we find that increasing mechanical leg stiffness allows our hexapod to run faster. A similar effect was observed on surfaces of different compliance, where more compliant surfaces such as carpet padding and grass allowed the robot to run faster and more efficiently (with and without a payload) than was achieved on carpet. We also found that for our platform there is an optimal leg stiffness to maximize speed, and legs that are too stiff result in slow and inefficient locomotion. Lastly, we also report a marginal improvement in turning agility at higher leg stiffnesses.

Another important contribution of this thesis work is the construction of a hierarchical set of design objectives that should be considered at the outset of any attempt to design tunable legs. These objectives are generated within the framework of axiomatic design which offers a systems level approach to design. What emerges from the creation and implementation of these design objectives are two novel tunable leg designs that innovate on the method of structure-controlled stiffness and serve as example implementations. Furthermore, during the course of addressing each of the design objectives we document lessons learned which we anticipate will serve as a valuable resource future leg innovators.

This thesis also details an approach to understand the non-linear behavior of RHex's C-legs under load. For the purposes of modeling, the C-leg has typically been simplified to a single linear spring even though under load the toe clearly deflects in two dimensions. Other attempts have tried to model it as a two degree of freedom system by two orthogonally placed linear springs [44]. We propose a simpler model to capture the spatial compliant properties of a tunable leg using a combination standard beam bending theory and the pseudo-rigid-body (PRB) model, which represents leg stiffness as a torsion spring at the effective center of rotation.

A last contribution of this work has been the innovation of new robotic hardware to increase the robustness and capabilities of EduBot. Most notable of these innovations is the integrations of a slip ring into the motor mount assembly, which enables the passage of power and communication between the robot body and its six continuously rotating legs. This was necessary to achieve reliable autonomous leg tuning; however, this development also enables future development of a more sophisticated leg sensory system as there is now a direct electrical connection between the legs and the robot body.

# Chapter 2

# Background

## 2.1 Review of Mammalian Legged Locomotion

Turning to nature for inspiration has been a growing practice in robotic research for the last few decades. The studies of legged animals in particular have revealed musculoskeletal spring behaviors that are common across a very diverse group of creatures. These insights into animal locomotion offer design principals (both in mechanics and controls) and benchmarks for the development of running robots. In this section, we highlight many of the findings from legged animal studies with a focus on the role of leg stiffness in locomotion. We begin by first introducing the Spring Loaded Inverted Pendulum (SLIP) model which is the basis for most of the work on legged locomotion both in biomechanics and robotics [37].

### 2.1.1 Review of Spring Loaded Inverted Pendulum (SLIP) Model

The Spring Loaded Inverted Pendulum (SLIP) is a reduced-order dynamic model that accurately captures the center of mass motion of high degree of freedom legged locomotion systems [23]. In its simplest form, the SLIP model represents a legged

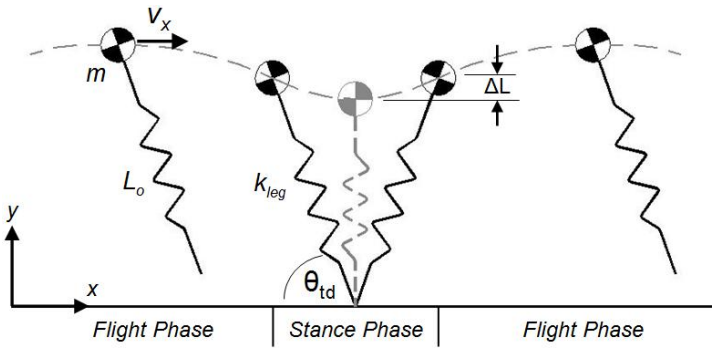


Figure 2.1: Spring Loaded Inverted Pendulum (SLIP) Model (adapted from [13])

.

animal as mass on top of a single linear spring which bounces like a pogo stick (see Figure 2.1). The motion in the sagittal-plane is characterized by two phases: an aerial and a ground contact phase. As it implies, the entire system is off the ground (i.e. ballistic) during the aerial phase. As the leg spring touches down with a certain velocity and touch down angle, $\Theta_{td}$, the kinetic energy is converted into potential energy as elastic strain energy in the spring. The point mass moves forward pivoting about the point of contact and sweeping an arc as the spring is loaded and unloaded. Once maximum compression is reached, generally some form of energy is inserted to mitigate energy losses (note: more sophisticated models include a damper in parallel with the spring to account for energy dissipation from the musculoskeletal system and ground contact) and the potential energy in the spring is converted back into kinetic energy. Within this framework, leg spring stiffness, $k_{leg}$, is calculated as the ratio of the ground reaction force, F, to leg compression, $\Delta$L, when the spring is maximally compressed [12].

$$k_{leg} = \frac{F}{\Delta L} \tag{2.1}$$

Locomotion is far more complicated than the SLIP model reveals as it simplifies the entire musculoskeletal system (i.e. muscles, tendons, joints and so forth) into a single leg spring. However, ignoring the inner workings of the musculoskeletal

system and characterizing the output through inverse dynamics to arrive at the SLIP model has proven very useful [27]. As Alexander claims, "The advantage of such an approach is to reveal basic principles that do not depend on the fine details of body structure" [3]. For example, one principle that has been identified through the SLIP model is the scaling of individual leg stiffness with body mass. In [23], a comparison of $k_{leg}$ across a wide range of animal sizes (0.1-140 kg) revealed that $k_{leg}$ increases proportional to $M^{(0.67)}$ where animal mass is given by M. The resulting resonant period of vertical vibration was found to be longer in larger animals, proportional to $M^{0.19}$. Furthermore, the foot ground contact time nearly matched the resonant period of vibration with increasing body mass [23].

## 2.2 Role of Leg Stiffness in Locomotion

In the following section we explore further the role of leg stiffness in locomotion by presenting experimental and simulation studies. In particular, we consider two aspects of legged locomotion that have some degree of dependency on leg stiffness which include work output and gait control. Additionally, we consider how these findings may be relevant to robotic locomotion.

### 2.2.1 Work Output

Biomechanical studies and the SLIP model suggest that tuned resonant running leads to energy efficient and stable locomotion [37]. Matching the leg stiffness to the stride frequency can minimize the amount of work that must be inserted during each stance phase. For example, one study estimated that horses generate 40% of positive mechanical work for trotting and galloping from the elastic coil of their tendons [10]. In another study, researchers estimated that the Achilles tendon conserves as much as 35% of mechanical work for each stride [41]. Full et al. studied the mechanical properties of cockroach (Blaberus discoidalis) legs and found the leg resilience in this

running arthropod to range from 60-75% [22]. There are other factors influence an animal's or robot's gait such as leg touch down angle, velocity, or terrain to name a few; Irregardless animal studies suggest there is an optimal leg stiffness for a given mass where $k_{leg} \propto M^{0.67}$ [23].

Evidence also suggests that tuned leg stiffness influences passive stability properties. A SLIP study by [64] concluded that for certain leg touch down angles the system becomes self-stabilized if the leg stiffness is properly adjusted and a minimum speed is exceeded.

Hurst also notes the consequences of incorrect leg stiffness for robots [37]. A leg that is too stiff results in energetically wasteful collisions with the ground, and may introduce high stresses (potentially damaging) to the robot body and electronics. On the other hand, leg stiffness that is too soft may experience loads that exceed the material limits or compression limits of the leg. For example, overly soft legs may cause the robot to bottom out and cause hardware damage. Soft leg springs also introduce another form of inefficiency as the robot must support its weight against gravity over a longer stance phase [37].

Biomechanical evidence also suggests that tunable leg stiffness may be useful for switching between work output (i.e. tuned resonant running) and high power activity modes. Passive elastic elements are an efficient means to reduce muscular work as they recycle energy; however, in animals they can not be turned off. Tendons will always store energy when the muscle is activated. Roberts claims that "for high power activities - those that require significant net mechanical work to increase the potential or kinetic energy of the body - the tendency of the tendons to stretch can potentially increase the work muscles must do" [59]. Therefore it has been suggested that stiffer spring elements offer better transmission of mechanical work for movements such as jumping or accelerating [2] [40] [11]. Tunable stiffness legs may then offer robots the ability to switch between these two modes as the situation arises such as jumping across a hole.

### 2.2.2 Gait Control with Tunable Legs

A system tuned for a particular environment and speed can produce energy efficient locomotion; however, changes in desired speed, payload, and terrain can quickly alter the locomotor's dynamics and produce energetically wasteful locomotion. A robot has significantly more utility if it can adapt to a changing environment. Both biomechanical and robotic research suggest that tunable leg stiffness is one effective method for gait control [4] [26] [57].

***Leg Stiffness vs. Speed***

Several studies have shown that tunable leg stiffness may be necessary to achieve a range of stable forward velocities. Alexander notes that if a leg is swung through the same angle while the foot is on the ground, a stiffer spring may be needed to achieve higher or lower speeds [4]. A simple version of this concept has been demonstrated in human hoppers. Farley et al. conducted human hopping experiments and found that vertical leg stiffness more than doubled as hopping frequency increased [24]. Even though hopping isn't running, there are considerable dynamic similarities between the two cyclic systems. Raibert and Koechling adjusted the air pressure of linear air springs in a planar biped to change the effective leg stiffness, and demonstrated stiffer springs lead to faster running [58]. Simulation results of a two-segmented leg also suggest that to achieve a large range of speeds and regions of stability, legs with adjustable joint stiffness are needed [61] [60].

With that said there are some differences of opinion in the biomechanical field as to the relationship between velocity and leg stiffness. Some animal studies suggest that leg stiffness does not vary with speed [27] [23] [28] [46], but rather animals increase stride length by their angle of attack at leg touch down. In this way the vertical travel of the center of mass ($\Delta$L) is reduced while keeping leg stiffness constant. Arampatzis et al. [7] on the other hand found that for humans running up to 6.5 m/s (14.5 mph), velocity does influence leg spring stiffness with an approximate 40% change in leg spring stiffness. Similar results were also found by [42] where there was

an observed increase in knee joint stiffness over a range of sprint running speeds. It is proposed that the discrepancy stems from the calculation methods employed [7]. Arampatzis et al. collected force plate and kinematic data while previous work used ground reaction force data and calculated the theoretical length change of the leg spring, which overestimated the length change of the leg spring [7].

***Leg Stiffness vs. Payload***

The SLIP model also suggests that tunable leg stiffness plays an important role in gait adaptation to changes in payload. A torque-driven SLIP study by Jun and Clark showed that for changes in a robots body mass (i.e. payload changes) adjusting leg stiffness without changing the controller adapted for a particular set of physical parameters, gives stability results in general better than those obtained by optimizing the controller alone [74]. This suggests that very efficient locomotion could be achieved with very little computing overhead. For example, one could imagine embedding a robot's gait parameters into its mechanical structure through clever gearing. Leg stiffness adjustment alone could be used to adjust the gait in response to changes in desire forward velocity (i.e. stride frequency) or payload. Furthermore it should be noted that for some designs, tunable leg stiffness also includes the ability to safely support heavier loads without failure.

***Leg Stiffness vs. Terrain***

Tunable leg stiffness may be useful for adapting to terrains of different stiffness. The hypothesis stands that during running, a compliant surface acts as a second spring in series with the leg spring. Changes in ground stiffness therefore affect the total stiffness of the system and can adversely affect the gait. Biomechanical studies suggest that tunable leg stiffness may be warranted to maintain a constant total stiffness of the series combination of the leg spring and surface, and thus preserving consistent center of mass mechanics across the range of surface stiffnesses. A study of humans hopping in place found that for a desired hopping frequency, leg stiffness increases as much as 3-fold as the compliance of the running surface increases while

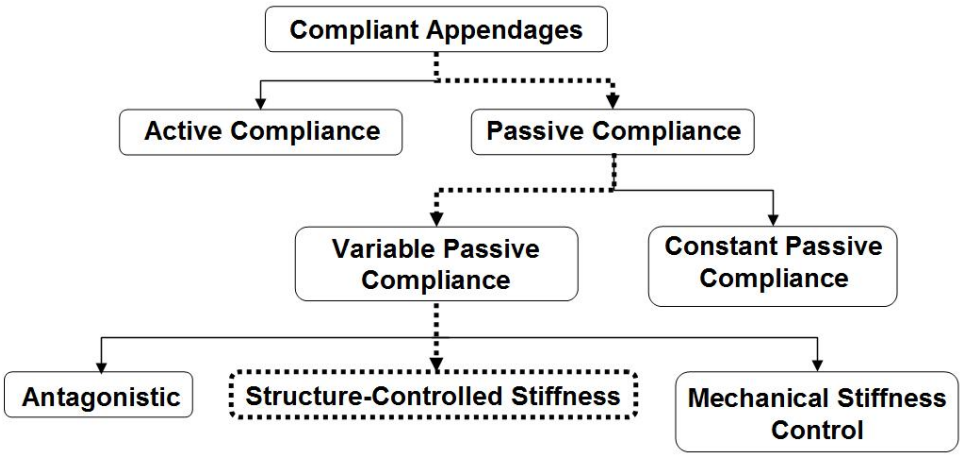


Figure 2.2: Taxonomy of tunable compliance methods.

the total stiffness remained relatively unchanged [25]. The same study also noted that impact of ground stiffness changes on a gait are dependent on the animal size [25]. For example, the leg stiffness of a horse with a body mass of over 600 kg is affected more by the series combination with the ground stiffness than is a mouse weighing 30 g.

## 2.3 Compliant Actuation Methods

Leg compliance plays an important role in locomotion especially with regards to gait stability, efficiency (i.e. energy storage and return), and forward speed. Animals control leg compliance with a very complex system of muscles and tendons that work together to add and store energy to achieve rather efficient forward locomotion. Simplifying these behaviors into a robust mechanical device is a topic of interest within the legged robotics community. Several variable stiffness mechanisms have been created in recent years for use in robotic legs and various robotic joints; each with varying degrees of success. While the bulk of this thesis focuses on variable passive leg compliance, in the following section we present an overview of compliant actuators used in legged (and some non-legged) machines. We will discuss the

advantages and disadvantages of each in order to provide context for the following chapters where we discuss the development and design of a tunable stiffness leg. In this section we treat the topic of compliance very generally and present examples of each case in the following sections.

The taxonomy of compliant actuators as they relate to legged locomotion can be represented in hierarchical form as shown in Figure 2.2. Compliant actuators are devices which can accommodate a certain amount deviation from an equilibrium position of some end effector or joint without actuator input. This is contrasted with stiff actuators which track a predefined path and supply the actuator force necessary to correct any deviations. Within the first sub-group, active compliance and passive compliance offer two very different approaches to compliant actuation.

Active compliance, also known as force control, is essentially a stiff actuator that achieves compliance through software. In the case of a robotic leg, this is done by coordinating the systems response to deviations from the leg's target position. Generally, as the deviation increases the restoring torque (or force) increases [70]. Active compliance offers several useful applications in manufacturing and human-robot interactions for improving safety of the robot and those around it; however, for implementation in dynamic legged locomotion, this form of software controlled compliance comes with several drawbacks which include 1) slow reaction to sudden impacts (reaction rate depends on sampling rate), 2) significant input power required to accelerate the end-effector, and 3) increased mass (i.e. motors are heavy). The most significant drawback of active compliance stems from the fact that motors transmit rotational torque and are not capable of storing and returning energy. As a result, active compliant locomotion platforms such as Sony's Asimo bipedal robot or Aibo robotic dog, require power for every motion and any kinetic energy that is generated is lost as an inelastic collision with the ground.

Passive compliance is generally thought of as the combination of actuators and mechanical elasticity [52]. In this case, an actuator may drive an elastic element such

as a spring, and the element deflects in response to applied loads or impacts. Some of the useful benefits of such devices in legged locomotion include 1) a seemingly unlimited bandwidth to impacts compared to active compliance, 2) the capacity to store and return energy, and 3) reduced power requirements [38]. Within passive compliance there are two subgroups shown in Figure 2.2: constant and variable passive compliance. Constant passive compliance features an elastic element with fixed stiffness properties, and generally features simple designs with few, if any, moving parts. This increases the mechanism's reliability and minimizes weight. Much design effort is therefore invested to determine the leg spring geometry that will integrate harmoniously with the overall mechanical design and yield dynamic gaits. Variable passive compliance on the other hand can offer a range of stiffness settings, which for legged locomotion applications leads to the ability to change the natural dynamics of the system. The added capability also introduces added complexity as the design must typically incorporate at least one motor for altering compliance, sensors for detecting the compliance setting, and so forth.

Variable passive compliance can be achieved through several methods including antagonistic, mechanical stiffness control, and structure-controlled stiffness (shown in Figure 2.2). Antagonistic methods offer a means to control joint stiffness and usually require two motors that work against each other to control the joint stiffness. Compliance is added by inserting springs between the motors and the joint. Of the variable passive compliant methods, the antagonistic approach is the most bio-inspired, though, this doesn't necessarily make it the best approach. There is a high degree of complexity associated with these mechanisms as joint compliance and motor torque can not be decoupled [33]. Furthermore, antagonistic designs create considerable internal forces which necessitate a stronger and generally heavier support structure.

Mechanical stiffness control is a relatively recent method for joint stiffness control and uses two motors to control the compliance and the equilibrium position

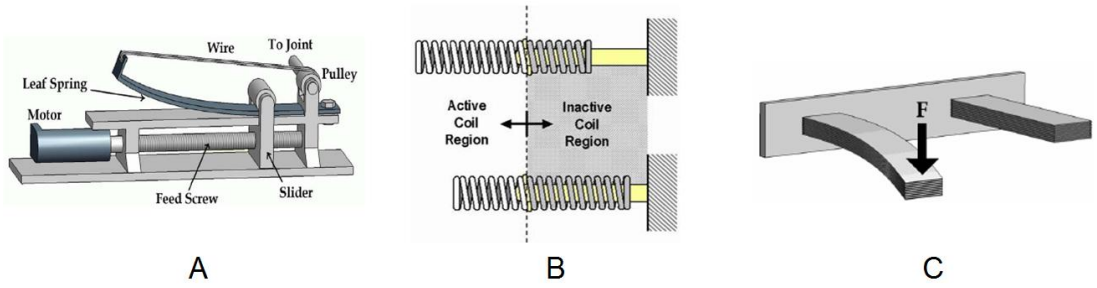


Figure 2.3: (A) Mechanical impedance adjuster changes spring stiffness by adjusting effective length of a leaf spring [51], (B) the Jack Spring changes the stiffness of a helical spring by adjusting the number of active and inactive coils [34], (C) the stiffness of stacked cantilever elastic elements can be adjusted by changing the connectivity between layers [66] [39].

independently of each other [68]. This method essentially creates the effect of a tunable torsion spring by adjusting the length of the moment arm that extends from one rigid body and is connected via a spring to the other rigid body. Compared to antagonistic joint stiffness control, mechanical stiffness control is much easier to implement and to control as the joint stiffness and equilibrium position setting are decoupled. This method does, however, require two motors which adds considerable weight depending on the desired size of the mechanism.

Structure-controlled stiffness is probably the simplest variable passive compliant method to control and implement. Stiffness is adjusted by changing the active structure of an elastic element such as its effective length or second moment of inertia. Figure 2.3 illustrates a few versions of this concept. In Figure 2.3A, the stiffness of a leaf spring is adjusted by changing the leaf spring's effective length with a slider [51]. For small deflections of a cantilever beam, the resulting stiffness, K, is related to the active length, l, through the following relation

$$K \propto \frac{1}{l^3} \tag{2.2}$$

Changing the effective length of the spring element can have a profound effect on the resulting stiffness since the length term is cubed. Figure 2.3B demonstrates another

variation of this idea with a helical spring. The effective stiffness of a helical spring can be adjusted by changing the number of active and inactive coils (i.e. changing the effective length) [34]. Figure 2.3C shows a passive cantilever spring element constructed from several layers of flexible sheets. The mechanical impedance of the passive element can be adjusted by controlling the connectivity of the layers through an external stimulus such as a vacuum [66] [39]. For example, when the layers are not connected the second moment of inertia, I, behaves as

$$I = \frac{nbh^3}{12} \tag{2.3}$$

where I is the second moment of inertia, n is the number of layers, b is the width of the elastic element, and h is the thickness. If the layers are connected, then the second moment of inertia increases significantly as the term for the number of layers, n, is now cubed.

$$I_{ConnectedLayers} = \frac{b(nh)^3}{12} \tag{2.4}$$

One must be careful, though, that the intended application does not saturate the elastic element [37]. However, in general, structure-controlled stiffness methods yield simpler designs that offer 1) large stiffness ranges, 2) configurations that are easy to scale up or down in size, 3) designs that behave like a constant passive compliant leg once locked into position, and 4) a lighter weight solution as one actuator is typically needed to adjust stiffness.

## 2.4 Robotic Legged Locomotion

Robotic legged locomotion derives inspiration from biology and is a topic that continues to fascinate and challenge biomechanists and roboticists [57] [5] [45]. In fact in 1893, the first bio-inspired locomotion patent was granted for human powered

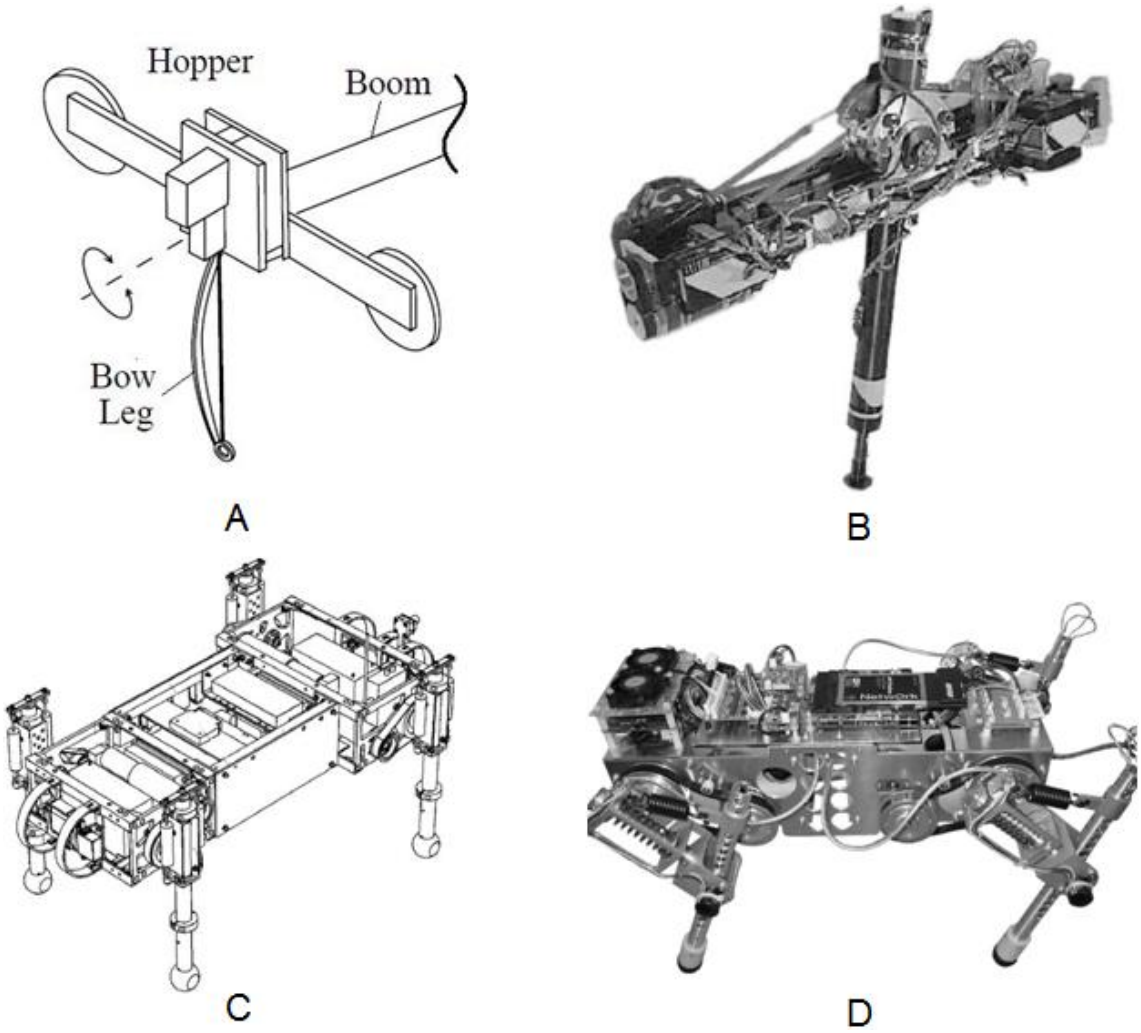


Figure 2.4: (A) Bow Leg Hopper from CMU [75]; (B) ARL Monopod II from McGill [1]; (C) Scout II from McGill [54] and (D) RUSH [76].

mechanical horse [57]. Many of the recent efforts have focused on trying to achieve locomotion with active compliance some of which include BIP2000, Johnnie, Rabbit, H6, Asimo and QRIO [37]. While these robots were designed to locomote and in some cases exhibit some dynamic behavior, the reliance on active compliance for joint stiffness and joint angle means they will always be energy inefficient. For this reason we look to robotic legged platforms that have demonstrated the usefulness of springs for achieving energy efficient and/or fast running.

Raibert's work was the first to break ground in this field with simple dynamic

hopping robots capable of achieving dynamically stable gaits. In particular, the Planar Biped featured an air spring in series with a hydraulic actuator which controlled the resonant bouncing motion, the air spring pressure (i.e. leg stiffness), and leg retraction. To our knowledge this platform demonstrated the earliest known implementation of robotic leg stiffness adjustment. Raibert et al. found that increasing the leg stiffness by increasing the air pressure in the legs allowed the robot to run faster [58]. It should be noted though that the Planar Biped was tethered to a compressed air source which is a rather inefficient method to pursue for leg stiffness adjustment in an autonomous vehicle.

The CMU Bow Leg Hopper shown in Figure 2.4A, used a physical spring constructed from fiberglass and lost only 20-30% of its energy during stance [75]. A thrust servo in the hip pulled on a bow string to pull the toe inward to insert energy into the leg during the flight phase. During the stance phase the string slacked and released the stored energy. The Bow Leg Hopper demonstrated that substantial energy efficiency could be achieved using a fixed stiffness spring. The design also showed that making the leg structure and the spring one in the same is an efficient method to minimize mass. The fiberglass bow leg structure weighs 30 grams.

The ARL Monopod series (I & II) is an under-actuated passive dynamic running robot leg that has demonstrated impressive efficiency [32] [1] (see Figure 2.4B for an image of the ARL Monopod II). Weighing 18 kg and standing 0.7 meters tall, the ARL Monopod II features two passive spring mechanisms; one as a helical spring built into the prismatic joint to store and return energy during the stance phase, and the other as a double pulley-spring system with surgical latex tubing as the spring to passively counter oscillations between leg and body at the hip.

Scout II [14] [15] [56] shown in Figure 2.4C, is another under-actuated quadruped robot that employs a single actuator per leg to control leg rotation in the sagittal plane. Each leg features a prismatic spring to passively store and return energy. Buehler et al. has shown very simple control laws (i.e. positioning the legs at a

desired touchdown angle) can achieve stable running at speeds up to 1.3 m/s [56].

Rush is a more recent under-actuated quadruped robot that features compliant kneed joints instead of prismatic ones. Shown in Figure 2.4D, the leg consists of an upper portion and a lower portion connected to form a passive knee joint. A linear spring connects two ends of this mechanism to create passive torsional stiffness at the joint. Rush has demonstrated stable and efficient locomotion at speeds up to 0.9 m/s [76].

These robots and several others share a common feature in that the leg stiffness is either manually tuned for the test environment or the gait is optimized for the stiffness of the mechanical system. Therefore, in order to change the stiffness of the mechanical system, the elastic element must be physically changed. This is where the value of tunable leg stiffness becomes apparent. For additional background material on legged robots the following are useful resources [57] [44] [37] [17].

## 2.5 Related Work on Tunable Legs

The Biped with Mechanically Adjustable Series Compliance (BiMASC) is the first leg that we are aware of that was designed with the intent of being a variable mechanical stiffness leg for a dynamic running robot [37] [38]. The design uses an antagonistic spring arrangement of non-linear fiberglass springs and a complex system of pulleys and cables to adjust joint stiffness. Its final configuration weighed approximately 30 kg (66 lbs) and stood about 1 meter tall. This prototype revealed that adjusting leg stiffness through antagonistic springs does not offer an efficient means of energy storage as one would think. Its creator found significant energy losses as joint deflection only causes one spring to compress to store energy while the other relaxes to transfer energy into the compressing spring. Furthermore, the antagonistic spring arrangement creates significant internal forces that increase the friction of the system and necessitate stronger (i.e. heavier) parts to support these

loads. A redesign of BiMASC produced Thumper which had approximately the same size and shape; however, the tunable joint stiffness capability was removed. Consequently the mechanical stiffness of the system could only be adjusted by physically changing the antagonistic springs. Thumper was able to demonstrate through simulation and experimentation that proper selection of spring stiffness could lead to energy efficient gaits [37].

A recent biped walker was designed with tunable joint stiffness using an antagonistic arrangement of pleated pneumatic artificial muscles (PPAM) where one actuator pulls while the other relaxes to control joint stiffness and joint angle [69]. Through a 1-DOF pendulum actuated by the antagonistic actuators, researchers were able to demonstrate that tuning actuator compliance to the natural frequency of the biped walker can significantly reduce energy consumption [69]. PPAM's technology, however, is not a viable solution for autonomous running as it requires a sizable power source to support the compressor, is difficult to scale down to small robots (less than 8 kg), and tends to be difficult to model and control.

The Mechanically Adjustable Compliance and Controllable Equilibrium Position Actuator (MACCEPA) is an example of a mechanical joint stiffness control mechanism [68] which was designed for a passive bipedal walker. Joint stiffness is controlled by two servo motors; one adjusts the angle of a lever arm which sets the equilibrium point, and the other pretensions the spring independently of the equilibrium position. The MACCEPA is a simple design and works well for controlled passive walking; however, the power and weight cost of supporting two motors to control a single joint stiffness makes it a difficult method to implement on a dynamic runner.

## 2.6 Description of EduBot

The research and development of tunable legs has in large part been inspired by RHex (see Figure 2.5), which uses a very simple clock-driven, open-loop tripod gait

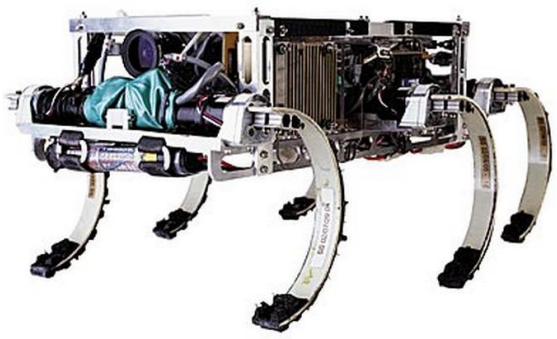

Figure 2.5: RHex

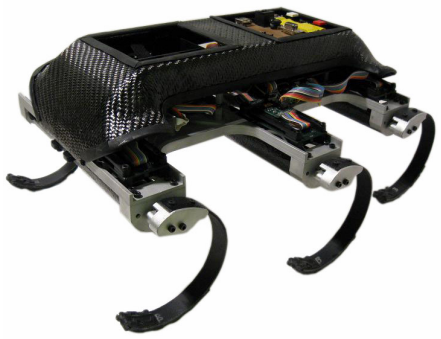

Figure 2.6: EduBot

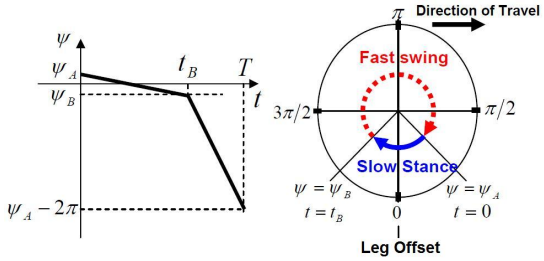


Figure 2.7: Shows the gait parameters of one leg revolution controlled by the Buehler clock (adapted from [74])

**Scaled Running (High Speed)**

| | RHex | Geometric Scaling Factor | Scaled to Edubot | Edubot (Penn 3) |
|---|---|---|---|---|
| Robot Length (m) | 0.48 | a = 0.75 | 0.36 | 0.36 |
| Mass (kg) | 8 | $a^3$ | 3.38 | 3.31 |
| Leg Length (cm) | 15.5 | a | 11.63 | 11 |
| Speed (m/s) | **2.7** | $a^{(.5)}$ | **2.34** | 2.5 |
| Speed (Froude) | 4.79 | --- | 4.80 | 5.79 |
| Speed (Bl/s) | 5.63 | $a^{(-.5)}$ | 6.50 | 6.94 |
| Specific Resistance | **0.84** | --- | **---** | **0.50** |
| Stride Freq. (Hz) | 4.76 | $a^{(-.5)}$ | 5.50 | 5.5 |

Figure 2.8: Geometric comparison of RHex and EduBot

to rotate six compliant C-legs to generate forward locomotion. A PD controller at each hip controls the leg's angular position and speed which are governed by a periodic function known as the Buehler Clock [62]. As indicated in Figure 2.7 there are six gait parameters for this locomotion system where 1) T is the stride period that specifies the rotation frequency, 2) the angle swept during stance phase is the difference between, $\Psi_A$ and $\Psi_B$, 3) the duty factor is a percentage of the stride period that specifies the rotation frequency during the stance phase, 4) the leg offset angle specifies the angular position of the stance phase (i.e. the leg offset is set to zero in Figure 2.7, 5) $k_p$ is the proportional gain, and 6) $k_d$ is the derivative gain. Careful

tuning off all these parameters can lead to very fast and efficient locomotion and impressive performance on even the roughest terrains [72].

EduBot shown Figure 2.6 is a smaller version of RHex weighing 3 kg with a leg diameter of 11.5 cm compared to RHex's 8 kg mass and 17.5 cm diameter C-legs. Using known scaling factors [5], Figure 2.8 uses published RHex data [72] to calculate the projected and actual performance values for EduBot. It is clear that the two platforms are geometrically similar; however, in terms of dynamics we find that EduBot can run faster with better efficiency (as measured by specific resistance which is covered in more details in Chapter 5), which suggests that EduBot is a better tuned mechanical system.

Aside from being similar to RHex, the EduBot platform was selected for tunable leg integration because 1) the mechanical configuration allows for direct integration of new leg designs without affecting sub-assemblies, and 2) the robot size is easier to handle.

It should also be noted that while EduBot can run faster than RHex, it is weaker compared to RHex. The stall torque for a RHex motor is approximately 3.6 Nm, while the stall torque for an EduBot motor is approximately 1 Nm. The ratio of stall torque to body mass reveals that EduBot has approximately 30% less torque output per unit mass than RHex.

## 2.7 Design Methodology

Tunable legs for dynamic locomotion is a relatively new area of study mainly for the fact that there are a only a few robots that can run dynamically and fewer still which can mechanically integrate new leg designs without affecting other sub-assemblies. With the introduction of most new mechanical designs, designers present visual models, equations that characterize the mechanism's behavior, and some experimental

results. What is not captured or entirely evident are the underlying design decisions that were driven by dependencies on other components (or sub-assemblies) and constraints unknown to the reader. It is true that many tunable leg designs will be more or less platform specific (i.e. bipeds, quadrupeds, hexapods); however, the evaluation of the usefulness of a proposed design for any platform could be improved through a clear explanation of the designer's intent. By intent we mean the design requirements the designer weighted most heavily and how those requirements impacted other aspects of the design.

In our particular case, the design of a variable passive compliant leg for a dynamic legged robot requires careful consideration of several components including the actuation method(s) for tuning leg stiffness, robot-to-leg communication, material selection, weight budget, manufacturability, cost, and so forth. Therefore it is important to have a design model to organize these objectives and capture the interconnectedness of these features. The motivation of any such model is to provide a method to objectively evaluate potential solutions and identify those with a higher probability of success. This section provides a summary of the design model known as axiomatic design (AD), which offers a scientific approach to design, and serves as a framework for presenting the mechanical implementations of our tunable legs.

### 2.7.1 Introduction to Axiomatic Design

Within engineering, design is often pejoratively referred to as a "soft science" as it lacks the scientific rigor and objectivity found in the "hard sciences." While it is true that one can not input design requirements into an equation and obtain the best design as the output, there clearly exists good designs and bad ones. This suggests that certain underlying features separate the two [65]. Axiomatic design offers a systems level approach to design and provides design rules or axioms for good design. As the theory's creator, Dr. Nam Suh explains, "The goal of axiomatic design is to make human designers more creative, reduce the random search process,

minimize the iterative trial-and-error process, and determine the best design among those proposed." The following section is provided as a general overview of AD to explain its use in the development of a variable passive compliant legs. A more detailed discussion and examples of this design method can be found in [65].

### 2.7.2 Axiomatic Design Process

The first step in AD is to attempt to define the problem or the need that must be addressed. Since you don't know what you don't know, the design process is iterative. Gradually one closes in on the perceived needs as new information is collected from literature, experimentation and so forth. Therefore at the beginning of this process, the problem definition is essentially an educated guess based on the knowledge, experience, and creativity of the designer.

The design process then becomes a game of decomposing the problem definition into design objectives, also known as functional requirements (FRs), which must be satisfied to reach a solution. The FRs are then paired up with design parameter's (DPs), which define the physical embodiment of "how"' the FRs will be achieved. For example, one FR may be to design a tool to open a metal capped bottle. Potential DPs include a tool that twists, pries, drills, or even cuts the cap off. Projects with multiple FRs require multiple DPs. Furthermore, FRs and DPs can be arranged in hierarchies such that DPs must be generated for $i$th level FRs before DPs can be generated for $i$th+1 level FRs.

In addition to defining FRs and generating DPs, design constraints much also be specified. There are two types of constraints: 1) input constraints which are constraints in the design specification (i.e. volume, mass, cost, and so forth), 2) system constraints are those that are imposed by the system in which the design solution must function. An example of system constraint would be the goal to design a robot to operate underwater. All subsequent FRs and DPs must be compatible with this decision.

Within in this framework of FRs and DPs, good design is governed by two Axioms [65].

**Axiom 1**: The independence Axiom. *Maintain Independence of FRs.*

**Axiom 2**: The information Axiom. *Minimize the information content of the design.*

Axiom 1 simply states that an optimal design has a one-to-one mapping between FRs and DP's. In matrix form, the FRs and DPs can be represented as vectors and the design matrix represents the relation between the two. In a one-to-one mapping only the diagonal elements of the design matrix are non-zero, which represents an uncoupled design. According to axiom 1, this is the signature of a good design as new DPs can be substituted to satisfy FRs without affecting the other FRs. Similarly, the signature of a bad design has a design matrix with non-zero off diagonal elements in which FRs depend on more than one DP. This situation can be problematic as it maybe difficult or impossible to find a combination of DPs that combine to satisfy multiple FRs.

Axiom 2 states that among the designs that satisfy Axiom 1, the best design has the least amount of information content where information may be in the form of drawings, operation instructions, manufacturing processes and so forth. In other words, the simpler solution is the better design.

### 2.7.3 Limitations of Axiomatic Design

Generating an uncoupled or decoupled design matrix does not necessarily mean that the task is complete especially in complex architectures where hierarchies with multiple FRs exist at each level. AD is merely a conceptual tool used to organize design objectives and proposed design solutions. It does not consider the technical feasibility of the physical integration of all the DPs into one entity [67]. In the shift from the design matrix to the actual product development (in our case the mechanical implementation of a variable passive compliant leg design) the challenge

is to preserve the FR-DP relationship through the selection and arrangement of components in the final configuration. This is an important feature to maintain as the FR-DP's may behave one way in isolation and a completely different as an integrated system [73]. Situations such as these require re-evaluation or adjustment of FR-DP's to achieve desired system performance. Maintaining FR-DP independence should make the outcome of tuning the components of the system more predictable. Another limitation or characteristic of AD is that it works best in a solution neutral environment [65]. Therefore one may not derive the greatest benefit from AD for incremental improvements on mature designs [67].

# Chapter 3

# Passive Variable Leg Stiffness with a Rigid Slider

In this chapter, we present the work surrounding phase one of two of our tunable leg developments which was presented in [30]. We begin by first stating the objective, the problem definition, known constraints, and the reasoning behind the selection of structural controlled stiffness as a tuning method. We then present some of our early prototypes which were fabricated for the purpose of exploring the design space and identifying poor assumptions. This eventually led to the development of a variable stiffness C-leg using a rigid slider. We present this development within the framework of Axiomatic Design (AD) as it offers a clear presentation of the development and reasoning process. Static and dynamic experiments were conducted to validate the strength and weaknesses of the design. We conclude this chapter with a discussion of the results and prescriptions for phase two development.

## 3.1 Mechanical Design

### 3.1.1 Problem Definition and Constraints

The problem definition formulated for this work was to create a tunable leg for EduBot by mechanically adjusting leg stiffness. The one system constraint was that the six legs must be able to rotate continuously. Input constraints were placed on the leg's mass and center of mass. Without legs, EduBot weighs approximately 3 kg. Consequently, the leg's mass is important since any addition (or subtraction) is multiplied by six. The target weight for each leg was set to 90 grams or less. The leg's center of mass was also a constraint as a center of mass located away from the motor shaft would demand more power from the motor to accelerate. Boundaries for the center of mass location were never specified, but every attempt was made to minimize its distance from the axis of rotation. Given the weight constraints and the need for a small and simple design led to the selection of structural controlled stiffness as an optimal tuning method.

### 3.1.2 Early Prototypes

Structure-controlled stiffness mechanisms range in size and configuration; however, the principal methods employed either change the spring element's effective length or the second moment of inertia. The former method was pursued as it was the most straightforward to implement. The effective spring leg length was adjusted using a rigid slider where the portion of the leg covered by the slider was considered rigid, while the remaining portion extending from the slider was considered compliant.

In the first few designs, the elastic element took the form of an epoxy compliant cantilever beam with a four-bar linkage system to control the slider position (see Figure 3.1 and 3.2). This concept was motivated in part by an earlier RHex leg that had a fixed four-bar shape with each link having some compliance [44]. Several

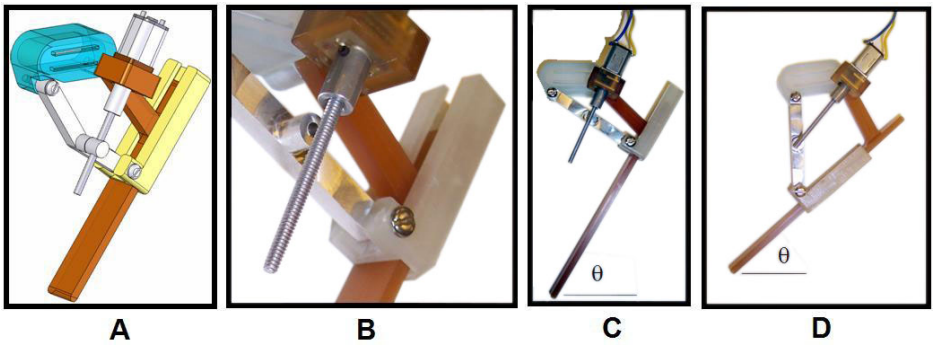


Figure 3.1: Images A-D illustrate the first concept of a four bar tunable leg design with a DC actuator located at one of the hip pivots which drove a lead screw to adjust the orientation of an opposing link and consequently the slider position.

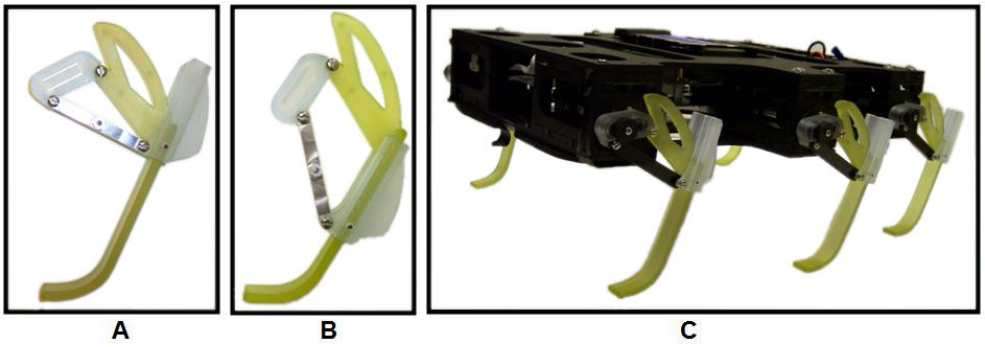


Figure 3.2: A simplified version (i.e. no motor) of the tunable four-bar configuration. The slider position was manually adjusted and fixed using set-screws. (A) Is the leg in a soft setting, (B) is a stiffer configuration, (C) illustrates the size of the legs compared to an earlier version of EduBot.

leg shapes were prototyped with the objective of learning more about the potential design weaknesses and challenges of developing structure-controlled stiffness tunable legs.

Preliminary running trials quickly revealed several flaws in this design including large impulse torques to the motors, low lateral stiffness, part loosening, and geometry complications. For instance, the cantilever beam design generated significant reaction torques. The moment arm measured from the leg motor shaft to the touchdown point at the toe was too long. This combined with the ground reaction forces during the stance phase, created a reaction torque that exceeded the capabilities of the motor. Often times the motor was unable to keep up with the PD controller and would skip rotation cycles. The four-bar design also raised structural issues. For example, it was difficult to design links that offered enough stiffness in the lateral direction and did not interfere with the slider. Running trials revealed that compliance in the linkage system allowed the legs to deflect under the robot body. The four-bar design also had too many parts. After relatively few trials, the joints would come loose and required constant maintenance. Lastly, the design raised geometric challenges as the 4-bar design also caused the angle of the cantilever portion to change with respect to the hip for different leg stiffness settings (see Figure 3.1C and D). While the controller could have adjusted the leg touch down angle for different leg stiffness settings, it was clear that calibration and monitoring would be troublesome.

The Z-leg in shown in Figure 3.3 was an attempt to resolve the problems with the 4-bar design. It featured fewer parts, added material in the hip to increase lateral stiffness, an arc extending back from the toe to reduce impulse torques to the motor shaft, and a slider adjustment method that used a rack and spur to fix the hip-leg orientation. Although this design achieved the objectives, new problems were introduced. The added toe weight shifted the center of mass further away from the axis of rotation. This in effect increased the rotational kinetic energy impacting the ground. As [4] notes, if the kinetic energy upon impact is too large, the ground reaction forces

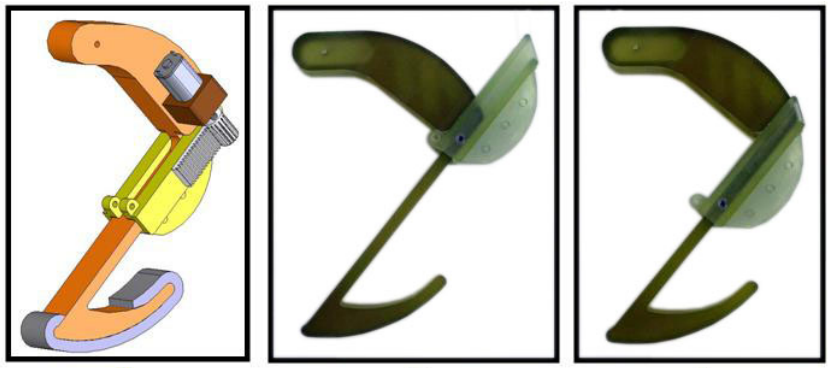


Figure 3.3: The Z-leg features a spur gear and rack configuration for controlling the slider position, and a larger toe to minimize impulse torques to the motor shaft.

may be large enough to cause the leg to rebound or "chatter." In this particular case the chatter disrupted the PD controller. Preliminary locomotion experiments failed to reveal any net positive impact which led to the eventual abandonment of this design.

### 3.1.3 Functional Requirements and Design Parameters

In the following section we propose a leg solution based on the lessons learned from the previous section. We present this solution within a three-level hierarchy of FRs and DPs (as depicted in Figure 3.4). Each FR and DP pair will be discussed in detail and serve as a framework for presenting the mechanical design.

We defined the components of the axiomatic design hierarchy as follows

FR (1,1): Vary the stiffness of a spring element
DP (1,1): Change the effective length using a rigid slider

FR (2,1): Maximize yield strength to flex modulus ratio of elastic element
DP (2,1): TP-4004 epoxy

FR (2,2): Ability to communicate to the legs
DP (2,2): Infrared communication to command stiffness changes

FR (3,1): Ability to adjust leg stiffness

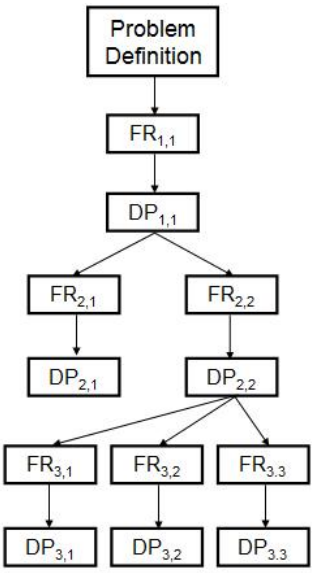


Figure 3.4: FR-DP hierarchy for proposed rigid slider leg design

DP (3,1): Attach a DC motor to drive the slider

FR(3,2): Detect stiffness setting
DP(3,2): Rotary potentiometer has geared connection to motor

FR(3,3): Ability to sense leg strain
DP(3,3): Embed a flex sensor into leg

Constraint 1: Device mass $\leq$ 90 grams
Constraint 2: Position center of mass near axis of rotation

**FR (1,1): Vary the stiffness of a spring element**

**DP (1,1): Change the effective length using a rigid slider**

Previous work on RHex development investigated several leg shape profiles with the most successful being the C-shaped leg [6] [62]. Riding on the success of this design, a tunable C-leg with a rigid slider was pursued. There are two features of the C-shape that make it suitable for the tunable leg design. First, the simple geometry offers several manufacturing options which will be explored throughout this document. Second, the symmetry and constant cross-section allow for easy integration of the rigid slider. Figure 3.5 depicts a tunable C-leg with a rigid slider

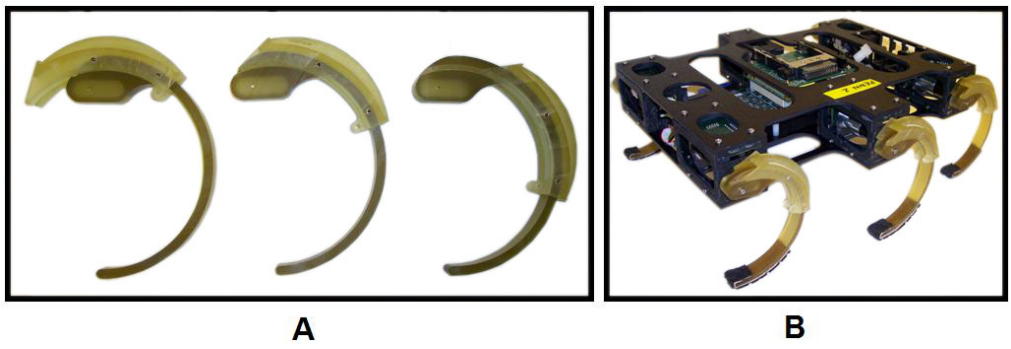


Figure 3.5: (A) Side view of C-leg with rigid slider at different stiffness settings, (B) An early version of EduBot with the C-legs mounted.

that moves along the length of the leg to change the effective length of the spring. Again, it is assumed that any portion of the leg that is covered by the slider is rigid while the remaining exposed portion of the leg is compliant.

**FR (2,1): Maximize yield strength to flex modulus ratio of elastic element**

**DP (2,1): TP-4004 epoxy**

The leg design process began with much uncertainty regarding optimal materials and manufacturing methods for robust leg construction. As a result, inexperience led to the erroneous assumption that we desired a manufacturing method that would offer considerable design flexibility to fabricate a range of leg geometries and sizes. The thought being that rapid output of different leg designs would allow us to learn more and faster than could ever be gained from a simulation. This learning curve was demonstrated to some extent in section 3.1.2 with the 4-bar and Z-leg designs. Nevertheless, it will be revealed that selecting a manufacturing method first had the effect of limiting our selection of materials which in our case was a class of high performance epoxies.

During this first phase development, energy and resources were spent building knowledge and experience with Shape Deposition Manufacturing (SDM), which we believed afforded the design freedom necessary to make robust tunable stiffness legs.

| Epoxy | E *(MPa)* | S *(MPa)* | S/E x $10^3$ HIB |
|---|---|---|---|
| TP-4000 | 690 | 21 | 30 |
| TP-4004 | 793 | 35 | 44 |
| TP-4007 | 2240 | 104 | 46 |

Table 3.1: Epoxy material properties from Innovative Polymers, Inc. (Saint Johns, MI) where E is the Young's modulus, S is the yield strength, and the ratio of S to E is the yield strength to Young's modulus ratio. Materials with a high ratio are desirable in compliant mechanism design.

SDM is a solid free form fabrication process which systemically combines material deposition with material removal processes. The general SDM design principles and techniques are covered in detail in [48], and have been applied to robotics [18–21]. SDM offers several advantages over traditional prototyping methods. Some of these include the ease of embedding components (i.e. actuators and electronics) that save volume and weight, the flexibility of combining dissimilar materials to create complex compliant mechanisms, the ability to create whole parts in a layered fashion, and the advantage of eliminating custom tooling [21]. For the fabrication of tunable leg designs, the SDM process offered the advantage of quickly iterating the leg shape and experimenting with different epoxies. For example, the overall leg stiffness can be adjusted by choosing an epoxy from a family of materials (see Table 3.1) of different Young's moduli, E, or by changing the second moment of inertia, I.

Early research [35] suggested that the most suitable epoxy to act as a compliant element is one that maximizes the strength-to-modulus ratio. A high ratio will permit larger leg deflections before fracture. For example, nylon (type 66) has a strength-to-modulus ratio of about 20. The class of epoxies used in the leg designs have a ratio as high as 46 (see Figure 3.1). TP-4004 (Innovative Polymers, St. Johns, Michigan, USA) was eventually selected as it offered a relatively low Young's modulus with a favorable strength-to-modulus ratio.

**FR (2,2): Ability to communicate to the legs**

**DP (2,2): Infrared communication to command stiffness changes**

The legs on most robotic platforms swing back and forth like a pendulum to generate forward locomotion. Thus passing communication from the leg to the body is very straight forward. The legs on RHex-like robots are rigidly attached to a motor shaft, and rotate continuously to generate forward locomotion. This avoids toe stubbing as the legs do not retract, but also precludes a wired connected between the robot body and the legs. Enabling autonomous leg stiffness adjustment then requires a different means in which the robot can command the legs to adjust overall stiffness, and a way for the legs to report leg stiffness status back to the robot. Slip rings were initially considered as they provide a continuous electrical connection through stationary brushes on rotating contacts; however, at the time, the limited availability of small, off-the-shelf configurations combined with the high cost (approx. $1000 for six) steered the design in the direction of a wireless configuration using an IrDA. In particular, the TFDU4300 is a low profile (2.5 mm maximum dimension) infrared transceiver module which is compliant with the latest IrDA physical layer standard for fast infrared data communication, and supports IrDA speeds up to 115.2 kbit/s. This platform was chosen for its small size and relatively high bandwidth (at least compared to the 6 Hz maximum stride frequency of the legs). The drawback of this solution stems from the fact that IR requires line of sight. Therefore during a full leg rotation there would be a small window ( $< 15°$) in which the communication could occur. A wireless solution also requires each leg to have its own power supply capable of supporting a microcontroller and the actuator for leg stiffness adjustment.

Figure 3.6 offers a high level block diagram description of the proposed system. In this figure, the robot body and the legs have their own microcontroller, IrDA encoder/decoder and infrared transceiver. The legs have additional components such as a H-bridge, motor and potentiometer, which will be discussed in the next section. The proposed communication path from the robot to each leg would be as follows. Leg stiffness change commands issued by the robot would be converted to an infrared

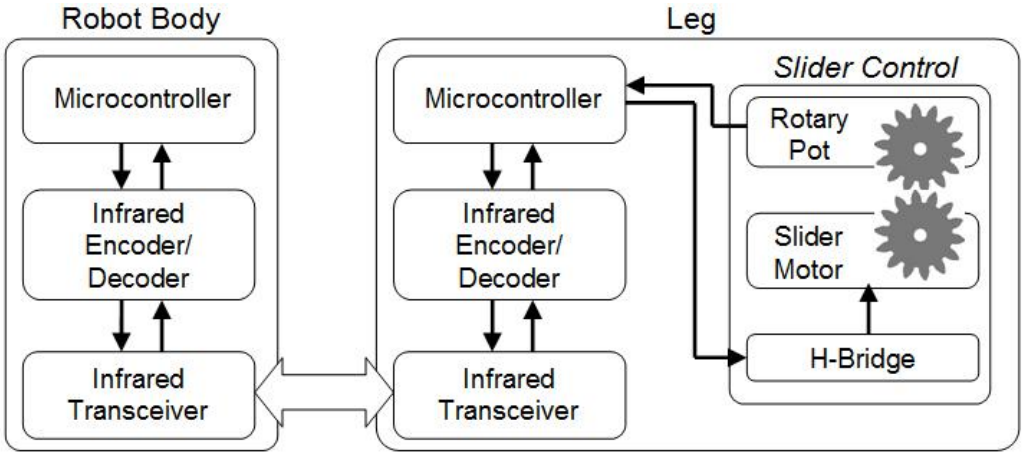


Figure 3.6: Schematic illustrating a wireless solution to control leg stiffness between the robot body and the continuously rotating legs. IRDa transceiver/receiver pairs are mounted on each motor mount and on each leg (12 total). IR commands are sent from the robot to the leg's microcontroller to change leg stiffness.

signal by the encoder. The infrared receiver on the leg side would then decode the message, and the microprocessor on the leg side would then execute the command by activating the actuator to change the leg stiffness. The rotary potentiometer, which has a geared connection to the motor, allows the leg microcontroller to detect the leg stiffness setting. The communication direction could also be reversed to update the robot on leg stiffness setting or pass information regarding other sensors that may be integrated into the leg.

**FR (3,1): Ability to adjust leg stiffness**

**DP (3,1): Attach a DC motor to drive the slider**

The decision to use SDM to fabricate the leg offered weight saving possibilities by embedding components into the leg as well as the option to minimize the number of exposed parts that could be damaged from wet environments or collisions. Figure 3.7 below illustrates the desired components for inclusion in the final design which include the motor, potentiometer, microprocessor, IrDA, and so forth. One additional sensor was included in the design, a flex sensor, to demonstrate the capabilities of SDM.

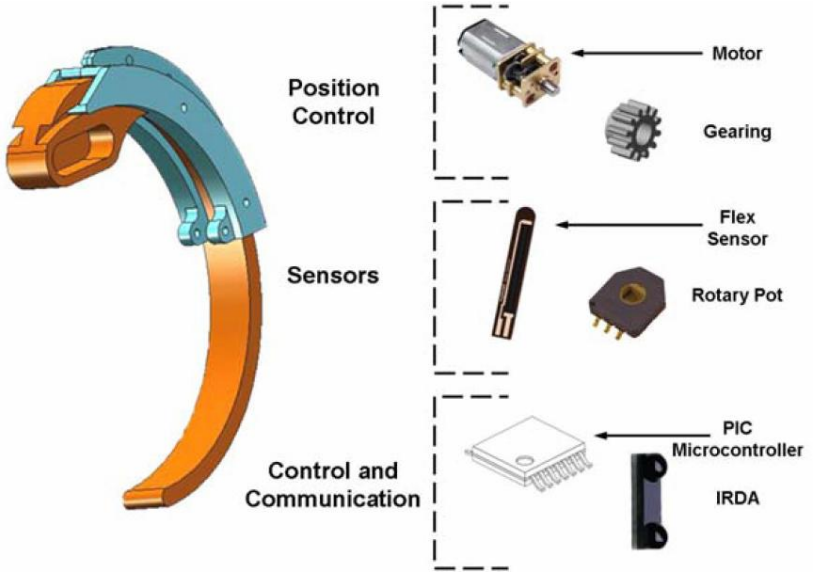


Figure 3.7: Illustration of the C-leg rigid slider design with desired components for inclusion in final configuration.

In the proposed design, the stiffness is adjusted using a small, geared DC motor to drive the rigid slider back and forth. The motor was embedded into the hip structure with the motor shaft exposed. A spur gear was attached to the motor shaft. The SDM process offered a unique opportunity to machine gear teeth along the length of the rigid slider as depicted in Figure 3.8. A summary of the SDM process is outlined in Figure 3.9, and Figure 3.10 contains an image of the first prototype.

**FR(3,2): Detect stiffness setting**

**DP(3,2): Rotary potentiometer has geared connection to motor**

Another functional requirement for the proposed tunable leg centers on the ability to detect the position of the slider and hence the overall leg stiffness. This was satisfied by embedding a small potentiometer into the hip region and attaching a gear to mate with the actuator gear. While the potentiometer offered the capability of continuous rotation, it could provide measurable changes in resistance up to 340°. As result, the pitch diameter of the potentiometer's gear was sized so that a 340° rotation matched the entire slider travel length.

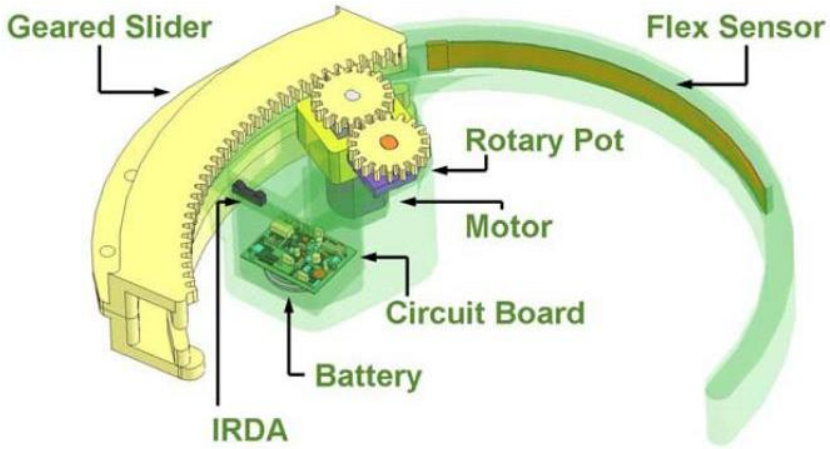


Figure 3.8: A C-leg rigid slider assembly with desired components incorporated into the leg structure.

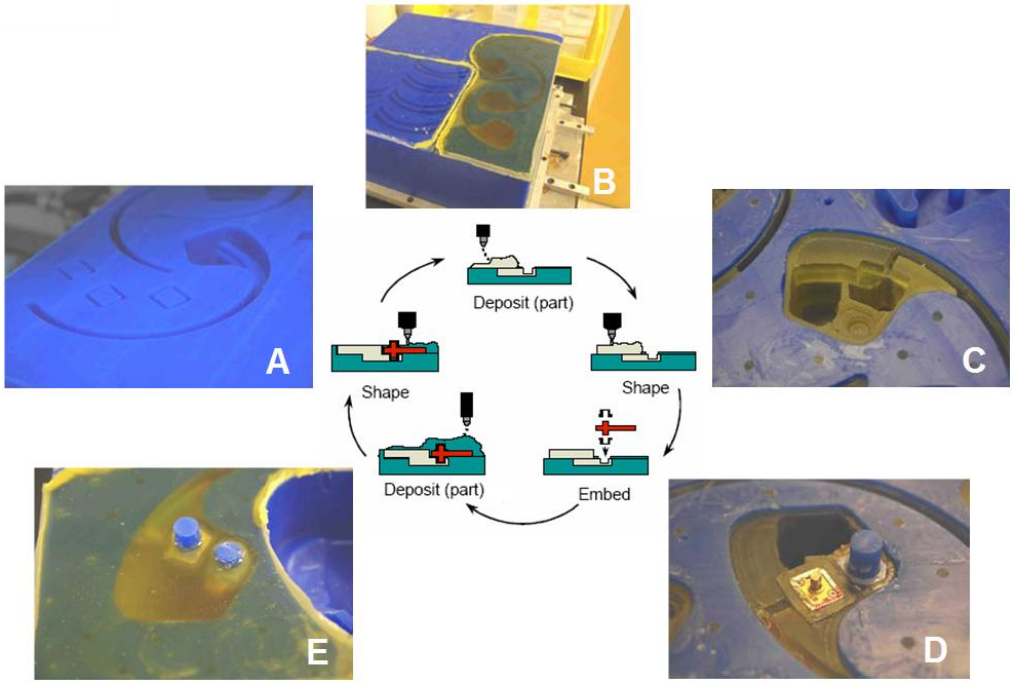


Figure 3.9: A step-by-step outline of the shape deposition manufacturing process. (A) Machine the negative of the leg shape into a block of machinable blue wax, (B) deposit part material (TP-4000 epoxy), (C) Machine pockets for components into cured part material, (D) insert components, (E) deposit more part material to fully embed components and then machine finished parts out of the mold and assemble (see Figure3.10)

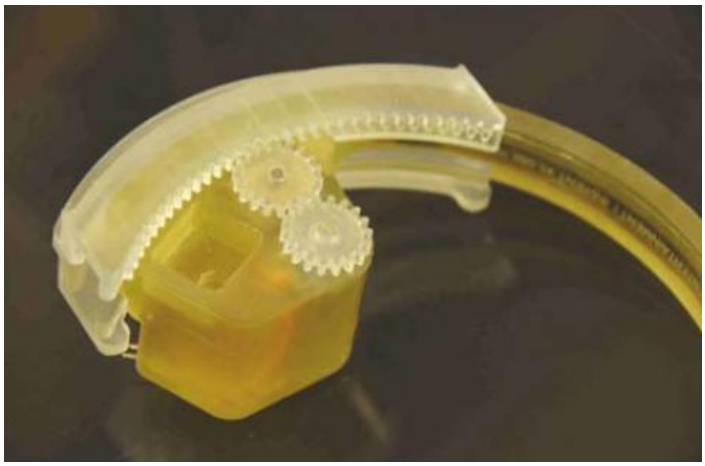

Figure 3.10: Photo of first assembled prototype with embedded components including dc motor and rotary potentiometer.

**FR(3,3): Ability to sense leg stress**

**DP(3,3): Embed a flex sensor into leg**

For the last functional requirement we desired the ability to include additional sensors as needed to augment leg functions. For example, a "pain" sensor could provide valuable feedback to the robot. One of the challenges of using passive compliant legs stems from the fact that robot does know how much stress its legs experience for a given gait. For untuned gaits, the loading stresses can break these passive compliant legs. To extend the robot's knowledge of its legs, we selected a flex sensor by Jameco which offers variable resistance readings depending on the curvature of the bend. Measuring 6.35 mm wide x 112 mm long x 0.5 mm thick, the flex sensor was suitable for embedding into the leg. There are three advantages to embedding the sensor as opposed to applying it to the surface which include 1) increasing robustness (i.e. protected from environmental hazards) 2) minimizing potential damage from shear forces, 3) eliminating interference with other components. SDM was used to embed the flex sensor at the mid-point between the inner and outer surface of the C-shape as shown in Figure 3.8. In preliminary experiments the leg was mounted to the leg loading apparatus shown in Figure 3.16 (see section 3.2.5 "Measuring Leg

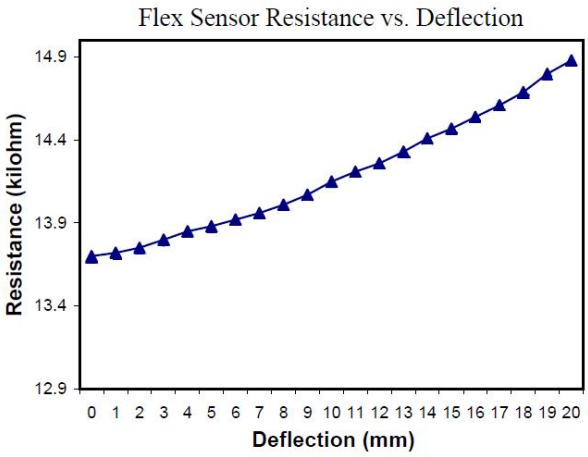


Figure 3.11: Embedded flex sensor resistance vs. leg deflection

Stiffness" for more details) and the resistance was measure for a range of vertical hip deflections. The preliminary results showed a nearly linear increase in resistance as leg deflection increased (see Figure 3.11) [53]. It should be noted that this reflects the resistance change for the leg near its most compliant setting. Unfortunately, this solution is not suitable for detecting leg stresses at higher stiffness settings as the rigid slider reduces (if not eliminates) bending that could be detected by the flex sensor.

## 3.2 Analysis of Rigid Slider Tunable Leg

It is necessary to identify some form of test or analysis to determine whether or the not the design satisfies the functional requirements. For this particular leg design, two features were tested including 1) the stiffness range under static loads, and 2) the ability to store and return energy. For the first feature, we desired a simple analytical solution that could predict the stiffness range as well as capture the spatial compliance and factor of safety of the design. Such a tool would allow us to design variable passive compliant legs to achieve certain performance ranges, and minimize the time spent conducting trial-and-error experiments. For this we have adapted

the pseudo-rigid-body model from compliant mechanism theory to characterize leg compliance. For the second feature, we present a simple test to measure the ability of the design to store and return energy under controlled dynamic loading conditions.

### 3.2.1 Compliance Characterization: Previous Work

There have been several iterations on RHex's compliant leg design [49], with the initial leg built from a curved rod of delrin which was quickly abandoned for its inappropriate stiffness compliance and low fracture toughness. The second major iteration was a 4-bar linkage design whose compliance was generated by the deformation of two fiberglass components on the internal 4-bar linkage mechanism [44]. This planar mechanism was easier to model, and had better deflection properties, but still had robustness issues as it was assembled from more than 20 parts [49]. The current leg design is a semi-circular shaped fiberglass structure. The curved shape of the leg aids in standing from rest and allows for the contact point to roll during stance. Despite its success, little work has been conducted to understand the C-leg's non-linear behavior under load. For the purposes of modeling, it has typically been simplified to a single linear spring even though under load the leg end clearly deflects in two dimensions (see Figure 3.12A). In [44], it was modeled as a two degree of freedom system by two orthogonally placed linear springs (see Figure 3.12B). Although, the two spring model captures the force-deflection behavior of the compliant leg, it is difficult to work with due to the number of parameters needed to specify the orientation and magnitude of the springs. We propose a new model to capture the spatial compliant properties of the leg using a combination of the pseudo-rigid-body (PRB) model (see Figure 3.12C) and standard beam bending theory. This model represents an implementation of the pseudo-rigid-body model for curved beams, where the leg stiffness is represented by a torsional spring at the effective center of rotation.

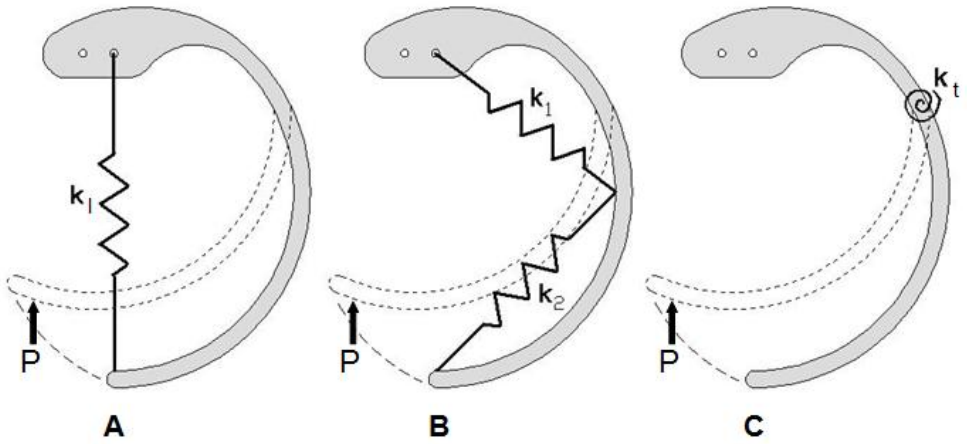


Figure 3.12: Illustrations of different spring models used to understand C-leg compliance under load, P, where (A) represents the linear model, (B) represents the 2-dimensional model, (C) represents the pseudo-rigid-body model where stiffness is characterized by a torsional spring.

### 3.2.2 C-leg Compliance in the Sagittal Plane

In the pseudo-rigid-body model, flexible members are represented as rigid links connected via pin joints with torsional springs (see Figure 3.13). This approach was chosen for two reasons. First, the deflection path followed by the toe is nearly circular. Thus, representing the leg stiffness as a torsional spring best captures the large non-linear deflections of the leg under load. Second, the PRB model offers design and time saving advantages. For example, it is significantly easier to estimate the leg stiffness for different configurations and dimensions using the PRB model than it is to update a solid model and constraints in a finite element program. In this model, the initial curvature and the length of the pseudo-rigid-body link are related through the non-dimensionalized parameter

$$k_o = \frac{l}{R_i} \tag{3.1}$$

where $l$ is the leg arc length measured along the centroidal axis of the leg from the point of deflection to the loading point, and $R_i$ is the initial radius of the C-leg.

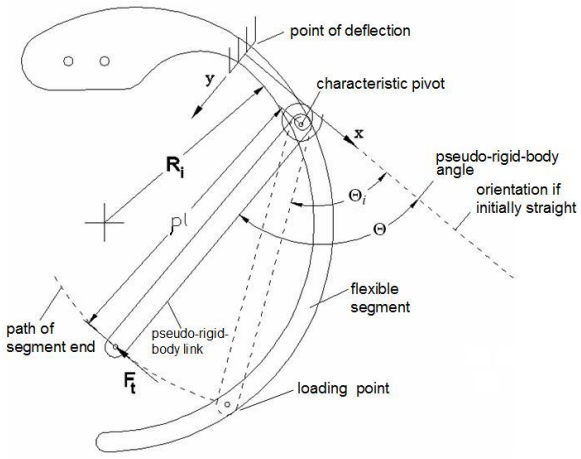


Figure 3.13: Pseudo-rigid body model applied to the C-leg. Adapted from [35]

Figure 3.13 details the components of the PRB model where the characteristic radius factor, $\rho$, is used to determine the location of the characteristic pivot and the length of the pseudo-rigid-body link. The PRB angle, $\Theta$, specifies the angle of the PRB link while, $\Theta_i$, defines the initial angle of the PRB link. Detailed explanations of the PRB model can be found in [35]; however, for the purposes of this work we are primarily interested in the magnitude of the torsional spring constant, $K_t$, which is given by

$$K_t = \rho K_\Theta \frac{EI_s}{l} \tag{3.2}$$

where $K_\Theta$ is the stiffness coefficient, E is the material's Young's modulus, and $I_s$ is the second moment of inertia in the sagittal plane. For initially straight beams, $K_\Theta$ is a function of the angle at which the load is applied. For initially curved beams with $k_o$ values near 1.0 and higher, $K_\Theta$ is relatively constant for tangential and compressive beam loading. This means that $K_\Theta$ can be approximated from $k_o$. In the same way, for given $k_o$ values, $\rho$ can also be averaged for a range of loading conditions. These approximations have been captured in a simple look-up table in [36]. Therefore, once the design inputs have been determined (i.e. E, $I_s$, $R_i$, and $l$) calculating $K_t$ is straight forward as $rho$ and $K_\Theta$ are functions of $k_o$.

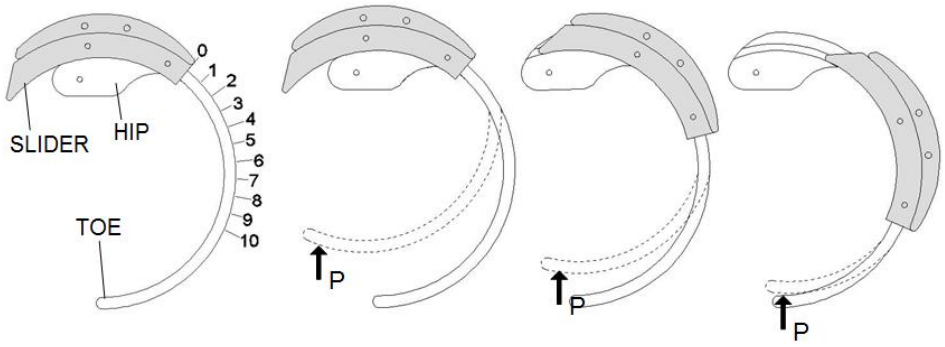


Figure 3.14: An implementation of a structure-controlled stiffness mechanism applied to a C-leg. The rigid slider highlighted in gray can slide along the length of the leg to change the C-leg's spring length.

### 3.2.3 Compliance in the Lateral Direction

The C-leg also has compliance in the lateral direction or the direction normal to the sagittal plane. The leg stiffness in this direction, $K_l$, can be characterized by the standard cantilever beam bending equation

$$K_l = 3\frac{EI_l}{L^3} \tag{3.3}$$

where L is the linear distance from the point of deflection to the loading point, and $I_l$ is the second moment of inertia in the lateral direction.

It is important to note that $K_t$ and $K_l$ can be independently specified by changing the second moment of inertia. This feature increases design flexibility and allows one to adjust spatial compliance in the lateral direction independent of the sagittal plane. Our model assumes that small deflections in the lateral direction causes a negligible deflection in the sagittal plane, allowing us to consider the motions effectively decoupled.

In Figure 3.14, the slider can move continuously between the 0 and 10 markings where 0 is the most compliant configuration and 10 is the stiffest. Using the PRB model and the lateral stiffness equation, we can predictably design the tunable leg to operate within a range of stiffnesses as long as a portion of the slider is supported

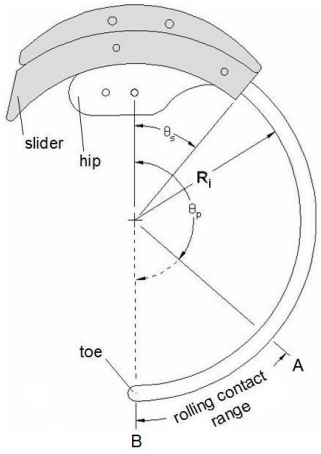


Figure 3.15: Application of PRB-model to tunable a tunable leg where leg stiffness can be defined by the slider position and the loading point.

by the hip region. For example, if the slider moves past the 10th marker it loses support from the hip region and the leg will begin to deflect from both ends of the slider.

It is important to note that moving the slider will affect the stiffness in all directions in a coupled manner. Fortunately the intuition offered from the primary biomechanical running models–the Spring-Loaded Inverted Pendulum model [12] in the sagittal plane and Lateral Leg Spring model [63], suggest that the change in stiffness in each direction should increase with running frequency or robot load. Although the optimal nature of this coupling for a many-legged spatial robot has not yet been worked out in detail, our design couples these changes in the correct direction.

### 3.2.4 PRB Based Leg Model

Thus far the PRB model has been presented with a single loading force where the loading point does not change. During operation of the robot, however, the loading point changes significantly. Generally, the leg touches down at around Point A (see

Figure 3.15) and rolls through to about Point B during the stance phase. The value of $K_t$ decreases from A to B according to Equation 3.2 as the value of $l$ increases. Although calculating the effective stiffness using PRB-based model of bending is more complex than with a simple linear prismatic spring, there are two notable features about the C-leg that make it difficult to reduce it to the simple spring model. First, there exists a coupled two-dimensional compliant behavior in the sagittal plane. Second, as the leg rolls during the stance phase, the moving point of contact creates two behaviors that can not be captured by a prismatic model. The first is that the stiffness of the leg decreases as the leg progresses from touch down to lift off. The PRB model captures this behavior as changes in $l$, but the linear model can not. The other non-linear spring behavior is that the rest length $l$ increases as the leg rolls through the stance phase. Our experience in designing and testing alternative legs is that failure to incorporate these behaviors leads to the design of legs with poor performance characteristics. This has to some extent been shown through simulation by [61] where it was shown that a softening leg spring is able to perform self-stable running behavior in significantly broader ranges of running speed and control parameters (e.g. control of angle of attack at touchdown, and adjustment of spring stiffness) than an linear prismatic one.

Even though stiffness varies along the length of the leg, it is not critical to determine the exact stiffness of the leg for each loading point since the robot will be optimized for different stiffness settings. In the design stage, it is more important to consider the range of stiffnesses, or relative stiffness of the leg. To calculate the range of stiffnesses for the C-leg presented in Figure 3.15, $k_o$ can also be represented as

$$k_o = \theta_p - \theta_s \tag{3.4}$$

where in radians $\theta_p$ specifies the loading point, and $\theta_s$ species the angular position of the slider or point of deflection. Thus to design a C-leg for a range of stiffnesses in

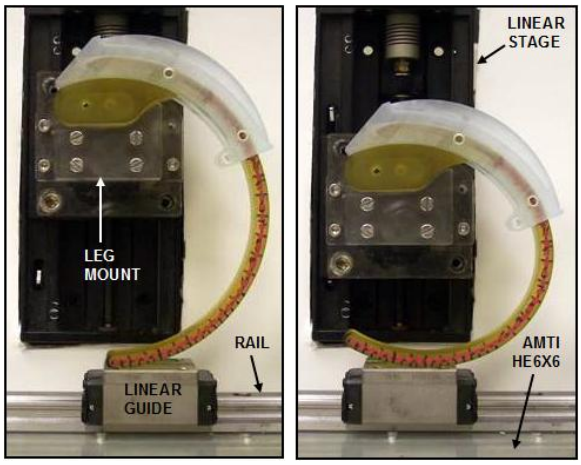


Figure 3.16: Relaxed and compressed images of a C-leg in the experimental set-up

the sagittal plane there are several design variables in the model that can be adjusted (e.g. $\theta_s$, $E$, $I_s$, and $R_i$).

### 3.2.5 Measuring Leg Stiffness

The $K_t$ for a shape deposition manufactured C-leg was collected at each of the even numbered slider positions shown in Figure 3.14. The leg was mounted to a Micos linear stage for ease of repeatability and the deflection of the leg against an AMTI HE6x6 force plate was visually captured (see Figure 3.16). The linear stage has a resolution of one micrometer and is capable of traveling 80 mm at rates as high as 14 mm/s. The AMTI HE6x6 is a six axis force plate capable of measuring loads as large as 16 pounds at 200 Hz with 12-bit resolution. Five measurements of the linear stage pressing the leg into the force plate at 10 mm/s where collected.

The $K_t$ was obtained by marking evenly spaced colored dots along the centroidal axis of the leg. An image capture system was created to compare the relaxed and compressed images to determine the loading point, point of deflection, the characteristic pivot, the arc length, $l$, and the value of the PRB-angle, $\Theta - \Theta_i$.

The analytical $K_t$ was calculated by inputting the specified material properties, and $l$ into Equation 3.2. The value for $K_\Theta$ and $\rho$ were determined from the look-up table in [36].

The experimental $K_t$ was calculated by first measuring the resultant torque, $T_R$, about the characteristic pivot using the force data and the horizontal and vertical distances measured from the characteristic pivot to the loading point. The resultant torque along with the PRB-angle, $\Theta - \Theta_i$, were then applied to the torsional spring equation below to determine the experimental torsional spring constant.

$$K_t = \frac{T_R}{\Theta - \Theta_i} \tag{3.5}$$

The stiffness in the lateral direction was determined by using the same force plate and linear stage. The toe was deflected in the lateral direction by pushing it into an obstruction rigidly anchored to the force plate. This experiment was repeated ten times for each even numbered slider position. A force-deflection graph was generated with the data, and a linear curve fit was applied to each experiment for a given slider position. The slopes of the linear curves were averaged to determine the average lateral leg stiffness for each slider position.

### 3.2.6 Results

For the sagittal plane stiffness, we found a reasonable correlation between the PRB model and the experimental results (see Figure 3.17). The error between the analytical and average experimental torsional stiffness measurements was less then 3%. For slider positions 0-8, the analytical results fall within the error bars, however this not the case for positions 9 and 10. This deviation can be attributed to deflection at the hip end of the slider. As mentioned earlier, as the slider moves to higher settings it is supported less and less by the hip region. For example, at slider position 10, there are noticeable deflections at both ends of the slider. Since this behavior is not

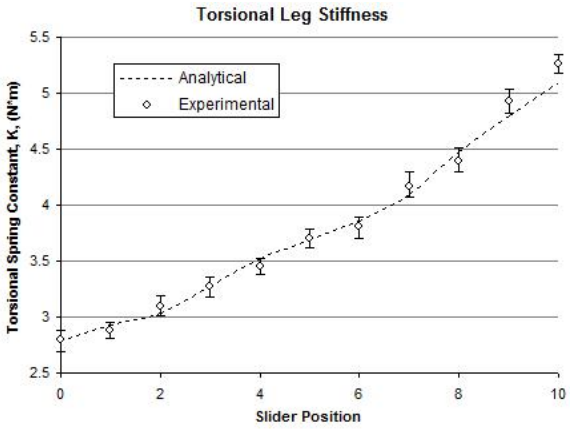


Figure 3.17: Experimental validation of the PRB-model for estimating torsional spring constant.

accounted for in the PRB model, it introduces another source of error.

### 3.2.7 Dynamic Loading

The objective of the following analysis was to observe the dynamic response of the variable stiffness C-shape leg for a range of payloads, when it was allowed to travel in the vertical direction only. A linear stage was created using precision ground steel rods and linear bushings. The linear bushings on each rod were connected via a laser cut acrylic platform. The platform served as a mounting structure for the leg and the payload. Steel plates were used to create a 500 g and a 1 kg payload. In each experiment the platform was raised and allowed to drop a distance of 113 mm (Figure 3.19). An IR marker was attached to the platform and an Optotrak 3020 motion capture system was used to record the position of marker with sub-millimeter precision at a rate of 1500 Hz (see Figure 3.20). This data was then used to determine the frequency of the stance phase (i.e. the amount of time spent loading and unloading) and the coefficient of restitution as measured from the rebound height.

In these experiments, we expected the ground phase frequency to increase as leg

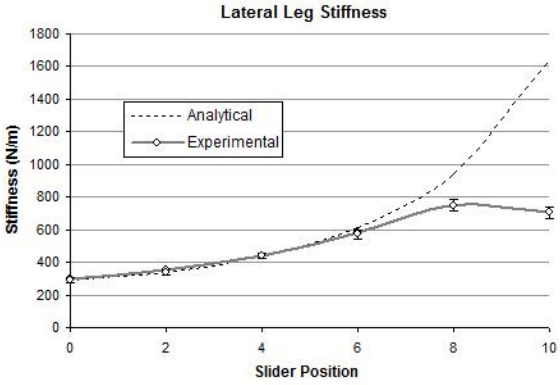


Figure 3.18: Experimental validation of the cantilever beam bending model for estimating lateral leg stiffness.

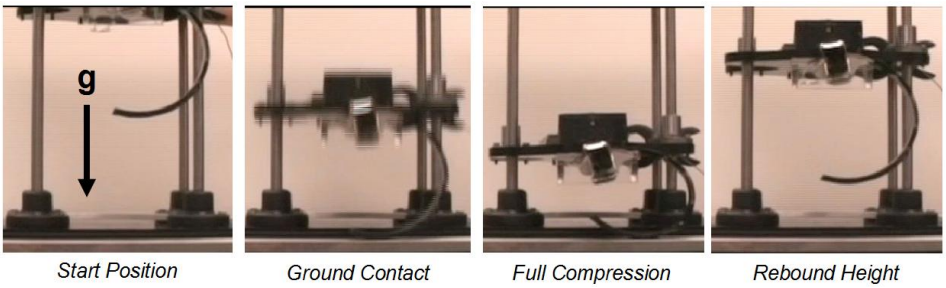


Figure 3.19: Side view of linear stage bounce test showing progression of leg loading and unloading.

stiffness increased; however, we observed the opposite trend (see Figure 3.21). These results revealed first hand that in addition to changing leg stiffness, the rigid slider was also changes the deflection path of the loading point. In essence the rigid slider design changes the shape and the stiffness of the spring in a way that can not be decoupled. For example, this was most noticeable at leg stiffness setting four where there is a noticeable drop in the ground phase frequency and coefficient of restitution. At this intermediate stiffness setting, the toe prefers to initially deflect more in the x-direction than in the y-direction which leads to significant frictional energy losses.

Pursuing this design poses a problem during running experiments. The coupled

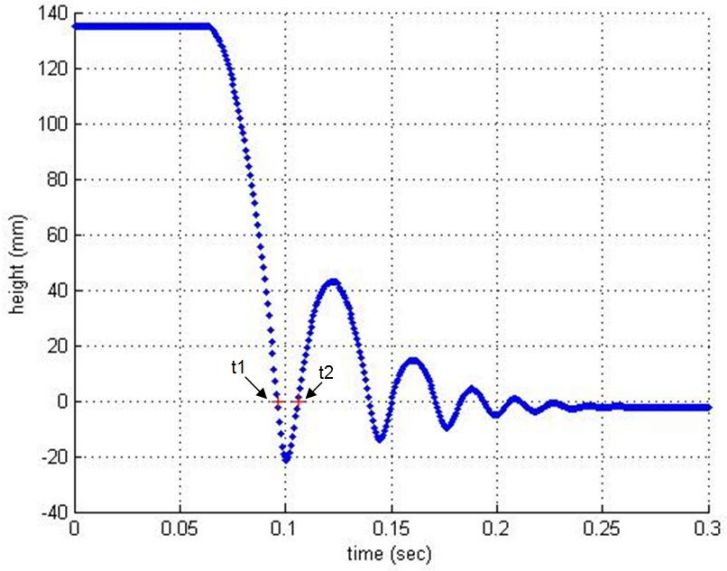


Figure 3.20: Sample of motion capture output where y-axis is the rebound height with y=0 specifying the undeflected leg hip position and x-axis measures elapsed time where t1 indicates leg touch down and t2 indicates leg lift off. The ground phase frequency is calculated as 1/(2(t2-t1)).

nature of a stiffness and shape changing spring makes it difficult to isolate the contribution of leg stiffness adjustment to the robot's locomotion. Therefore, what is desired is a leg that can change its effective stiffness without significantly altering the shape of the spring. In other words, can these two effects be uncoupled or at least minimized.

## 3.3 Preliminary Running Trials

Despite the coupled shape and stiffness changing nature of the leg design, preliminary running trials were conducted to test the material limits and learn more about the design. Observations collected from these experiments revealed two significant flaws in the design. The first flaw concerned the fatigue yield strength of the epoxy. After less than 600 meters, legs began to break especially the middle and back legs.

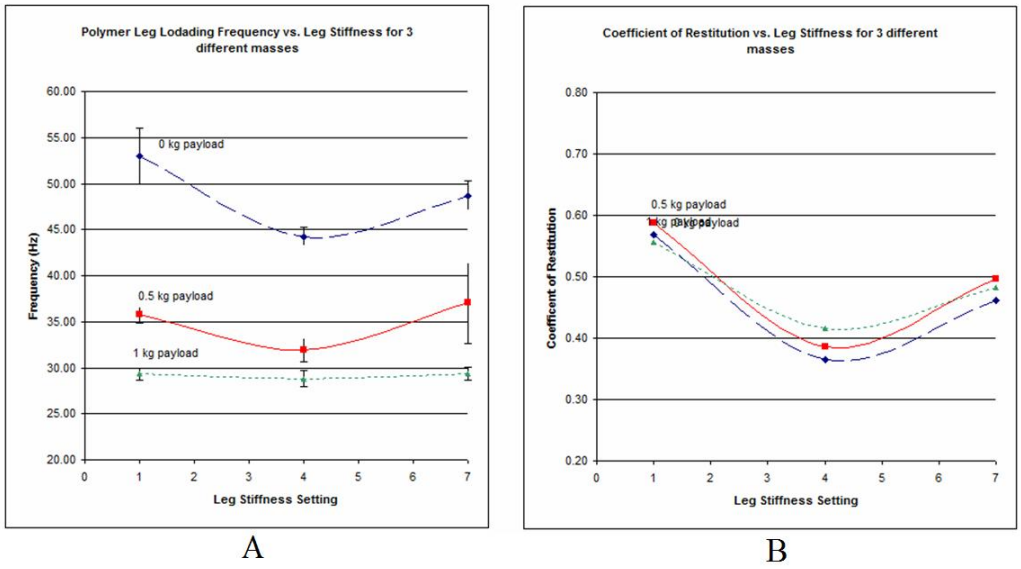


Figure 3.21: (A) Shows the ground phase frequency which is a measure of the loading and unloading of the leg for different payloads and stiffness settings. (B) Shows the coefficient of restitution for the leg at various leg stiffness settings and payloads.

Further research revealed that other material features must be considered including the density, energy density, fatigue life, and so forth. A high yield strength-Young's modulus ratio was not enough to guarantee robust passive compliant legs.

The other flaw in the design, while not apparent at first, was the rigid slider itself. One of the novel features of the original passive compliant C-shaped legs [50] is that they enable the robot to navigate rough terrain by allowing compliant ground contact anywhere along the length of the leg. A leg design with a rigid slider effectively limits the leg length that is capable absorbing impacts. This is important to consider as legs are generally stiffer at higher speeds or with larger payloads where the potential for damage from collision is greatest. Preliminary running trials revealed that poorly tuned gates allowed the rigid slider to impact the ground and in some cases damaged the slider.

## 3.4 Summary of Variable Passive Compliant Leg with Rigid Slider

The method of shape deposition manufacturing was explored extensively as a means to create variable passive compliant legs of arbitrary geometries with epoxies of different flex moduli and yield strengths. The method proved very useful for rapidly prototyping various leg structures; however, the epoxy materials themselves proved to be too weak to handle the cyclic load requirements of our dynamic running robot.

The pseudo-rigid-body model was applied to the rigid slider tuning method and was found to be a suitable analytical model for capturing the spatial compliance of the C-leg and the stiffness range. Despite the effectiveness of the model, dynamic loading tests revealed that in addition to changing leg stiffness, the rigid slider also changes the shape of the leg spring. The coupled nature of these effects makes it impossible to evaluate the robot performance based singularly on leg stiffness adjustment. Furthermore, from a pragmatic view point, the rigid slider narrowed the window of non-destructive leg touch down angles, which is not acceptable for this particular dynamic running robot.

# Chapter 4

# Passive Variable Leg Stiffness with a Compliant Slider

In this chapter, we present the work surrounding phase two of our tunable leg developments which was presented in [31]. In the first phase, a tunable C-leg design was presented whereby stiffness was adjusted by sliding a rigid element along the leg length (see Figure 3.14). The portion of the leg covered by the element was assumed to be rigid, while the remaining exposed portion was considered compliant. It was demonstrated that the overall stiffness could be varied by as much as 90%; however, there were undesirable features coupled in the design including: shape changing of the spring and an increased probability of the rigid slider impacting the ground.

Maintaining a relatively consistent toe deflection path for the continuous range of stiffness settings is an important feature to consider in a tunable leg. In the rigid slider design, each stiffness setting altered the deflection path of the leg spring causing the leg to respond differently to applied loads depending on the stiffness setting. The effect of this deflection behavior was observed using a one dimensional bounce test. While this is not an ideal testing method, a stronger design would be one that exhibits a monotonic increase in leg stiffness even under one dimensional loading conditions.

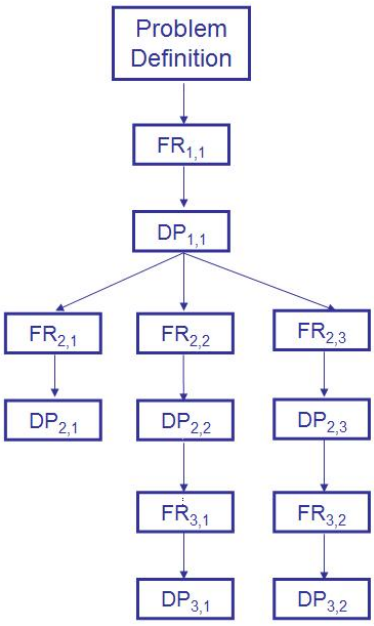


Figure 4.1: FR-DP hierarchy for proposed variable passive compliant leg design.

In the following chapter, we present a new tunable passive compliant leg which improves upon the shortcomings of the rigid slider by employing a compliant tuning element. As in the previous chapter, the developments of this work are presented within the axiomatic design framework.

## 4.1 Mechanical Design

In this second proposed solution, we defined the components of the revised axiomatic design hierarchy as follows

FR (1,1): Vary the stiffness of a spring element
DP (1,1): Change the second moment of inertia using a compliant slider

FR (2,1): Must use a springy material and robust material
DP (2,1): Fiberglass

FR (2,2): Ability to communicate to the legs
DP (2,2): Slip Ring

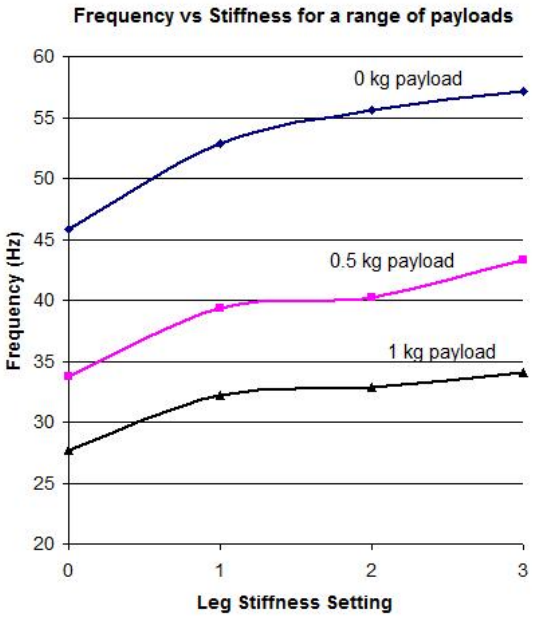


Figure 4.2: Leg bounce test results with compliant slider tuning element.

FR (3,1): Ability to adjust leg stiffness
DP (3,1): Attach a DC motor to drive the compliant spine

FR(3,2): Detect stiffness setting
DP(3,2): Potentiometer directly connected to DC motor shaft.

FR(3,3): Ability to sense leg strain
DP(3,3): Embed a flex sensor into leg

Constraint 1: Device mass $\leq$ 90 grams
Constraint 2: Position center of mass near axis of rotation

**FR (1,1): Vary the stiffness of a spring element**

**DP (1,1): Change the effective leg stiffness using a compliant spine**

During the final stages of development of the rigid slider design, we were also investigating the manufacturing process and properties of composite materials for leg construction (the properties of which will be discussed shortly). Several one-dimensional drop tests were conducted to validate an early design using a composite C-leg and a compliant tuning element which we have termed a compliant slider. We hypothesized that a compliant slider would be able to store and return energy

while not significantly affecting the shape of the spring in the sagittal plane. The preliminary results proved very favorable (see Figure 4.2) where it is shown that the ground phase frequency increased as leg stiffness increased. This suggests that the compliant spine configuration is a stronger design than the rigid slider.

**FR (2,1): Choose a springy and robust material**

**DP (2,1): Fiberglass**

The material selection for the rigid slider design was dictated in large part by the manufacturing process. At the time, SDM was the most familiar and versatile prototyping method available, which quickly narrowed the material options to a small family of epoxies. Preliminary experiments presented in Chapter 3 demonstrated though that the epoxies lacked the cyclic fatigue strength to sustain the loading requirements for RHex-like locomotion. Furthermore, narrowing material options by maximizing the yield strength-Young's modulus ratio did not consider all the important features for a compliant leg design. This has led to the development of a material feature space for leg springs which is an attempt to capture the important material properties for passive compliant legs.

### 4.1.1 Material Feature Space

Springs are a very inexpensive and reliable option for converting kinetic energy to potential energy and back again. They do not require an external power supply; response time to impacts is instantaneous (since it is not slowed by sensors or processors); the stiffness can be designed for the particular task at hand; the geometry can be a designed to fit within particular dimensional constraints; energy losses can be small. With that said, springs also have their limitations which generally stem from the choice of material.

Material selection, aside from leg shape, is the most important decision in a compliant leg design. The following section does not contain any new findings in

materials research, but rather serves as a model to highlight relevant material properties that must be considered at this critical juncture in the design process. The feature space for leg springs considers the materials energy density, fracture toughness, loss factor, and manufacturability (including cost). Before discussing these material properties, however, we first provide definitions of the modulus of elasticity, yield strength, and fatigue yield strength as they will used often in the discussion of the leg spring feature space.

**Modulus of Elasticity**

The overall stiffness of any spring element is proportional to the product of the modulus of elasticity, E, the second moment of inertia, I, and to the inverse of the spring length, L, cubed

$$K \propto \frac{EI}{L^3} \tag{4.1}$$

where $I = bh^3/12$. For isotropic materials the modulus of elasticity is the same in every direction and can not be varied. According to equation 4.1, the stiffness of a spring element with isotropic mechanical properties (i.e. aluminum, steel, and epoxy) can only be changed by adjusting the spring length and/or the second moment of inertia. For spring design, however, it is desirable to have as much design freedom as possible. This includes the ability to change the modulus elasticity. Anisotropic materials such as composites laminates (i.e. fiberglass and carbon fiber) have the property wherein the Young's modulus may be different depending on the orientation along which the property is measured. This means that a spring element can be designed to have more than one modulus of elasticity. For example, in the case of the C-leg, the modulus of elasticity in the sagittal plane and the lateral direction can be varied without changing the second moment of inertia. Achieving the same range of stiffness with an isotropic material may lead to designs that do not fit within the dimensional constraints that the leg must operate.

### Yield Strength

The yield strength of a material specifies the stress at which the material plastically deforms. A material will elastically deform for any load below its yield stress and will return to its original shape once the load is removed. While the Young's modulus, spring length, and second moment of inertia essentially define the stiffness of the spring element, it is the yield strength that specifies the loading limits as the stress in bending increases with the distance from the centerline of the beam to the outside surface. Therefore a balance must be struck in the geometry of the design such that the stiffness of the structure is in line with the dynamics of the system, and that the loads do not exceed the material limits.

### Fatigue Yield Strength

The fatigue yield strength, when available, provides a much better measure of the potential life span of the spring element. All cyclically loaded materials eventually fatigue and fail. The cyclic longevity of the spring element depends on a number of factors including the load frequency, the strain or load amount, the temperature, and the geometry to name a few. Generally a spring element does not survive many cyclic loads or strains that approach the material's yield strength. A spring that is subjected to loads near or below the fatigue yield strength will typically last much longer. This was a failure in the design of the SDM epoxy leg. Much time was devoted to finding a geometry that would satisfy a certain radial stiffness and lateral stiffness while not exceeding the yield strength and space constraints, and little time was devoted to characterizing the fatigue strength of the epoxy.

### Energy Density

The energy density of a material is a measure of the potential energy storage capacity in a body by virtue of an elastic deformation and is calculated as

$$U = \frac{\sigma^2}{\rho E} \tag{4.2}$$

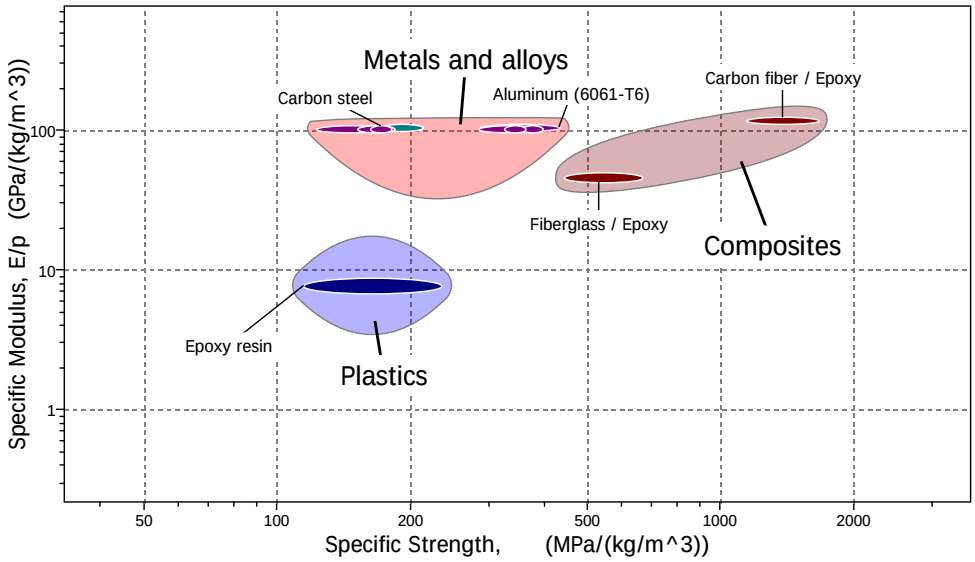


Figure 4.3: Energy density of a range of materials. This plot was generated from the Cambridge Engineering Selector (CES) by Granta.

U is the energy density, $\sigma$ is the yield strength, $\rho$ the material density and E the elastic modulus of the material. We divide by $\rho$ to identify spring materials that are lightweight [8]. Figure **??** plots the specific modulus against specific strength for a selection of materials including plastics, composites, metals and alloys. Light weight energy dense materials occupy the upper right-hand portion of the graph. It is worth highlighting that compared to composites, epoxies are an order of magnitude less energy dense. For spring designs, however, it is better to consider fatigue yield strength rather than the yield strength. According to equation 4.2, potential energy storage is maximized by selecting materials with a high fatigue yield strength, and a low density and elastic modulus. As can be seen in Figure 4.3, composite materials, Ti alloys, and rubber offer high energy density values compared to other materials.

### Fracture Toughness

Fracture toughness is measure of a material's resistance to the propagation of a crack which is an important property to consider for passive compliant legs that are cyclically loaded. A plot of fracture toughness against Young's modulus for a range

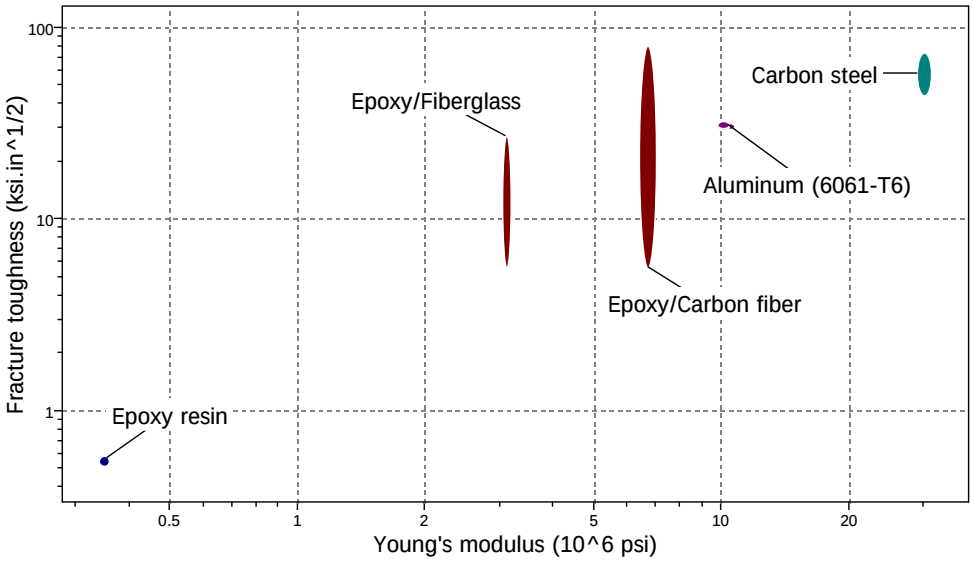


Figure 4.4: Fracture toughness of a range of materials. This plot was generated from the CES by Granta.

of materials in Figure 4.4 reveals that composites are an order of magnitude tougher than epoxies. Metals and alloys have approximately the same fracture toughness with a much higher Young's modulus.

### Loss Coefficient

The loss coefficient is a measure of a material's intrinsic damping. This in an important property to consider as a material with a large loss coefficient is likely to be inefficient at storing and returning energy. However, a material with a very low loss coefficient may produce robot dynamics that are hard to control or do not lead to passively stable gaits. Figure 4.5 demonstrates that composites have a loss coefficient that is approximately an order of magnitude smaller with metals posting values that even smaller.

Table 4.1 captures many of these material properties and what we find is that fiber composites are one of the best materials for spring structures, and least expensive. S2-6781 pre-preg fiberglass (from Applied Vehicle Technologies, Indianapolis, IN), was selected as the material of choice for several reasons including its relatively low

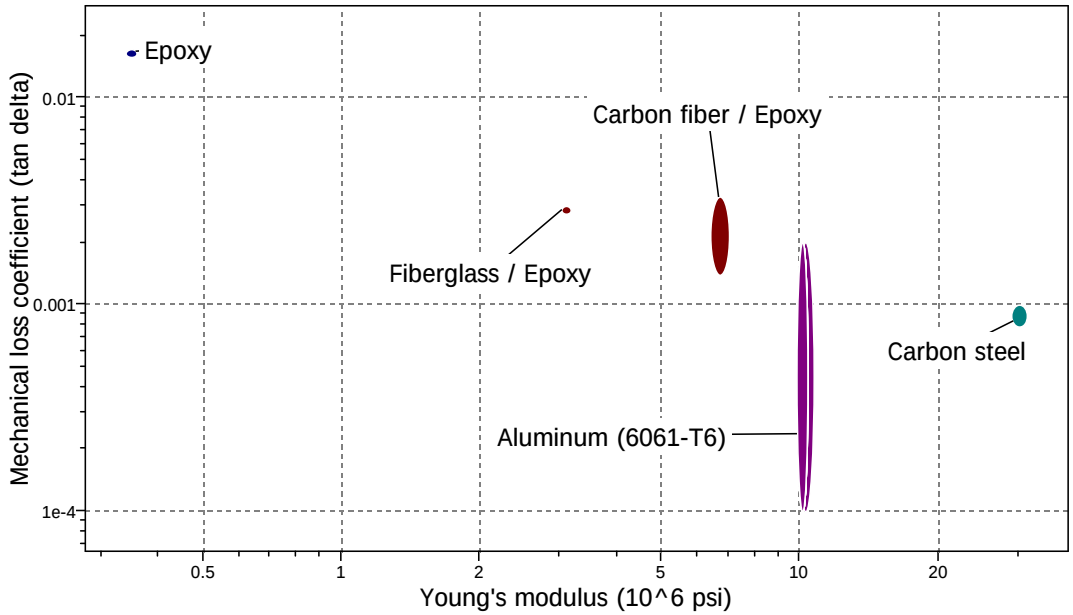


Figure 4.5: Loss coefficient of a range of materials. This plot was generated from the CES by Granta.

| Material | ρ (g/cc) LIB | E (Gpa) LIB | S (Mpa) HIB | (S/E) x10$^3$ HIB | U (kJ/kg) HIB | $ (USD) per leg LIB |
|---|---|---|---|---|---|---|
| Nitinol | 6.50 | 1 | 1000 | 1333 | 6.8* | 30+ |
| Fiberglass (S2-6781) | 2.25 | 22 | 520+ | 23.6 | 5.46 | 3 |
| TP-4004 (Epoxy) | 1.17 | 0.80 | 34 | 42.5 | 1.24 | 6 |
| Aluminum 7075-T6 | 2.81 | 71.7 | 500 | 7.0 | 1.24 | 1 |
| Steel (4140 Q&T@400) | 7.75 | 207 | 238 | 1.1 | 0.04 | 2.5 |

*Duerig et al., "Engineering Aspects of Shape Memory Alloys," 1990.

Table 4.1: Comparison of material properties.

density and Youngs modulus, high yield strength, comparatively high specific strain energy capacity and low material cost. In addition to these properties, composite laminates expand the available design space by offering the ability to vary the Youngs modulus value by adjusting orientation of the plies.

**FR (2,2): Ability to communicate to legs**

**DP (2,2): Slip ring**

The desire to communicate and power the legs led to a slip ring based motor assembly. While a wireless a solution is technically feasible, we foresaw many problems including the need to constantly remove and charge batteries on each leg, dropped signals, noise from the environment affecting the IRDa's and so forth. A slip ring on the other hand, offers a direct electrical connection between the leg and the robot. In this way, the legs and sensors are powered by the batteries on the robot, and sensor signals can be passed in the same manner. This solution is not without disadvantages including operating near the recommended RPM limit, a cycle life, and added resistance to rotation caused by the sliding electrical contact. In light of these drawbacks, a slip ring offers a more robust configuration to enable accurate collection of data, and more importantly, will expedite the locomotion experiments by minimizing robot downtime. In the proposed slip ring motor assembly, a six contact slip ring was sourced from Keyo Electric Company in China and can operate at 300 RPM continuously handling as much at 2 amps per circuit. Figure 4.6 below details the entire motor mount assembly, which is the first implementation of a slip ring for a RHex-like locomotion system. An aluminum shaft extension was created to accommodate the added spacing between the robot and the leg caused by the slip ring's rotor and stator. Furthermore to reduce the load on the motor shaft, a flange bearing (similar to the method used in RHex) was also incorporated.

**FR (3,1): Ability to adjust leg stiffness**

**DP (3,1): Attach a DC motor to drive the compliant slider**

In the proposed design the C-shape is anchored to an aluminum hip structure

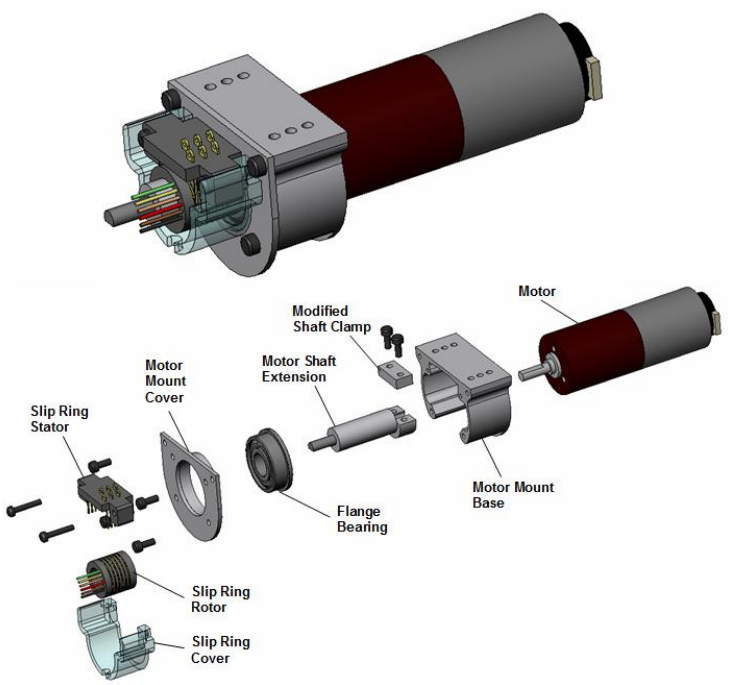


Figure 4.6: An assembled and exploded view of the slip ring incorporated into the motor assembly to allow legs to continuously rotate and source power from the robot power supply.

which also supports the drive mechanism. A thin, flexible rack is anchored to the back of the compliant slider, and controls the slider position without significantly altering the compliant slider stiffness. The position of the slider can be adjusted by activating a small, geared DC motor mounted to the hip, which simultaneously drives a nylon worm and spur gear (see Figure 4.7). A small plastic guide is attached at one end of the spine and wraps around the C-leg. The guide holds the spine against the C-leg, and acts as a mechanical stop when the spine is actuated to softest stiffness setting. The spacing between the C-leg and the compliant spine is approximately 2 mm. It is important to maintain this spacing so that the two compliant elements deform together under load. To enforce this condition, small spacers were attached to the inside surface of the compliant slider. During operation, the motor can rotate clockwise or counterclockwise to move the slider through the continuous spectrum of leg stiffnesses. When the slider reaches a target stiffness setting, the motor shuts off, and the worm provides sufficient resistance to rotation in either direction; thus acting as a natural self-locking mechanism. Hence no power is required to maintain the desired leg stiffness during locomotion. This also results in a robust and efficient spring as there are no moving parts for a given stiffness setting. In its final configuration, the tunable C-leg has a 114 mm inner diameter and weighs less than 85 grams.

An additional feature of the design is a mechanical stop, which is not found in previous fixed stiffness legs. In Chapter 5, we present empirical evidence that suggests EduBot, but more generally RHex-like robots, run more efficiently and faster with very compliant legs. This presents a challenge in that these low stiffness legs reach their material limits during uneven tripod stance phases. In other words, the challenge has been to identify a solution where low stiffness legs can support large loads and deflections without failure. We currently have been unable to identify a contemporary material that is as economical and easy to handle as composites and still capable of surviving the loading extremes. Therefore, the current design includes

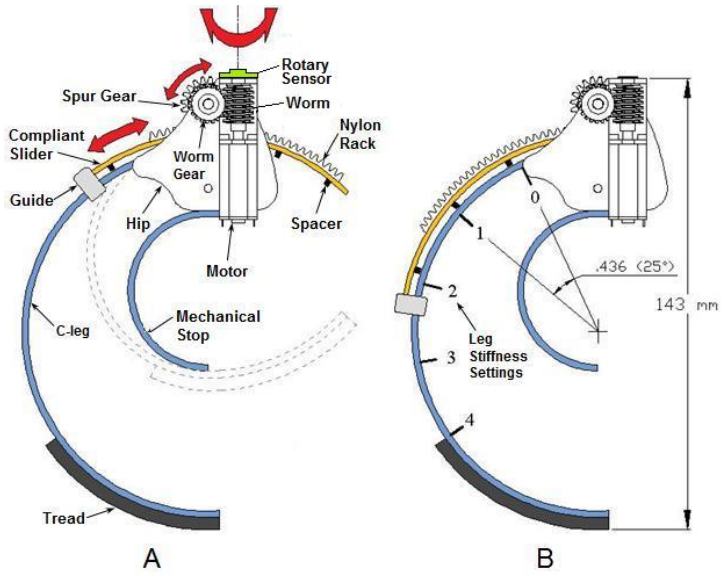


Figure 4.7: A side view of tunable stiffness composite leg design. A) Illustrates the rotation directions of gears B) shows the compliant slider adjusted to a higher stiffness setting.

a C-shaped mechanical stop to prevent the robot from deflecting the legs into regions where failure may occur and to prevent the robot from bottoming out.

**FR(3,3): Ability to detect leg stiffness setting**

**DP(3,3): Attach a rotary sensor to motor shaft**

We again offer a simple solution for detecting the leg stiffness setting using a continuous rotation sensor. In the proposed configuration the rotary sensor in connected to the worm's aluminum shaft which is the same shaft the DC motor rotates (see Figure 4.7). A full rotation of the motor shaft corresponds to the advancement of one tooth of the rack on the compliant slider. Therefore, counting rotations (clockwise and counterclockwise) can be mapped to the overall leg stiffness.

**FR(3,3): Ability to sense leg stress**

**DP(3,3): Embed a flex sensor into leg**

As discussed in the Chapter 3, we still desired a method to measure leg stress. In the first implementation, SDM offered considerable flexibility for embedding a flex sensor into the C-leg. Composite processing is a very different prototyping method;

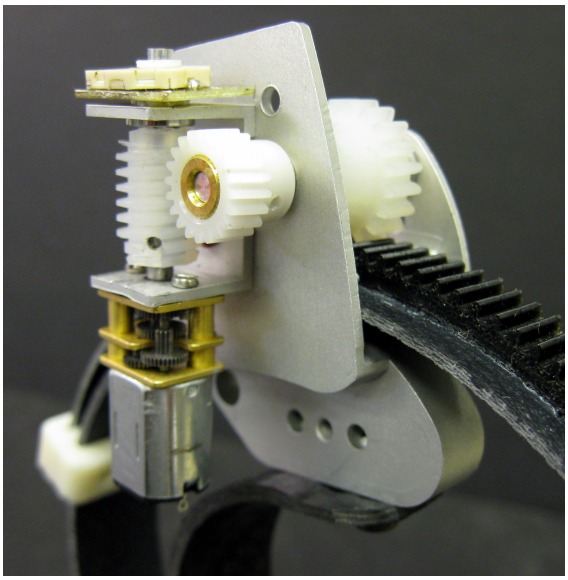

Figure 4.8: Active component of the tunable stiffness composite leg design.

however, it still offers the capability of embedding a flex sensor. This is achieved by following the fabrication steps outlined in Appendix A, and simply inserting the flex sensor once the first half of laminate layers have been applied. Care must be taken to protect the wire connections during the curing process. The Jameco flex sensor has an operating temperature of 80°C, but can withstand the pre-preg fiberglass curing cycle of 1 hour at 120°C without damage.

A tunable leg with an embedded flex sensor was inserted in the leg deflection fixture (see Appendix B), and the resistance was measured for a range of deflections. The results shown in Figure 4.9 are very similar to those presented in Figure 3.11, with the exception that we are now able to measure the stresses on the leg for the continuous range of leg stiffness settings. In this particular example the resistance-deflection signature is nearly the same for the different stiffness settings (SS) even though there is an 90% change in leg stiffness between SS0 and SS3. It should be noted that while we demonstrate the capability of including a flex sensor in the leg, we do not explore this feature any further in this work and instead leave it as a topic for future research.

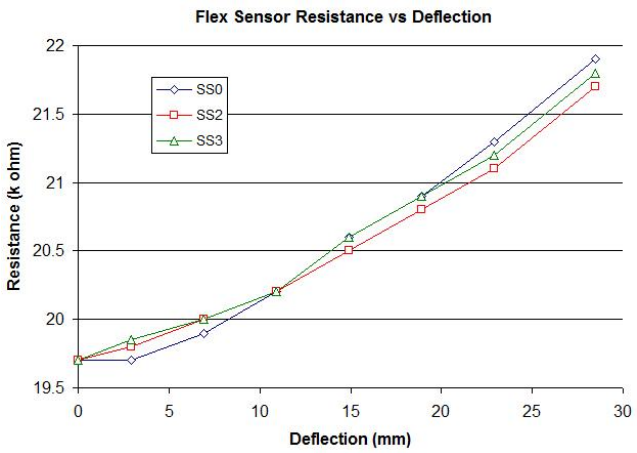


Figure 4.9: Flex sensor vs. deflection results for various leg stiffness settings.

### 4.1.2 Integration and Testing

In Figure 4.10, we present the integration of all these design parameters (with the exception of the flex sensor) into our hexapedal robot. Six tunable legs have been attached to the motor mount assembly shown in Figure 4.6. A PIC18F2553 micro controller is used to drive each of the DC motors in the worm gear mechanism and to detect the compliant slider position by counting revolutions of the rotary pot. These actions are carried out using the slip rings presented in Figure 4.6.

For the experimental results presented in Chapter 5, it should be noted that while this tunable leg design was tested, the active leg stiffness adjustment was not part of the optimization experiments. Instead, the tunable stiffness legs were adjusted to predetermined settings for which the robot's gait parameters were optimized. This was done primarily for the fact that we were and still are learning about the role of tunable stiffness legs and did not want to be burdened with the complexities of an active tuning component. With that said, the purpose of this section is to document that the active leg stiffness adjustment design does work. In a simple set of walking experiments, EduBot was able to stop, change its leg stiffness, and continue walking. After performing these tests, we suspect that in future developments EduBot should not have to stop, but instead could actively adjustment its leg stiffness while moving.

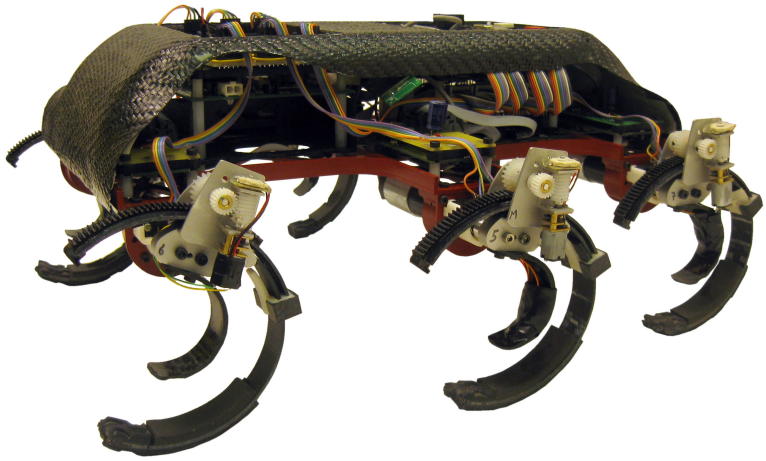

Figure 4.10: Assembled EduBot with tunable stiffness legs.

Figure 4.11 shows three images of EduBot actively adjusting its front left leg.

## 4.2 Analysis of Compliant Spine Tunable Leg

### 4.2.1 Compliance Characterization

To estimate the stiffness range of the compliant C-leg with a compliant spine, we again employ the pseudo-rigid-body (PRB) model [36]. A more detailed explanation can be found in chapter 3; however, for this work we are primarily interested in the magnitude of the torsional spring constant, $K_t$, in Equation 3.2. As it was noted earlier E, $I$, $R_i$, and $l$ are the only values needed to approximate $K_t$. Currently the PRB model can only be applied to approximate the stiffness of the C-leg at its softest and stiffest settings.

When the tunable leg is at the stiffest setting, we have found that the second moment of inertia is best expressed as

$$I = I_{leg} + I_{slider} \tag{4.3}$$

where $I_{leg}$ is equal to $b_{leg}h_{leg}^3/12$ and $I_{slider}$ is expressed as

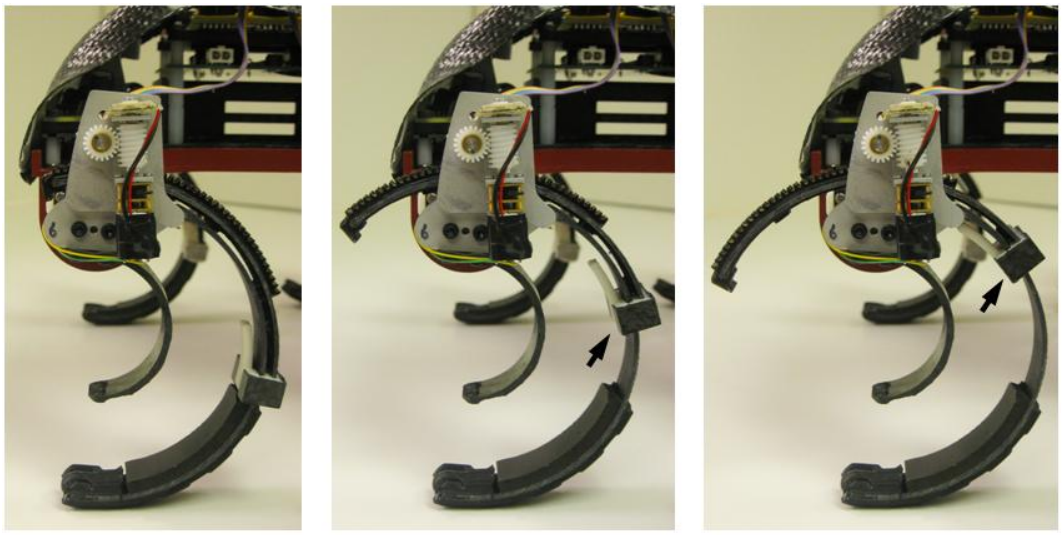


Figure 4.11: Side view of the leg actively adjusting its leg stiffness where A) the leg is at its stiffest setting, B) the slider position moves up to a softer stiffness as indicated by the black arrow, C) the slider has traveled as far as possible where the leg is at its softest stiffness setting.

$$I_{slider} = \frac{E_{slider} b_{slider} h_{slider}^3}{12 E_{leg}} \tag{4.4}$$

This formulation is an adaptation of the one presented in [39]. The ratio of $E_{slider}$ to $E_{leg}$ is a common expression used to account for situations in which members subject to bending are made of more than one material. With composite materials it is easy to fabricate the leg and spine for two very different Young's moduli. When the tunable leg is at its most compliant setting, we assume that $I_{slider} = 0$.

Since the PRB model assumes a uniform cross-section, it cannot be used to estimate the leg stiffness range and tip trajectory at intermediate stiffness settings. The finite element method can be used to produce the needed information; however, this requires a larger investment of time. To expedite the design process, we have determined that a stiffness setting near the angular position of 50° (see Figure 4.7B) leads to the greatest tip trajectory deviation. Therefore if one can design the tip trajectory at this setting to approximately match the behavior at the stiffness extremes,

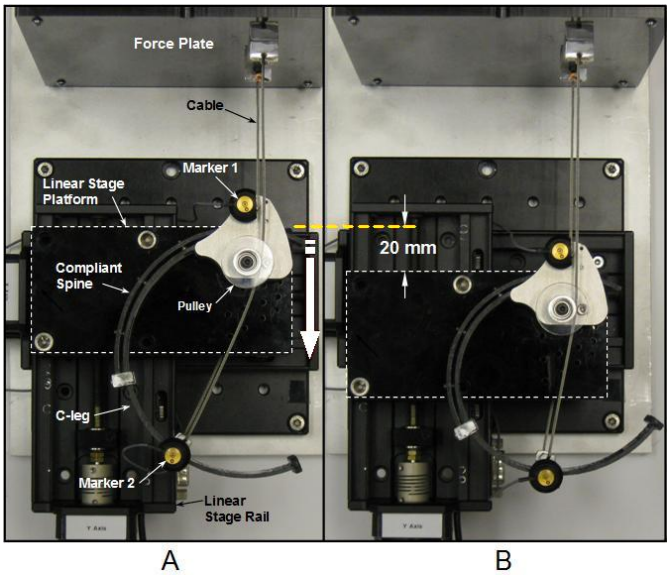


Figure 4.12: Top view of experimental set-up. A) Linear stage is in the home position and leg is undeflected. B) Platform has been moved a distance, d, and leg is deflected.

then the intermediate settings should also closely approximate the same behavior.

### 4.2.2 Static Leg Loading Experimental Set-up

To observe the leg deflection behavior and to validate the PRB model, an experimental apparatus was constructed to measure an applied load and to record the resulting deflection path. In the present experiment a Micos linear stage and an AMTI HE6x6 force plate were rigidly connected to an aluminum base plate. The linear stage has a resolution of one micrometer and is capable of traveling 80 mm at rates as high as 14 mm/s. The AMTI HE6x6 is a six axis force plate capable of measuring loads as large as 16 pounds at 200 Hz with 12-bit resolution. The C-leg's aluminum hip was anchored to the linear stage platform and the C-leg was cantilevered out from the platform. An aluminum leg clamp was affixed to the leg at the position indicated by Marker 2 in Figure 4.12A. One end of a flexible steel cable was anchored to the force plate while the other was connected to the leg clamp. A pulley was anchored to

the hip to provide a rolling contact point and to make the cable normal to the force plate's surface. The linear stage was commanded to translate (see Figure 4.12B) the hip a distance of 20 mm at 10 mm/s in the y-direction (given by the large downward pointing white arrow on the right side of Figure 4.12A). The force plate collected the reaction forces at the loading point (Marker 2) at a sampling rate of 200 Hz. An Optotrak 3020 motion capture system was used to capture the position of Markers 1 and 2 also at a sampling rate of 200 Hz. This was repeated for each of the leg stiffness settings 0-4 by shifting the compliant slider (see Figure 4.7B) along the length of the C-leg. The 6-ply fiberglass C-leg and slider were constructed with an alternating 50/50 blend ratio where 50% of the plies where angled at 45° while the other half were angled at 0°. The leg inner diameter is 114 mm with a thickness of 2.25 mm and a width of 18 mm. We estimate the Young's modulus value to be 9.65 GPa.

### 4.2.3 Static Leg Loading Results

Figure 4.13 plots the experimental results of the force versus radial deflection and demonstrates that the stiffness increases monotonically. The stiffness, which is indicated as a slope value, k, next to each curve, doubled between the two stiffness extremes. This was expected as the only difference between the two extremes was a doubling of the moment of inertia. It is also worth noting that the stiffness increase from leg stiffness setting (LSS) 0 t0 LSS1 is approximately 9% for this configuration. In the future, LSS1 could be the home position to allow the leg to reach higher stiffness settings faster without significantly limiting the stiffness range.

### 4.2.4 Deflection Results

In Figure 4.14 the xy-deflection path of the leg is presented. The bottom right image in Figure 4.14 provides a bearing for the location and orientation of the xy-axis while the rectangle reflects the results window. For the tested range of the stiffness

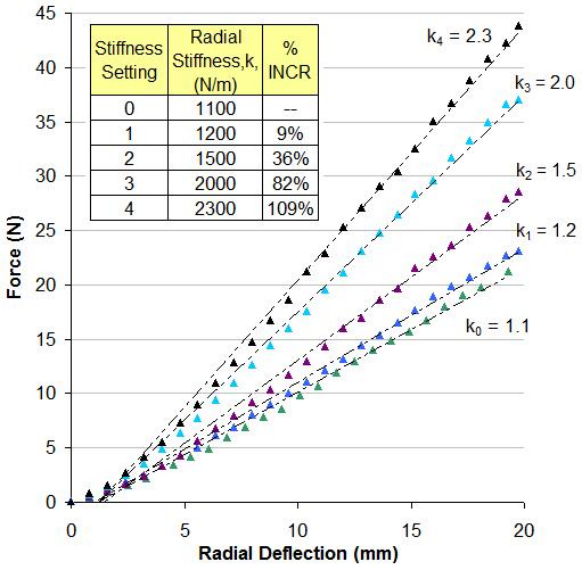


Figure 4.13: Tunable stiffness leg force-deflection response at four different stiffness settings each with a curve fit (dotted line) applied the data.

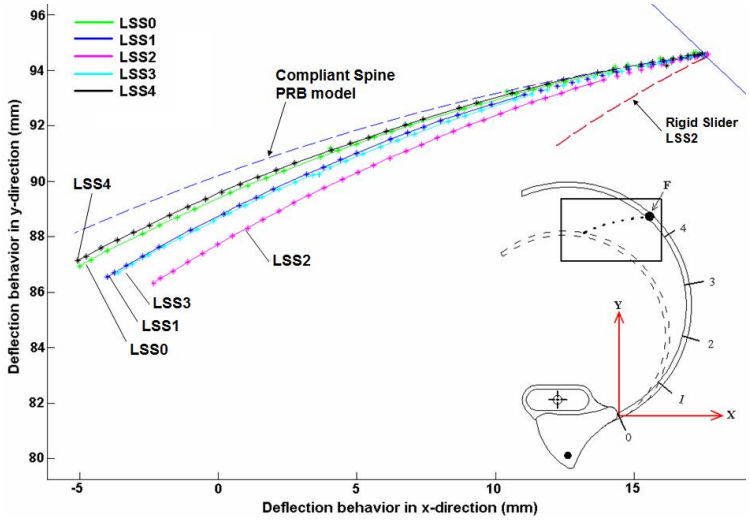


Figure 4.14: Deflection path of the loading point, F, for the tunable leg at various stiffness settings. Experimental results show that proper selection of slider stiffness can produce relatively consistent deflection paths for a large range of leg stiffnesses.

settings, the deflection paths showed low variability. In particular, the deflection paths of the two extreme stiffnesses (i.e. LSS0 and LSS4) were almost identical and varied by no more than 0.5 mm from each other. At maximum deflection, these results were also within 1 mm of the deflection path predicted by the compliant slider PRB model, which for a total deflection of 20 mm in the y-direction, represents about a 5% estimation error. As expected, the deflection path at LSS2 showed the most deviation. At maximum deflection, the y-component deviation was approximately 2 mm which represents roughly a 10% difference from the compliant spine PRB curve. For comparison purposes, the same tangential force that produced the deflection path for LSS2 was applied to a rigid slider PRB model also at LSS2. The rigid slider tuning method clearly produces very different spring behavior (see curve labeled 'Rigid Slider LSS2'). The stiffness is much larger, which is given by the short deflection path, and the smaller characteristic radius. It should be noted that achieving consistent deflection behavior for all stiffnesses while achieving a large deflection range are two competing objectives. If the compliant spine is too soft then the deflection path will be consistent; however, the stiffness range will be very small. Similarly, if the compliant spine is too stiff, the deflection path and stiffness range will begin to reflect the rigid slider model. Therefore, while deviation in deflection behavior is expected through proper material selection and geometries this can be minimized while still achieving a considerable stiffness range.

### 4.2.5 Dynamic Leg Loading Experimental Set-up

To better capture the energy storage and return properties of the compliant spine design, a new dynamic leg loading apparatus was created as shown in Figure 4.15. The improved design uses roller bearings which have less energy losses compared to the linear bearings used in the apparatus presented in Figure 3.19. The hip is still constrained to translate vertically; however, the toe is now allowed to deflect in the horizontal and vertical directions and does not touch the ground. A fixed length

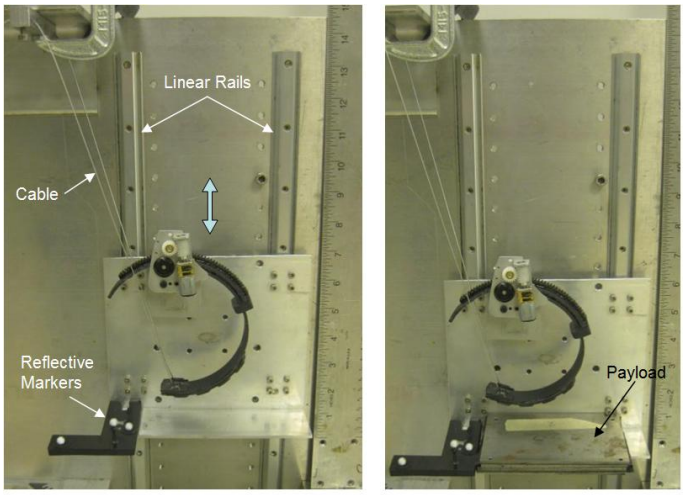


Figure 4.15: Front view of the dynamic leg loading apparatus. A) Shows the leg in unloaded state while B) shows the leg partially deflected with and also demonstrates how payloads can be added.

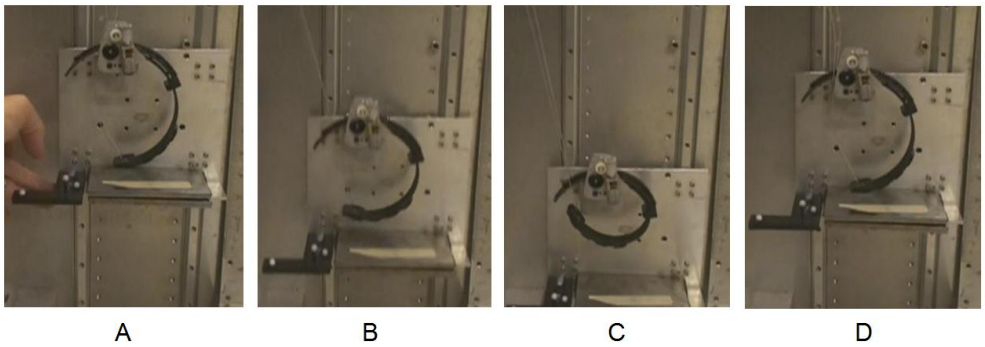


Figure 4.16: Snap shots of the tunable dynamically loaded. A) Platform is raised up, B) Platform is released and falls storing strain energy in the leg, C) Leg reaches full compression for given payload and stiffness setting, D) Rebound height.

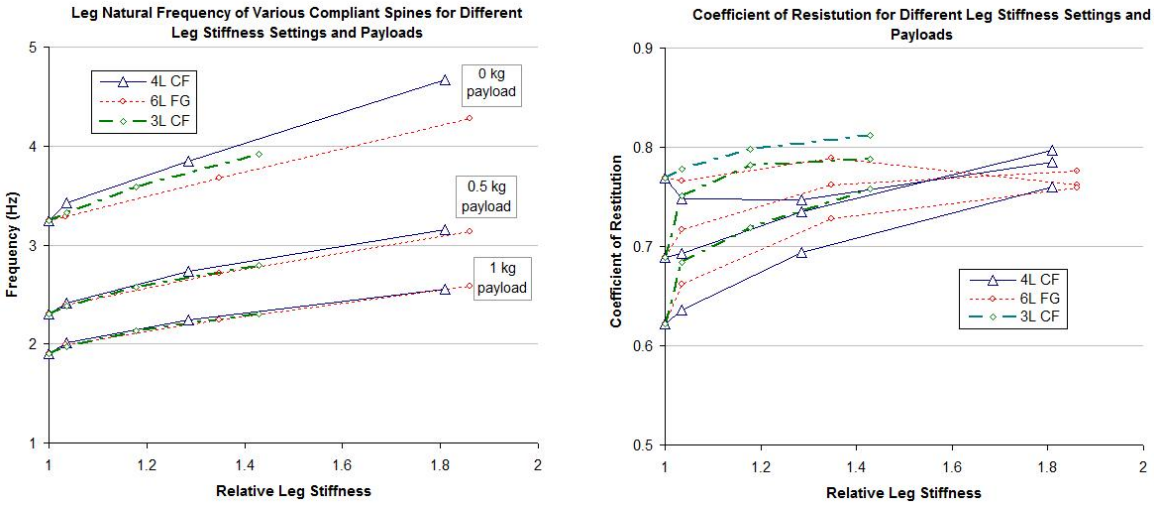


Figure 4.17: Leg bounce test results with 4 layer carbon fiber spine

cable connects the toe to the anchored test frame while the hip is anchored to the linear stage and is allowed to move up and down.

The objective of this new experimental set-up was to determine roughly what slider stiffness and material type offered the widest stiffness range, and the best energy storage and return. Three different compliant spines were prototyped including 1) a six layer S2-6781 pre-preg fiberglass spine (6L FG), 2) a four layer 11.7 ounce 2x2 twill carbon fiber spine (4L CF), and 3) a three layer 11.7 ounce 2x2 twill carbon fiber spine (3L CF) (note: all the layers for the sliders were oriented at 0 degrees). The C-leg itself was composed of six layers of S2-6781 pre-preg fiberglass. Three different payloads (0, 500g, and 1kg) were tested at four different leg stiffness settings as depicted in figure 4.7B. The stiffness of each leg-spine configuration was measured (see Appendix B) at each stiffness setting to determine the relative leg stiffness. The stiffness of the 6-ayer fiberglass C-leg measuring 18 mm wide with an 11.5 cm diameter and no compliant slider is used as the reference leg and has a relative leg stiffness (RLS) of one.

### 4.2.6 Dynamic Leg Loading Results

For the different compliant slider configurations, the 4L CF and 6L FG sliders offered the widest range of mechanical stiffness adjustment as shown in Figure 4.17. Although the materials were different, the effective stiffnesses of these sliders were designed to be the same. This is evident in their RLS ranges of 1 to 1.8 shown in Figure 4.17. Each produced approximately the same coefficient of restitution at the highest stiffness setting for each payload. The coefficient of restitution results also indicate that for the 0.5 and 1 kg payloads, energy storage and return increases as leg stiffness increases. This is a feature that was not captured in the dynamic leg loading apparatus presented in Figure 3.19.

## 4.3 Design Weaknesses

The compliant slider design overcomes many of the drawbacks of the rigid slider design; however, it does introduce a new set of problems. One weakness, which is more of a property of structure-controlled stiffness designs, has to do with slider length. Softer leg settings leave the unused portion of the compliant slider susceptible to damage as it extends out from the hip. Therefore, one must carefully consider the desired stiffness range as well as the overall length of the compliant slider.

All materials that are cyclically loaded eventually fatigue and fail and composites are no exception. The particular composite we are using is thermoset composite which means heat is required to cure the epoxy matrix to set the final shape of the part. Cyclic loading causes micro cracks to form in the epoxy which contribute to an effect known as stiffness softening where the effective Young's modulus decreases. For thermoset composites this stiffness softening can be as much as a 15-20% drop [43]. This effect is nearly impossible to characterize analytically as the properties of the part vary depending on the epoxy, fiber type, manufacturing process, loading conditions, and so forth [43]. Therefore an attempt was made to characterize the

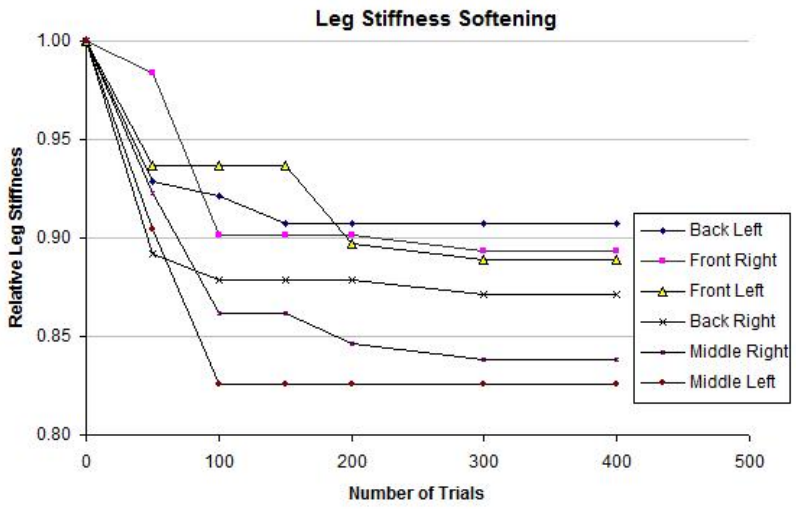


Figure 4.18: Leg stiffness softening of C-legs that are cyclically loaded from running.

stiffness softening of the C-legs by subjecting six legs to controlled running trials. In this experiment, six fiberglass C-legs were measured before being subjected to any cyclic loading. A medium-speed gait was selected (forward velocity of 1.2 m/s) and a 0.5 kg payload was added to increase the stress on the legs. Four-hundred trials were run where in each leg experienced approximately 15 loading cycles per trial (roughly 6000 loading cycles in all). The stiffness of each leg was measured at six different points during the experiment.

The results shown in Figure 4.18 suggest that the legs soften 10-18% depending on location with the most softening occurring in the first 100-150 trials. This percentage decrease is inline with related work on thermoset composites [43]. Additionally, the middle legs appear to soften the most which is not surprising as they must support the most load in a tripod gait. Two conclusions can be drawn from these results. First, the legs must be broken in via cyclic loading before optimization experiments (see Chapter 5) can be run. Second, due to the nature of stiffness softening, leg stiffness should be carefully monitored during experimentation as the legs may gradually continue to soften. We can also claim another benefit for tunable leg stiffness. Gaits are typically tuned for specific leg stiffnesses, but stiffness softening creates a moving

target. Tunable leg stiffness extends the utility of softened legs such that gaits of known performance for a given leg stiffness can be implemented.

## 4.4 Other Materials

Thermoset composites are relatively inexpensive, easy to work with, offer relatively reproducible parts, and require only a small capital investment to get started. There is, however, a better albeit more expensive material for passive compliant legs, namely thermoplastic composites. Thermoplastics (especially PEEK) are much tougher than epoxies as they offer superior resistance to impacts and can handle higher strain rates. Furthermore, under cyclic loading conditions thermoplastic composites demonstrate an insensitivity to fatigue damage [9] [55]. It should be noted though that we suspect thermoplastics may be more damped than thermosets; however, we were unable to confirm this as most companies do not test or publish this material property. Regardless, future work on passive compliant leg design should consider this class of composites. This material option was not pursued as it simply exceeded the allotted funds. Thermoplastic composites become a more economical option when high volumes are considered.

For the purposes of documentation, nitinol was also considered as a compliant leg material. Also known as shape memory alloy, nitinol offers a high energy density and fracture toughness (see Table 4.1). Some other material properties include the ability to recover from bending strains as large as 10% without plastically deforming (note: spring steel can manage about 0.2% strain before plastic deformation), and a low Youngs modulus. However, nitinol has less desirable properties, including a high raw material cost (approximately $30 per leg), limited available stock geometries, hysteresis, and difficulty to form various geometries with tight tolerances. For example, in order to achieve a desired curvature, nitinol must be clamped to a custom mold and baked at temperatures of 530°C. Several legs were fabricated using this

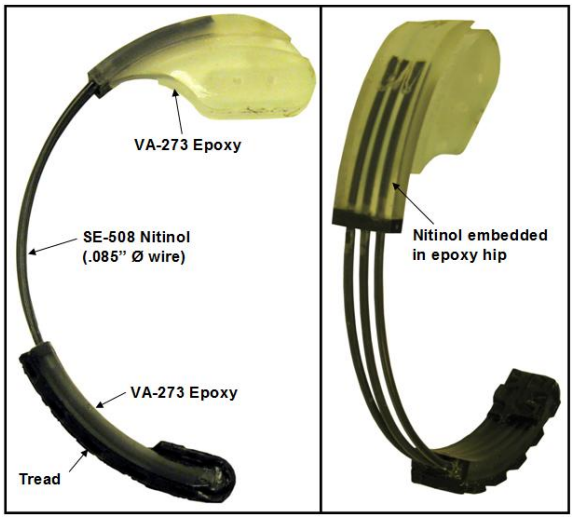


Figure 4.19: C-leg with nitinol spring element

technique to bake 0.085"' diameter nitinol wire in a C-shape. SDM was used to embed C-shaped wires into a plastic hip structure (see Figure 4.19); however, achieving consistent radius and stiffness values from one leg to another proved very difficult.

## 4.5 Summary

Considerable energy has been spent identifying the mechanical design, materials, and manufacturing process that will yield robust, tunable leg springs. In Figure 4.10, we present what we believe is the first implementation of an autonomous dynamic legged robot with variable leg compliance capabilities. The evolution of the leg design reflects the challenge of creating tunable legs for dynamic locomotion. Out of this work, we have articulated our reasons for shifting from epoxies to composite materials as composites offer a significantly higher energy density, superb fracture toughness, and low loss factor. Additionally, we presented a modified structure-controlled stiffness tuning method whereby a compliant slider rather than a rigid one slides along the length of the leg to change the effective leg stiffness. The goal of which was to preserve the toe deflection path for the range of leg stiffness settings

and to eliminate inelastic collisions of a rigid slider with the ground. As part of this work two important tools where developed, one to measure leg stiffness and the other to measure the dynamic properties of the leg which include the natural frequency range and the coefficient of restitution. We also have a better understanding of the weaknesses of different materials as spring elements especially the stiffness softening that occurs in composites. In response we have developed a practice to mitigate the influence of this particular weakness by running the robot to break in the legs.

# Chapter 5

# Experimental Results

In the following chapter we now shift from mechanical development to experimental validation of the structure-controlled stiffness leg on our hexapedal runner, EduBot. We present our method for optimizing locomotion gaits for a range of leg stiffnesses and the subsequent empirical results.

## 5.1 Optimization Method

Early attempts to identify good gaits with EduBot relied on manual teleoperation to control the robot as it ran back and forth on a path of fixed length. There were several problems with this arrangement as it required four people to run the experiment; one to control the robot, one to time, one to adjust the gait parameters, and one to turn the robot around. Furthermore, the results tended to be very difficult to repeat as it was hard to maintain a straight heading for many gait settings.

We improved our experimental procedure by developing an automated optimization routine similar to the method used to optimize RHex gaits [71]. A Nelder-Mead optimization scheme was used to tune EduBot's six gait parameters. Nelder-Mead is a nonlinear optimization technique that can find a locally optimum solution for systems with several variables. In [71] Nelder-Mead was employed to optimize RHex

gaits and was able to identify gait parameters that enabled a nearly 3x increase in forward velocity over the best hand-tuned gait. The system relied on an automated gait tuning configuration whereby a camera mounted to RHex allowed it to collect visual data to run toward engineered beacons thereby removing the human element from the experiment. EduBot gait tuning relied on a similar arrangement using a Vicon motion capture system to control the robot during all aspects of the experiment. Reflective tracking markers mounted to the robot shell allowed the controller to accurately and repeatably steer the robot from one end of the test arena, known as an *end zone*, to the other. The length of each run measured approximately 25 feet with the first 35% reserved for acceleration, and the last 5% reserved for deceleration. The robot's center of mass was tracked with sub-millimeter precision at a frequency up to 120 Hz. During each trial (i.e. running from one end zone to the other), the average power and average velocity were recorded. These values were used to calculate the specific resistance, $f_{sr}$, which is a dimensionless parameter that characterizes energy efficiency as the ratio of average power in over average power out. First introduced in 1950 by [29], specific resistance remains a standard parameter for comparing the energetic performance across a range of locomotion platforms including legged ones. It is typically written as

$$f_{sr} = \frac{P_{avg}}{mgv_{avg}} \tag{5.1}$$

where $P_{avg}$ is the average power consumed, m is the mass of the robot (EduBot weights 3.3 kg), g is gravity, and $v_{avg}$ is the average velocity recorded for a given set of gait parameters. It should be noted that for all of the running experiments $P_{avg}$ is measured at the battery and therefore includes the power needed to run the microprocessor as well as the motors. The power consumed by an idle EduBot (i.e. no motor actuation) is approximately 10.7 Watts. For purpose of comparison, the specific resistance for different locomotors as a function of speed is depicted in Figure 5.1. This figure is adapted from [1] where the red filled circular markers

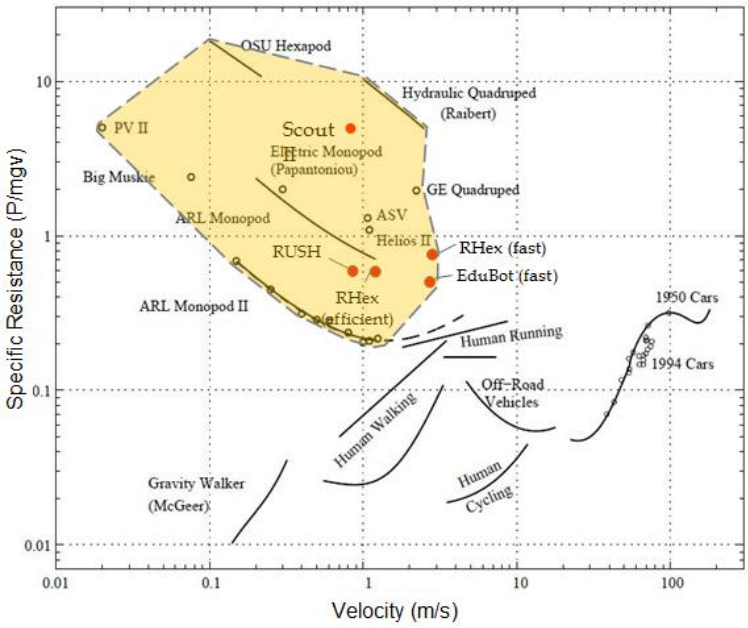


Figure 5.1: Specific resistance values as a function of speed for a range of locomotors [1].

reflect specific resistance values for more recent legged robotic platforms. The shaded polygon highlights the results posted by several legged robots. One can see that RHex and EduBot push the boundary for speed and efficiency among the legged robotic platforms. It is interesting to note that EduBot can run almost as fast as RHex with an almost 40% reduction in specific resistance. We suspect this due to the fact that in a scaled comparison, RHex legs are significantly stiffer than EduBot legs (see Appendix C for calculation). As we will show in the following experiments, legs that are too stiff converge to slower and less efficient gaits.

As noted in [71], for situations in which we want to identify fast running gaits a modified version of specific resistance takes the form

$$f_v = \frac{P_{avg}}{mgv_{avg}^3} \tag{5.2}$$

It was found in [71] that Nelder-Mead optimizations with $f_{sr}$ as a cost function

typically converge to dynamic, though relatively slower gaits (on the order of 1 – 1.2 m/s). Optimizations with $f_v$ as a cost function converge to faster gaits (on the order of 1.6–2.6 m/s depending on leg stiffness and payload), though, these gaits tend to be more unstable to perturbations at higher speeds as one would expect. It should be noted that for the purposes of experimentation we assume that low $f_{sr}$ and $f_v$ values are the signature of a relatively stable gait. An unstable gait is energetically wasteful with high $f_{sr}$ and $f_v$ values. Visually this takes the form of excessive body pitching and rolling with considerable slipping. Figure 5.2 provides a sample output from the data collected during an optimization, which highlights the range of gait parameters tested during a single optimization. In the first two rows of this figure, we plot the specific resistance recorded for each of the six gait parameters. The plot offers a high level view of the range of gait parameters tested where each dot represents one trial. In particular, portions of the graph with a higher density of dots indicate the gait parameter values that yield low specific resistance values. In the bottom left graph, we plot specific resistance against forward velocity and find that this optimization routine using $f_v$ as a cost function converged to gait parameters with a forward speed of about 2.2 m/s. In the bottom middle graph, we find that the forward velocity increased with stride frequency up to 5.3 Hz at which point forward velocity quickly drops. This suggests the natural frequency of the mechanical system was too unstable at higher stride frequencies. One can also find in the bottom right graph that as the trial number increases the optimizer converges to gaits with a lower specific resistance.

### 5.1.1 Optimizing Leg Stiffness for Speed

Previous optimization studies on RHex primarily focused on boosting robot performance through gait parameter adjustment [71]. A constant stiffness C-leg was used, however, no other leg stiffnesses were explored. This begs the question "Would a softer or stiffer leg have allowed RHex to run even faster or more efficiently?" In

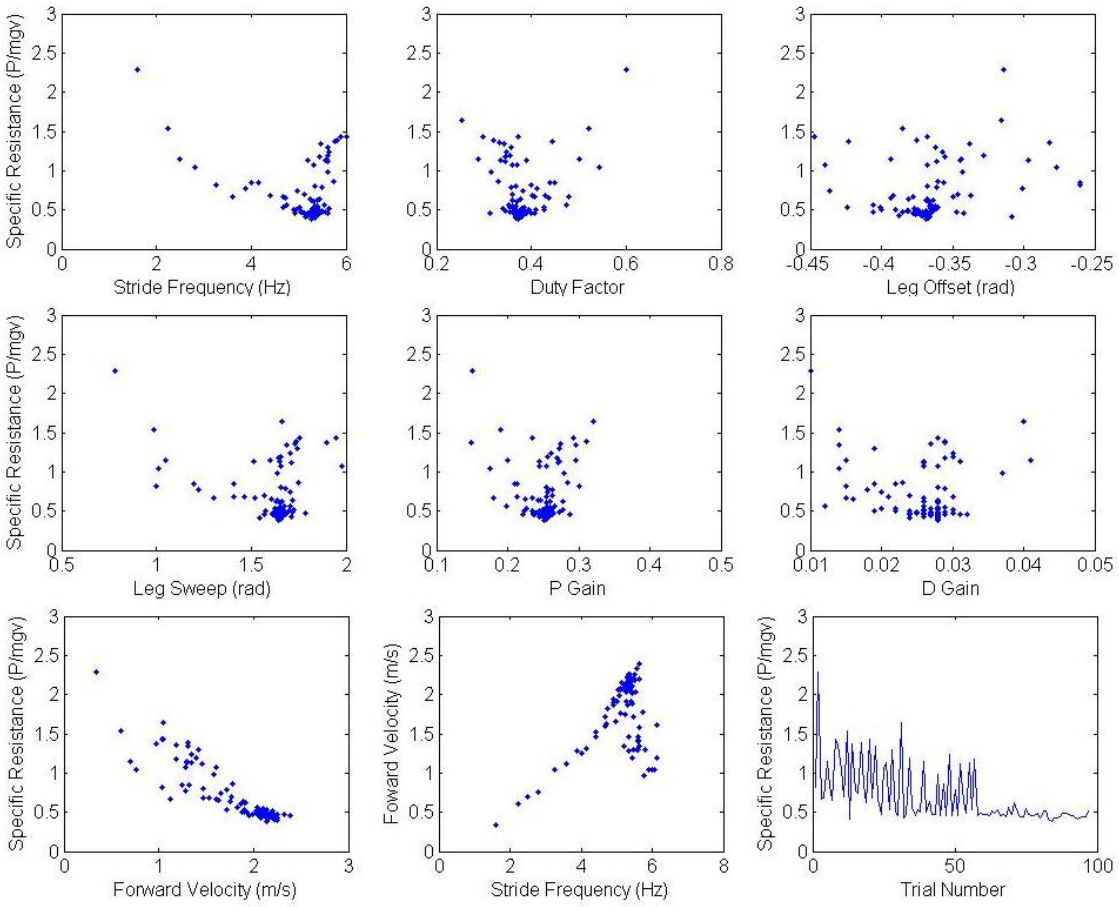


Figure 5.2: Data of gait parameters investigated during a Nelder-Mead optimization. The first two rows plot the six gait parameters against the resulting specific resistance. In the bottom left graph we plot specific resistance against forward speed. The bottom middle graph plots forward speed against stride frequency where optimal speed occurs at a drive frequency near 5.3 Hz. The bottom right graph plots the specific resistance value recorded for each trial. We find that the optimization routine eventually converges to gait parameters that yield efficient and fast locomotion.

Figure 2.7, we show that EduBot and RHex are geometrically similar, however, dynamically speaking, EduBot is faster and more efficient. Therefore we anticipate that experimental results with EduBot can be considered together with the RHex body of data.

In preliminary optimization experiments, we sought to understand the role of leg compliance in EduBot. This topic was explored using fixed stiffness C-legs to eliminate any effects a tunable leg might introduce. Five sets of C-legs were prepared with the stiffest leg being approximately 3.6x the stiffer than the most compliant leg. The legs were constructed from S2-6781 pre-preg fiberglass according to the manufacturing process detailed in Appendix A. The leg stiffness was set during manufacturing by either changing the number of layers of fiberglass or the leg width. The softest leg used 5 layers (5L) while the stiffest leg used 9 layers (9L). The leg labeled 6.5L is actually a 7 layer (7L) leg with a width that was reduced from 18 mm to 15 mm. This was done in order to quickly obtain a leg stiffness that fell in between a 6L and a 7L. To compare the stiffnesses of these legs, we use a scale called *relative leg stiffness* (RLS), where a 6L leg is used as a reference leg and has a RLS value of 1. The table in Table 5.1 specifies the conversion of RLS to a radial stiffness value. A Nelder-Mead descent was performed for each combination of leg stiffness and two different payloads: 0 kg and 0.91 kg. The payload was in the form of steel plates that were secured to the belly of the robot and positioned so as not to shift the robot's projected center of mass.

Running gaits were optimized using $f_v$ as the cost function within Nelder-Mead. The same initial simplex was used for each experiment. The robot typically converged to suitable gaits after 70+ trials. In most cases as the optimizer converged on suitable gaits minor adjustments were made to the gait parameters on successive runs. We therefore used these similar gaits to calculate the average and standard deviation of the measured specific resistance as well as the resulting forward speed. The reported $f_v$ values have been converted to standard specific resistance, $f_{sr}$, by

| Fixed Stiffness C-leg | | | | | |
|---|---|---|---|---|---|
| Layers of Fiberglass | 5L | 6L | 6.5L | 7L | 9L |
| Relative Leg Stiffness (RLS) | 0.85 | 1 | 1.3 | 1.6 | 3.1 |
| Radial Leg Stiffness (N/m) | 1090 | 1280 | 1660 | 2050 | 3970 |

Table 5.1: This table specifies the conversion from relative leg stiffness to radial leg stiffness for the variety of fixed stiffness C-legs.

multiplying the resulting $f_v$ by the average velocity squared ($v_{avg}^2$).

The results are reported in Figure 5.3 and 5.4. It can be observed that stiffer legs ran more efficiently with the payload, but what is most striking is that the increasing leg compliance improved speed and efficiency up to a point. Figure 5.4 shows that the no-load average forward speed for a 9L, 7L, 6.5L, 6L, 5L is approximately 0.85, 1.31, 1.5, 2.51, and 1.9 m/s respectively (though under the right conditions we were able to attain forward velocities of 2.7 m/s with the 6L leg). These results indicate that the value of tunable leg compliance likely exists near a RLS of 1 or lower where $f_{sr}$ is lowest and achievable speed is highest.

We also suspect that the softer legs (5L and 6L legs) enable better robot performance because they are more capable of maintaining robot stability especially in the face of an uneven tripod stance phase. For example, if a stiff leg touches down early (i.e. closer to the hip than to the toe) then the leg essentially behaves as a rigid element absorbing little energy. The leg falls behind the desired leg position dictated by the PD controller, and consequently the robot inserts considerable torque in a short time interval. This has the effect of inserting poorly timed energy into the system which creates pitching and rolling moments of the robot body that cause instability on the next tripod. Therefore, the stiffer legs appear to narrow the region of stable gaits. Compliant legs on the other hand are more capable of deflecting and absorbing energy even if the leg touches down early, which minimizes the severity

of ground reaction forces imparted to the body. We suspect that adding mass helps improve efficiency as it forces stiffer legs to act more compliant and likely offer better traction. One may also hypothesize that adding mass also closes the gap between the driving frequency of the motors and the natural frequency of the mechanical system.

While the softer legs (especially the 5L and 6L) were the top performers, there was an increased occurrence of leg failure as the payload increased (see the shaded region labeled *low safety factor* in Figure 5.3). This is one of the drawbacks of the dual nature of passive compliant legs (i.e. as a structural support appendage and a spring). In fact, 5L experiments were terminated after adding only 0.45 kg because too many legs broke. Over the course of a Nelder-Mead decent the legs are subjected to many unstable gaits that create very uneven leg loadings and place considerable stress on individual legs. These conditions are indicative of the scenarios the legs may experience while running on rough terrain. One could reason that if a set of legs can not survive an optimization for a given payload then the legs are likely unsuitable for "real world" conditions. We therefore begin to see the value of adding a mechanical stop to the design, which we introduced in section 4.1.

### 5.1.2 Variable Leg Stiffness with a Fixed Gait

In this set of tunable leg experiments, we were interested in exploring the effect of fixing the robot gait parameters and adjusting the leg stiffness for a set of payloads. We attempted to add payload and adjust leg stiffness in an intelligent manner such that an increase (or decrease) in leg stiffness had a matching increase (or decrease) in payload to maintain the natural frequency of the system. The fixed gait (w = 3 Hz, duty factor = 0.386, leg offset = -0.201 radians, stance sweep angle = 1.197 radians, kp = 0.233, kd = 0.032) was chosen by optimizing the robot as it carried a 0.91 kg payload and ran with a RLS = 1.29. These gait parameters produce a stable gait with a forward speed of approximately 1–1.2 m/s depending on the leg

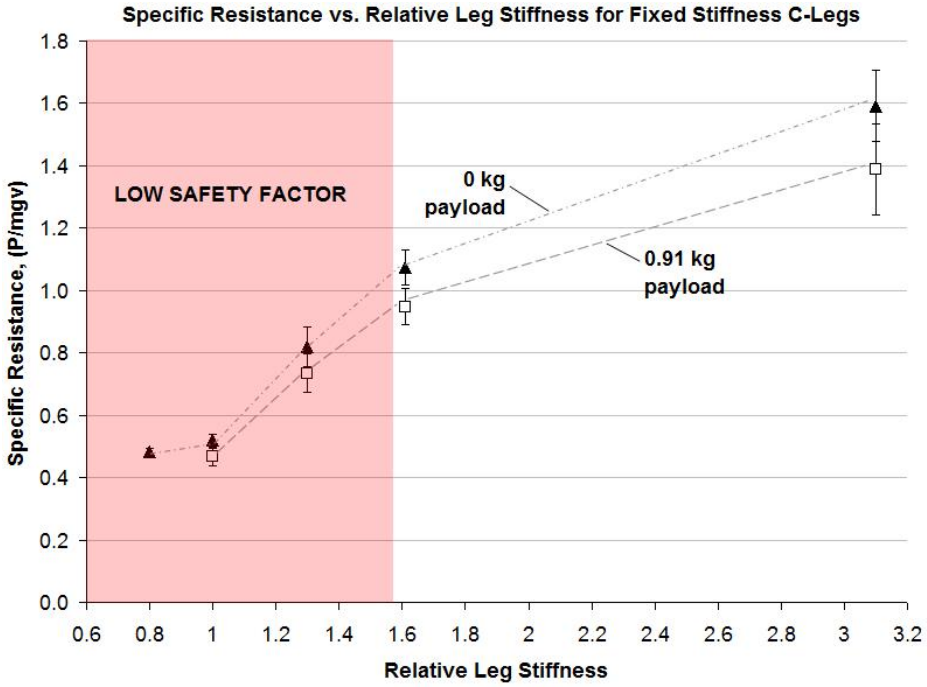


Figure 5.3: Data from fixed stiffness C-leg optimization experiments with specific resistance plotted against relative leg stiffness for two payload configurations. The 6L leg is the reference leg stiffness with a relative leg stiffness value of one.

stiffness. Two types of tunable legs were prepared to test a range of stiffness settings. One type had a relative leg stiffness range of 1 to 1.6 while the other had a range of 0.5 to 0.87 (see Table 5.2 for the conversion to radial stiffness). The payloads tested were 0 kg, 0.45 kg, 0.91 kg, and 1.365 kg. For each leg stiffness and payload combination the robot ran 20 trials with the fixed gait. The average $f_{sr}$ and forward speed as well as the standard deviation are presented in Figures 5.5 and 5.6. The results in Figure 5.5 reflect similar findings from the previous section in that softer legs tended to run faster and more efficiently than the stiffer legs. A relative leg stiffness of 1 or less in general produced more efficient gaits. The gaits were also considerably more stable in this stiffness regime evidence of which is given by the size of the standard deviation error bars. We also find more evidence that there may be a limit to the value of added compliance as the measured specific resistance either

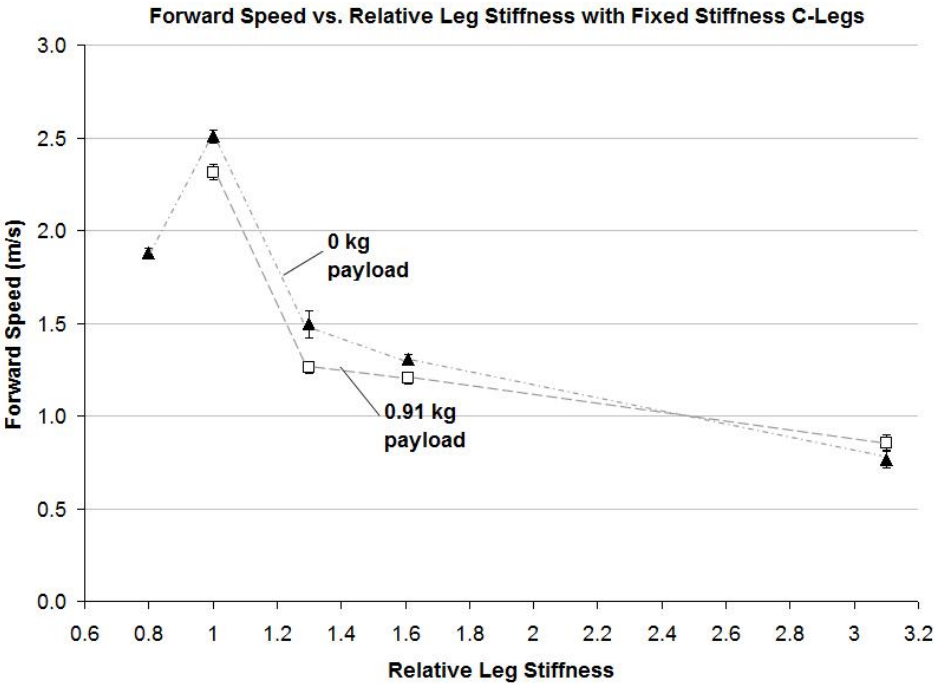


Figure 5.4: Data from fixed stiffness C-leg optimization experiments with the resulting forward speed plotted against relative leg stiffness.

plateaued or marginally worsened at the softest setting. There is also a noticeable trend for more efficient locomotion at higher payloads, suggesting that there is a better return for power input into the system when the robot carries larger loads. Figure 5.6 shows that the resulting forward speed with the fixed gait peaks with a RLS = 0.75. What is interesting is that the top speed was reached at the same leg stiffness for all payloads.

We should note that while the goal was to fix the gait parameters for a range of leg stiffnesses, the resulting gait turned out to be very different for many of the leg stiffnesses. For example, high payloads produced short or non-existent aerial phases and earlier leg touchdown events at softer settings compared to stiffer ones. Therefore, while the gait parameters may be fixed in the controlled the physical interaction of the legs with the ground is very different for each leg stiffness setting

| Tunable C-Leg | | | | | | | | | |
|---|---|---|---|---|---|---|---|---|---|
| Relative Leg Stiffness (RLS) | 0.5 | 0.63 | 0.75 | 0.87 | 1 | 1.13 | 1.26 | 1.4 | 1.6 |
| Radial Leg Stiffness (N/m) | 640 | 800 | 960 | 1110 | 1280 | 1450 | 1610 | 1790 | 2050 |

Table 5.2: This table specifies the conversion from relative leg stiffness to radial leg stiffness for the two tunable legs.

and payload. This may explain why we were unable to observe multiple peaks in efficiency and speed at the tested combinations of leg stiffness and payloads. An optimization for each payload and leg stiffness may have produced better efficiency results than those presented.

Overall the tunable leg design itself performed well. During the course of these experiments the legs were subjected to roughly 20 thousand leg compressions, ran a distance over 7k (4.3 miles), and were still capable of running more. It was clear that some legs experienced stiffness softening more than others. Consequently, the compliant slider was adjusted to slightly different positions to maintain uniform leg stiffness among all the legs.

### 5.1.3 Optimizing Tunable Leg for Speed on Carpet

For the next set of experiments Nelder-Mead optimizations were run with a tunable leg that offered a RLS range of 0.5 to 0.87. The cost function, $f_v$, was used to identify fast gaits. Experiments were run at the two relative leg stiffness extremes, 0.5 and 0.87, with a 0.91 kg payload and without a payload. Additional data were collected for RLS = 0.62 and 0.75, with a 0.91 kg payload and for RLS = 0.75 without a payload. Figure 5.7 is a plot of the top ten results from each optimization with specific resistance on the y-axis and forward speed on the x-axis. Here we assume good gaits occupy the bottom right hand corner of the graph where speed and efficiency are rewarded.

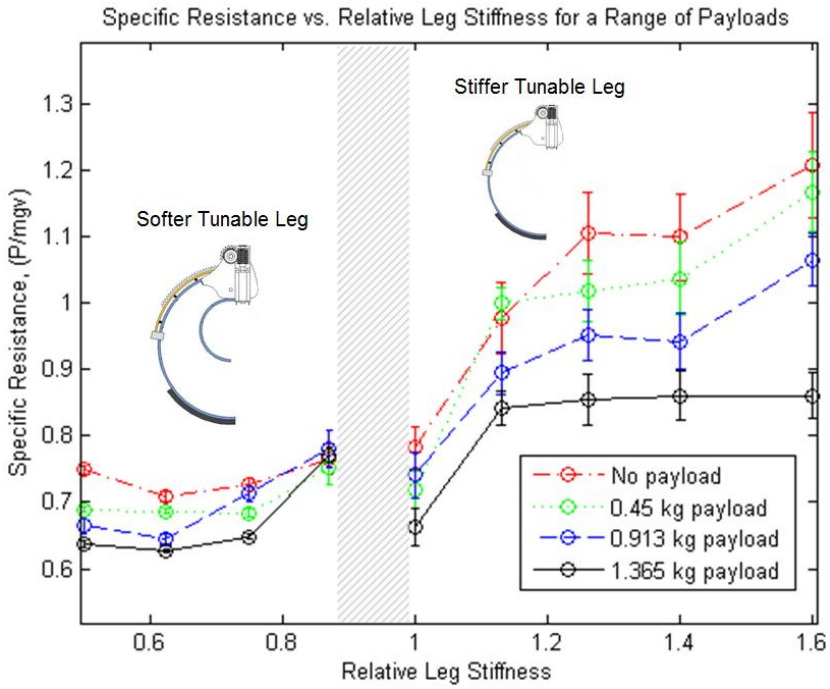


Figure 5.5: Data from fixed gait experiments shows the average specific resistance for various leg stiffnesses and payloads.

For the no payload configuration, the softest leg setting (RLS = 0.5) converged to gait with an average specific resistance of 0.56 +/- 0.03 (SD) and an average speed of 1.91 +/- 0.05 m/s. We find that if leg stiffness is increased, the robot converges to faster gaits. For a RLS = 0.75 the specific resistance was 0.51 +/- 0.02 and the average speed was 2.23 +/- 0.05 m/s. Increasing the leg stiffness by 50% allowed the robot to run about 10% more efficiently and with 16% increase in average speed. We found though, at the highest stiffness setting (RLS = 0.87) that there was a slight drop in efficiency and speed compared to RLS = 0.75 (see Figures 5.8 and 5.9). We suspect that this is due to a mechanical design oversight. The guide, which holds the compliant slider against the C-leg, protrudes about 2 mm past the thickness of the tread and is likely interfering during touch down. We would expect the speed and efficiency to be equal to or better than the results collected for RLS = 0.75.

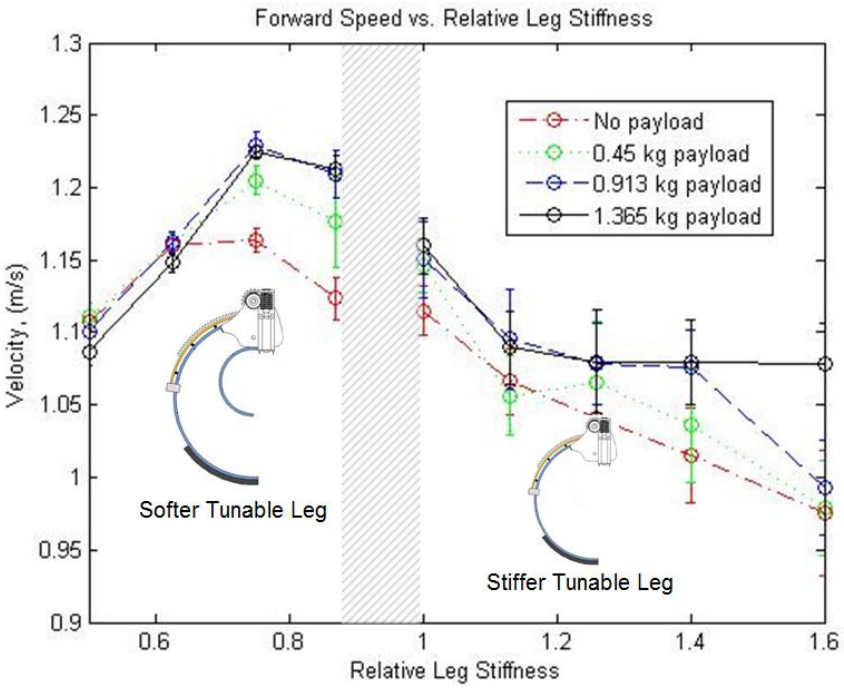


Figure 5.6: Data from fixed gait experiments shows the resulting forward velocity for various leg stiffnesses and payloads.

For experiments carrying a 0.91 kg payload, we observed a similar trend in that the robot was capable of running faster and more efficiently at the higher leg stiffness settings. A RLS = 0.87, allowed the robot to run at speeds up to 2.3 m/s with an average speed of 2.2 +/- 0.04 m/s and a specific resistance of 0.43 +/- 0.02. The results at the intermediate stiffness settings provide additional insights into the leg's capabilities. At a RLS = 0.75, EduBot ran on average faster (2.28 +/- 0.04 m/s), but less efficiently (0.46 +/- 0.02) than RLS = 0.87 (see Figure 5.8). At a RLS = 0.62, EduBot performed as one would predict; better than a RLS = 0.5, but not as well as a RLS = 0.75 or 0.87 in terms of both speed and efficiency. The leg at the softest setting with a payload posted an average speed of 1.84 +/- 0.06 m/s with a specific resistance of 0.56 +/- .05. The results suggest that the soft legs are speed limited especially when a payload is added. This result may be in part due to this

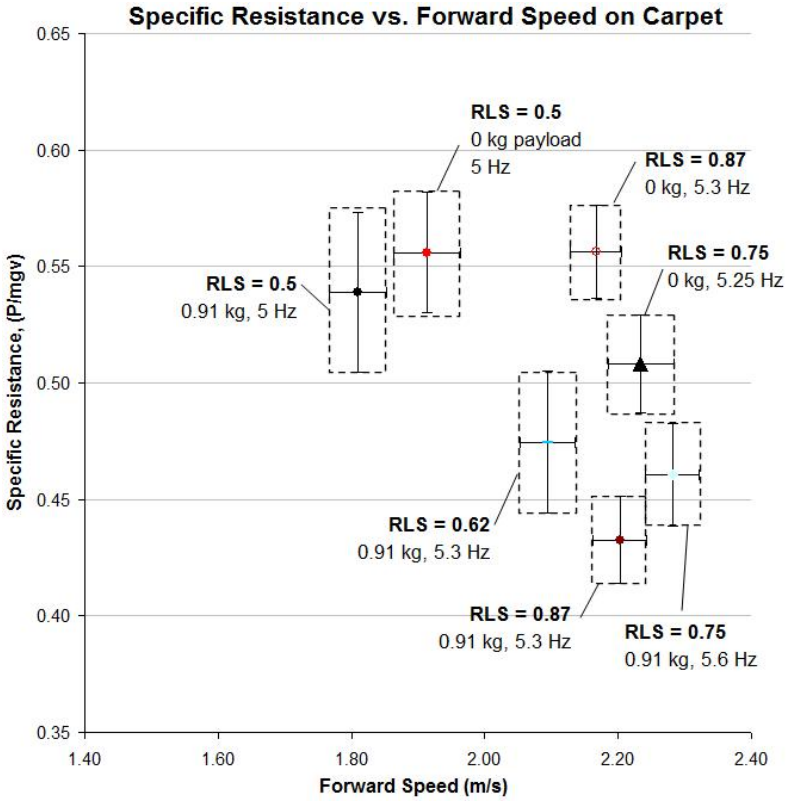


Figure 5.7: Specific resistance vs. forward speed results for EduBot running on carpet.

particular leg design. The configuration with a soft leg setting and a payload caused the C-leg to deflect into the mechanical stop. This most certainly prevented leg failure; however, the leg's collision with the mechanical stop imparts poorly timed impulse forces to the body which contribute to unstable gaits at high speeds. In spite of this we find evidence that this particular leg design enables the robot to adjust its leg stiffness to run efficiently for a range of speeds and payloads as depicted in Figure 5.7.

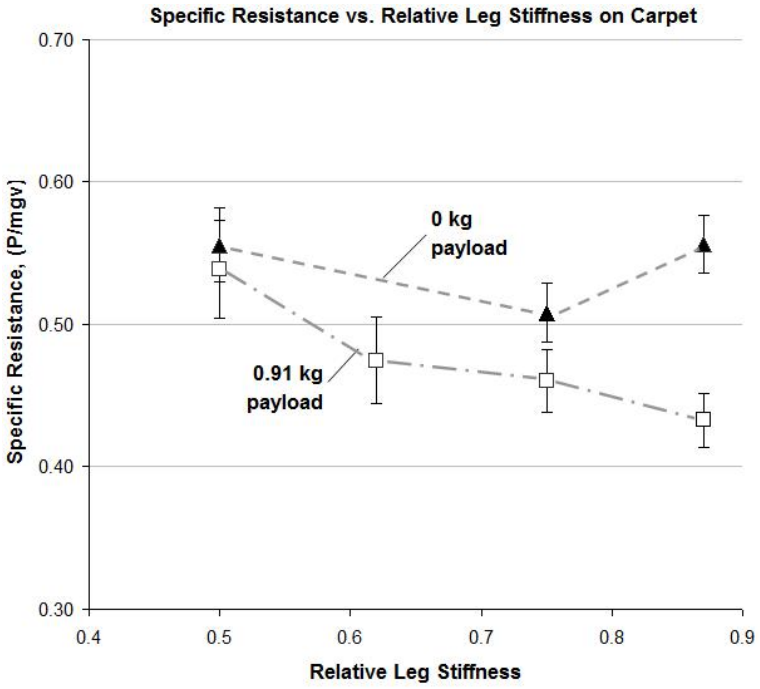


Figure 5.8: Specific resistance vs. relative leg stiffness results for EduBot running on carpet.

### 5.1.4 Optimizing Tunable Leg for Speed on Carpet Padding

In discussions with people who have worked with RHex, it was noted that the hexapod in general ran better on grass than on pavement. To evaluated the influence of surface compliance on RHex-like locomotors with tunable legs, the optimization experiments were repeated on 12.7 mm (1/2") thick carpet padding (see Figure 5.10 for a picture of the arena). A sample of the carpet and carpet padding where compressed in an Instron machine and the force-deflection data revealed that the stiffness of the carpet was on the order of 20 kN/m while the stiffness of the carpet padding was approximately 5 kN/m. This represents about a 4x change in surface stiffness. The experimental data in Figures 5.11 - 5.13 suggest a more compliant surface enables the robot to run faster and more efficiently for a range of leg stiffnesses and payloads. Again, we find that the stiffer leg settings enable EduBot to run faster

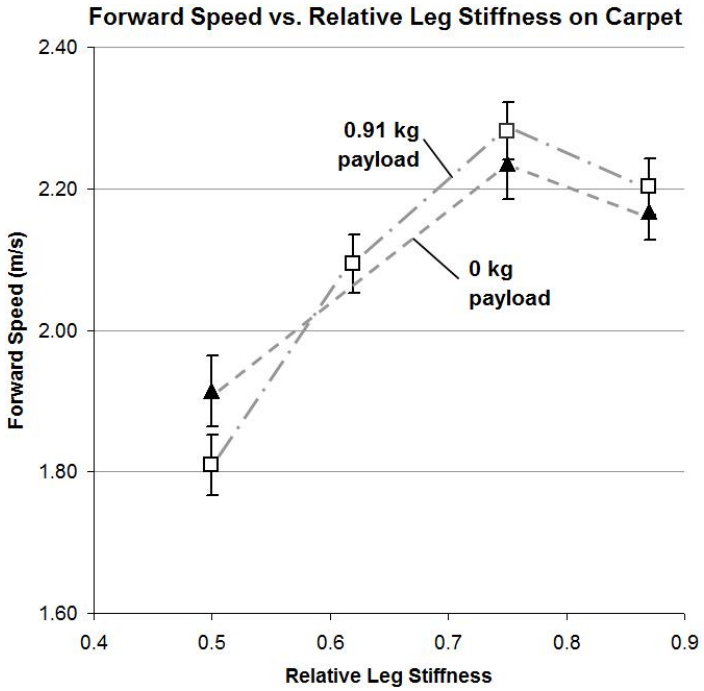


Figure 5.9: Forward speed vs. relative leg stiffness results for EduBot running on carpet.

and more efficiently for both payload configurations over the softer leg settings.

Running on carpet padding as opposed to carpet with a RLS = 0.87 with no payload, enabled EduBot to run 30% more efficiently (0.44 +/- 0.01) and approximately 13% faster ( 2.46 +/- 0.06 m/s). A RLS = 0.87 with a payload, allowed EduBot to run approximately 17% faster and 16% more efficiently (2.58 +/- 0.06 m/s, 0.37 +/- 0.02). The soft leg setting (RLS = 0.5) also demonstrated an increase in speed (20% increase without a payload, 25% increase with a payload) and about a 15% improvement in energetic efficiency. What is interesting though is that even though the soft leg setting converged to different gait parameters the resulting average forward speed on the carpet padding was about same at 2.3 m/s with and without a payload.

While the carpet padding increased the surface compliance there are other inherent physical properties that can not be decoupled. For example, the material does add more damping which may smooth out otherwise unstable gaits. Additionally, the padding allows the leg to sink in more than carpet which we suspect allows more contact area and better traction. There is some evidence that the improved traction allowed the robot to run faster. A relatively fast gait that was stable on carpet (RLS = 0.87, 4.79 Hz, duty factor = 0.397, leg offset angle = -0.330 rad, sweep angle = 1.473 rad, kp = 0.239, kd = 0.024) had a average forward speed of 1.75 m/s where as the same gait on carpet padding achieved an average speed of 1.92 m/s. We speculate that since this gait was stable on carpet, the damping effects of the padding had a small contribution to the observed speed increase. The improved traction may explain why the robot ran faster even at the softest leg stiffness setting. The added compliance of the carpet padding also has an impact on the robot's aerial phase. Preliminary data collected from high speed video suggests that the percent of time spent in the air during a leg rotation decreased from approximately 35% to 25% or lower for RLS = 1. For a soft leg setting (RLS = 0.5) it was difficult to observe any aerial phase. In summary, even though we may not fully understand the impact carpet padding has on the dynamics of EduBot, we do see that this particular leg design allows the robot to span a range of speeds and efficiencies for different payloads and terrains.

### 5.1.5 Optimizing Tunable Leg for Speed on Grass

In addition to running on man made surfaces, we also performed optimizations on a real world surface, namely grass. To maintain consistency in our optimization methods, a sod track measuring 6' x 25', was assembled in our motion capture arena (see Figure 5.14). The grass had an approximate blade length of 3 inches with about 3/4" of root and soil support. As in the previous tunable leg optimizations, the softest and stiffest leg settings with and without a payload (0.91 kg) were tested. The results from these experiments are plotted in Figures 5.15 - 5.16. These results

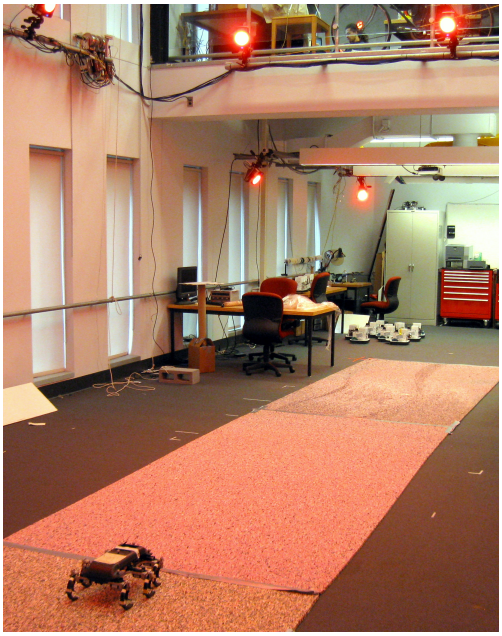

Figure 5.10: Image of the motion capture arena with carpet padding as the terrain.

show a resemblance to the results obtained from optimizing on carpet padding. We find from both figures that EduBot runs faster and more efficiently with and without a payload when the tunable legs are at their highest stiffness setting (RLS = 0.87). Two optimization experiments were also run with a 7L leg (RLS = 1.6) with and without a payload. The results support earlier evidence that these legs are simply too stiff and yield slower, less efficient gaits.

It is important to consider real world surfaces as there are generally interactions and behaviors that can not be produced in the lab with man made surfaces. In these particular experiments, we observed that some gaits performed poorly for the fact that the worm gear mechanism became tangled in the matrix of dead grass near the soil surface. Clearly a cover must be added for design, but this in an interaction that would otherwise have been difficult to observe on carpet.

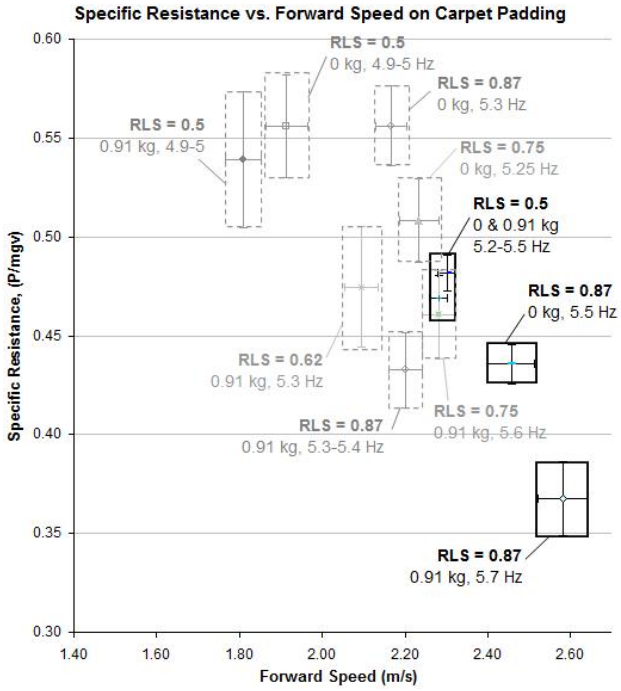


Figure 5.11: Specific resistance vs. forward speed results for EduBot running on carpet padding. The grayed portions of the graph offer a comparison of the results from running on carpet found in Figure 5.7. The data suggests that soft legs (RLS = 0.5) allow faster and more efficient locomotion on carpet without a payload; however, when a payload is added and/or the surface compliance increases stiffer legs offer better locomotion performance in both speed and efficiency.

### 5.1.6 Tunable Leg Optimization Discussion

We have shown that varying leg stiffness for a given payload and terrain can lead to a range of speeds and efficiencies. For the last part of this analysis we draw additional insights into the role of leg compliance by stitching together tunable leg and fixed stiffness leg experimental results. In Figures 5.19 – 5.21, the tunable leg results are plotted to the left of the gray divider and the fixed leg stiffness results are on the right. In Figures 5.19 and 5.21, one can see that the stiffness range of the tunable leg offers efficient locomotion for a range of fast speeds on carpet; however, there are two discrepancies between the results for the tunable leg RLS = 0.87, and the

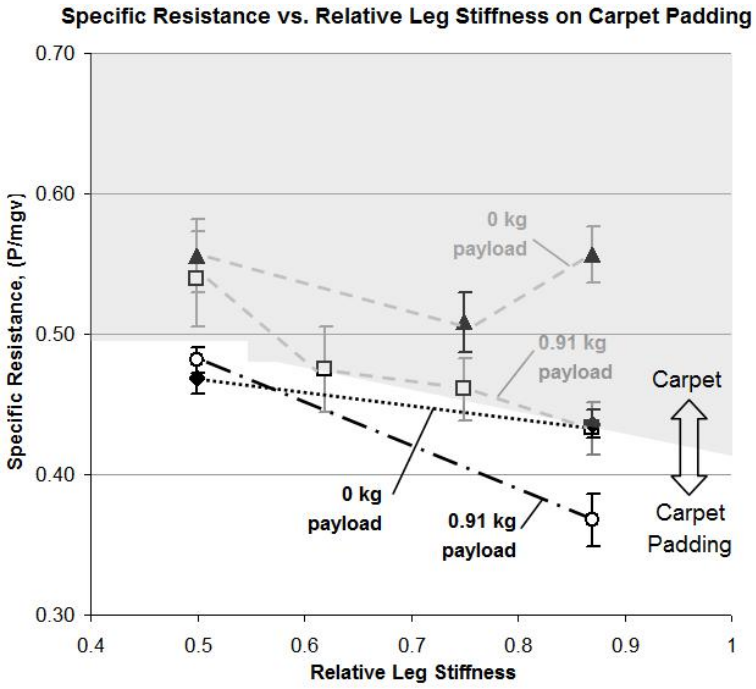


Figure 5.12: Data of specific resistance plotted against relative leg stiffness for EduBot running on carpet padding.

fixed stiffness 6L leg (RLS = 1). First, for the no payload configuration, the tunable performs noticeably worse in both speed and efficiency compared to the 6L leg. Second, when the payload is added we see that the tunable leg achieves a forward speed near that of the 6L leg with comparable efficiency; however, this does not occur at the highest leg stiffness setting, but rather at a RLS = 0.75 instead. There are several plausible reasons why the robot with a RLS = 0.87 failed to approach the speed of a 6L layer leg. In section 5.1.3, we speculated that the reduced speed was due to a mechanical design oversight in which the compliant slider guide extends about 2 mm past the tread thickness. This may narrow the region of acceptable touch down angles. It is also possible that the optimization failed to converge on an optimally fast gait, especially for the no payload scenario. These results also suggest that EduBot's leg stiffness tuning range should be increased to include at least the

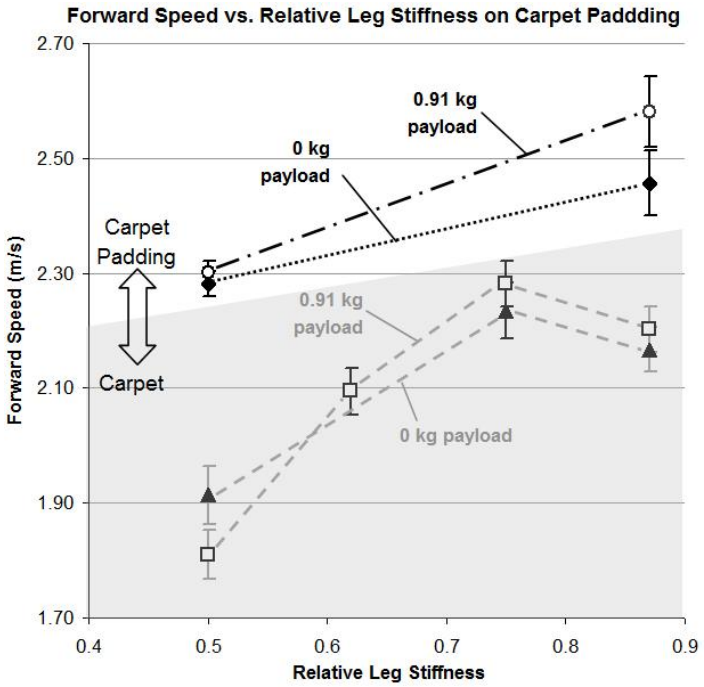


Figure 5.13: Data of forward speed plotted against relative leg stiffness for EduBot running on carpet padding.

stiffness of a 6L leg. However, their is strong evidence that extending the leg stiffness much beyond a 6L leg will result in slower and less efficient gaits.

For the carpet padding experiments the tunable leg performs as one would expect. EduBot is capable of running faster at the stiffer leg setting and the difference in forward speed with the 6L leg is minor. We suspect that the added surface compliance is more accommodating to the compliant slider fitting than the carpet. What is interesting though is that the stiffest tunable leg setting enables a lower cost of transport than the 6L leg.

For slow to intermediate speeds (1.2 – 1.8 m/s) we observed that softer legs enable very stable and efficient locomotion. In contrast to stiffer legs (such as the 6L leg) the aerial phase of the softer legs is very short or non-existent if the robot is carrying a payload. Unfortunately, we did not collect center of mass motion data

Figure 5.14: Picture of grass terrain

during our experiments and therefore can not provide a side-by-side comparison for the range of leg stiffnesses tested. Though, based on our observations it appears that soft legs reinforce stability as it severely limits body pitch and roll from one tripod touchdown to the next. As mentioned earlier, softer legs appear to accommodate the PD controller better than stiffer legs. If a softer leg touches down early, the reaction forces imparted to the body are smaller and occur over a long time period, which gives the controller more time to respond.

A topic that requires further investigation is the role of leg compliance for EduBot's slow to intermediate speeds (1.2 – 1.8 m/s). In our experiments, we optimized for speed and this generally resulted in gaits with forward speeds of 1.8 – 2.6 m/s. From these experiments we found that softer legs would not allow the robot to run as fast as stiffer legs, however their specific resistance values weren't significantly different even though they were running slower. To characterize this we look at another measure of efficiency which is joules per meter. To convert specific resistance to joules per meter one must multiply the specific resistance value by the robot mass and

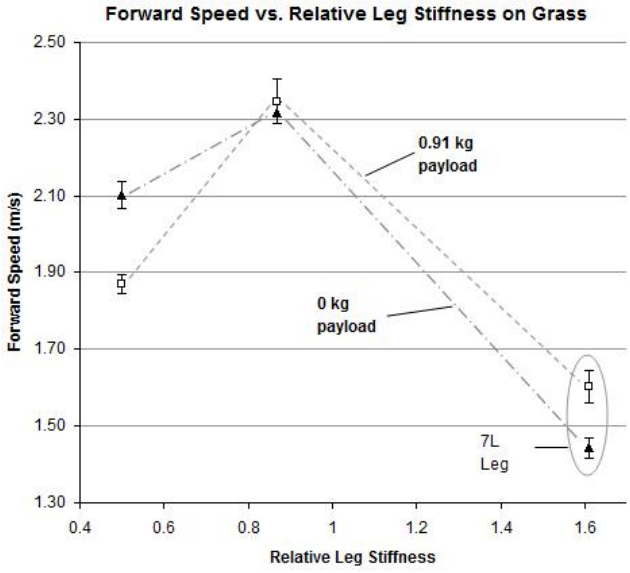


Figure 5.15: Data from the optimization experiments showing that the stiffest tunable leg setting (RLS = 0.87) ran the fastest. A constant stiffness 7 layer fiberglass C-leg (RLS = 1.61) was also optimized on the robot and shows that there is a limit to the value of increasing leg stiffness.

gravity. Therefore, joules per meter is the average power divided by the average velocity

$$\frac{Joules}{meter} = \frac{P_{avg}}{v_{avg}} \tag{5.3}$$

In more familiar terms, joules per meter can be thought of as the inverse of miles per gallon or gallons per mile. The advantage of thinking in terms of joules per meter is it actually places units on the cost of transport. Specific resistance is a dimensionless value that normalizes for weight, which in the majority of our experimental results, the robot appears to run more efficiently with a payload. When these results are converted to joules per meter we typically find that robot is consuming more joules per meter with a payload than without. When the experimental results for the tunable stiffness leg and the fixed stiffness legs are plotted as joules per meter against

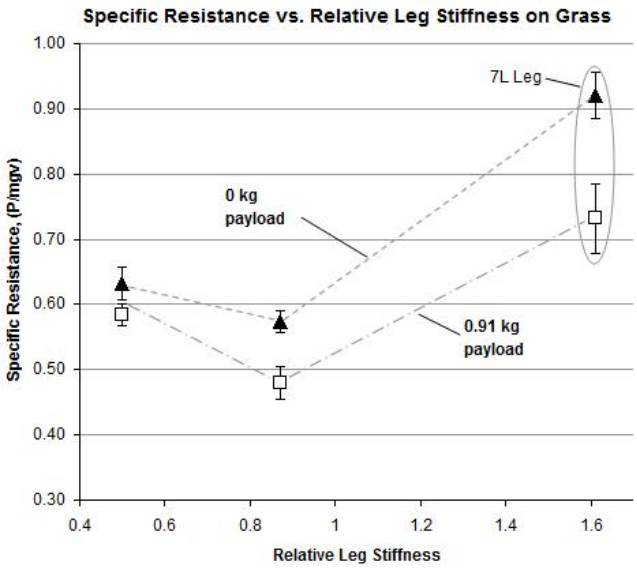


Figure 5.16: Data from the optimization experiments showing that the stiffest tunable leg setting (RLS = 0.87) on average ran most efficiently. The results also indicate that increasing leg stiffness much beyond RLS = 0.87, will lead to inefficient locomotion.

speed we find that the tunable stiffness leg and the fixed stiffness 6L leg (RLS = 1) consumed less than 19 J/m for a range of speeds (see small grayed box in Figure 5.18). The striped box highlights the range of intermediate speeds of interest. In this box, stiff legs (RLS = 1.3 and 1.6) are noticeably inefficient. Since we did not optimize the robot to run at these intermediate speeds, we can only plot results which were collected during the optimization experiments. More specifically, these results are the gaits that were tested during an optimization and are sorted in ascending order by specific resistance to yield the most efficient gait we can quickly obtain in this intermediate speed range. Therefore the results for RLS = 1 and RLS = 0.5 at the intermediate speeds in Figure 5.18 are preliminary results at best. However, they suggest that increasing leg compliance at the intermediate speeds will enable the robot to consume fewer joules per meter. Intuitively this makes sense as one would expect a lower leg stiffness to be better suited at lower driving frequencies.

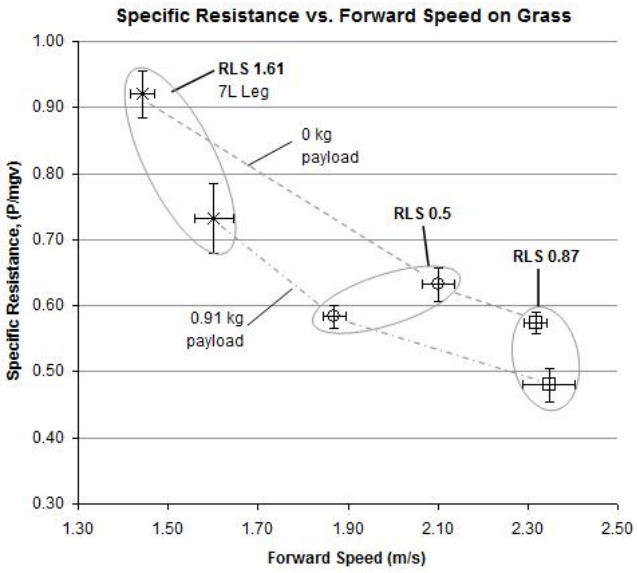


Figure 5.17: Data from the optimization experiments showing that the stiffest tunable leg setting (RLS = 0.87) on average ran most efficiently and fastest. The results also indicate that for this terrain increasing leg stiffness much above or below RLS = 0.87, will lead to inefficient and lower top speed.

At the moment we can only speculate, but there may be an added value to tunable legs at these intermediate speeds.

An additional observation that emerges from all of these experiments is a need for further refinement of the controller. The current open-loop PD controller achieves the very simple task of maintaining leg position and velocity by increasing or decreasing motor torque output during stance and aerial phases. The system relies on the natural frequency of the passive compliant legs to work in unison with the driving frequency of the motors to move the robot forward. At slow and intermediate speeds this method of control in general enables stable, efficient, and safe locomotion. At higher speeds, we have found this control scheme leads to gaits that can be rather unstable. There is a lot of kinetic energy in the high speed gaits and the slight disturbance or irregular leg touch down can send the robot into an irrecoverable tail spin where legs spin, the body pitches and rolls, but little forward motion is

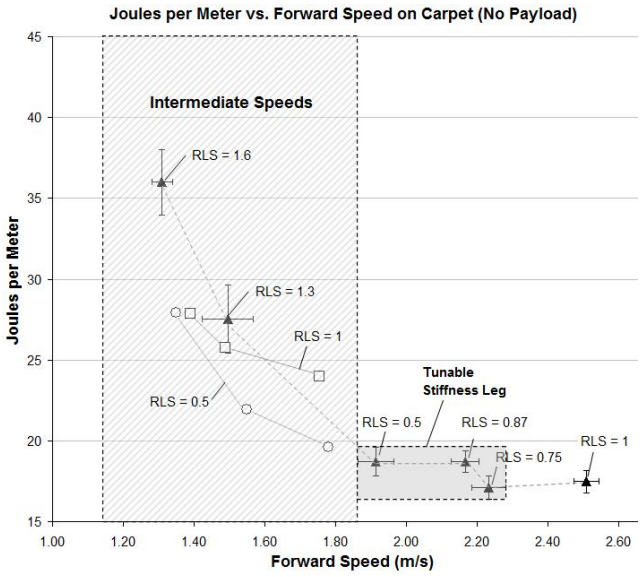


Figure 5.18: Data from the optimization experiments of tunable stiffness leg and fixed stiffness legs on carpet with no payload. Results are plotted as joules per meter against forward speed. Preliminary results suggest that a lower stiffness leg setting (RLS = 0.5) will allow the robot to run more efficiently for intermediate speeds than a stiffer leg (RLS = 1).

generated. What is needed is a method for dynamic stability control or the equivalent of a traction control system found in the car industry. Enabling the robot to measure the stability of its own gait, and to anticipate necessary gait adaptations would significantly increase its performance in the field.

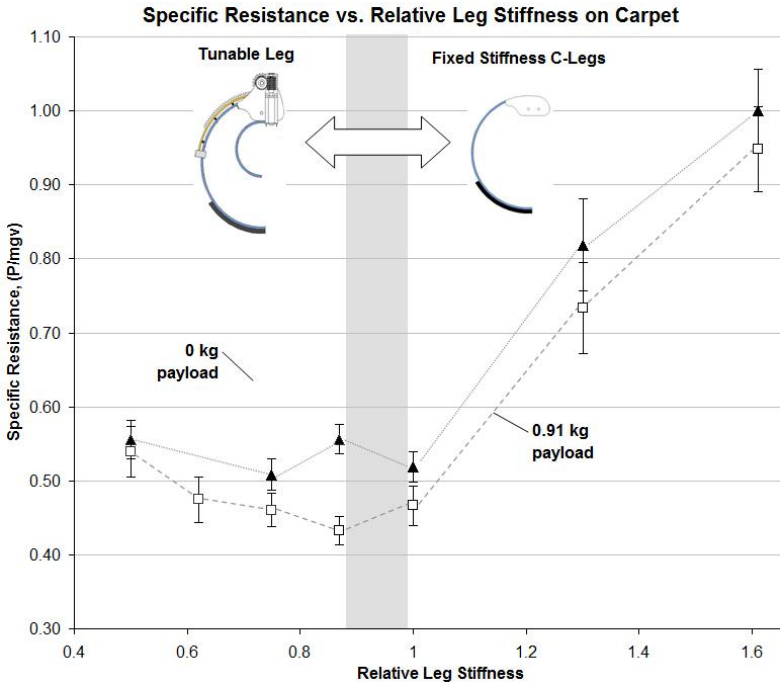


Figure 5.19: Data from the optimization experiments showing specific resistance results from tunable leg and fixed stiffness leg optimizations on carpet.

### 5.1.7 Tunable Stiffness Legs and Turning Agility

The present tunable leg design also offers a minor improvement in turning performance. Several turning experiments were performed with a 1.1 m/s jogging gait. As depicted in Figure 5.22, EduBot was commanded to run straight for four seconds, which was enough time to reach a steady state gait, and then commanded to make a sharp turn for 3 seconds. The sharpness of a turn is measured on a scale from -1 (left) to 1 (right). In these particular experiments the turn value was set to 0.7. It should be noted that we are not explicitly stating the sharpness of the turning angle, but rather are comparing the response of the robot to a given turn command for two different leg stiffnesses. The xy-position of the robot was recorded with a Vicon motion capture system. To characterize the turning agility, the resulting turning radius was measured by fitting a circle to the data by minimizing the sum of squared

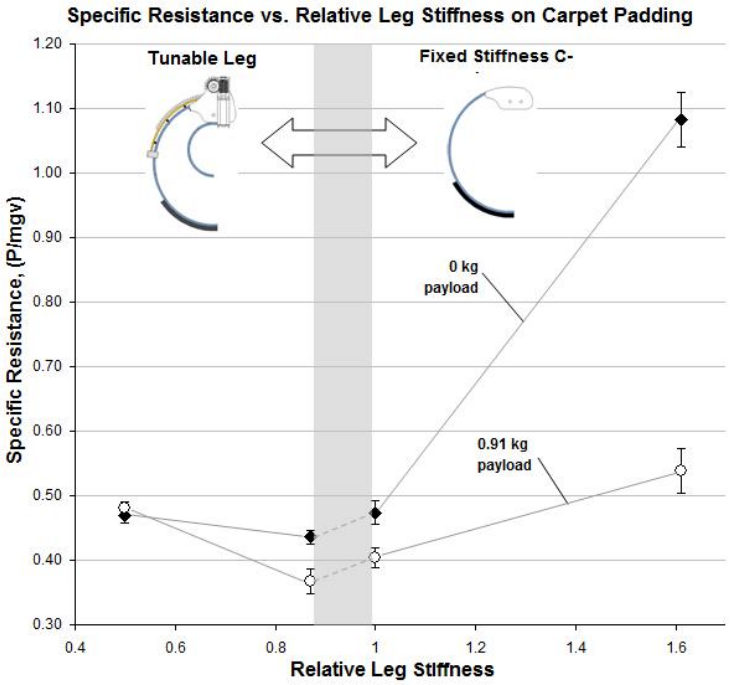


Figure 5.20: Data from the optimization experiments showing specific resistance results from tunable leg and fixed stiffness leg optimizations on carpet padding.

radial deviations. The robot carried a 1.365 kg payload and 10 runs were executed at a RLS = 0.5 and RLS = 0.87. As shown in Figure 5.23, the stiffest leg setting offered the best turning agility with an average turning radius of 4.12 +/- 0.24 meters. The turning radius for the softest leg setting was marginally larger at 4.88 +/- 0.28 meters. These results are not unexpected if we assume that turning performance is related to lateral leg stiffness. In the present design the lateral leg stiffness increases by 18% from the softest setting to the stiffest. In this particular experiment we see an 18% improvement between the two leg stiffness extremes. One draw back of the design is that the compliant slider contributes very little to the lateral stiffness as it is not rigidly anchored to the hip. This is one mechanical feature that could be improved in future designs.

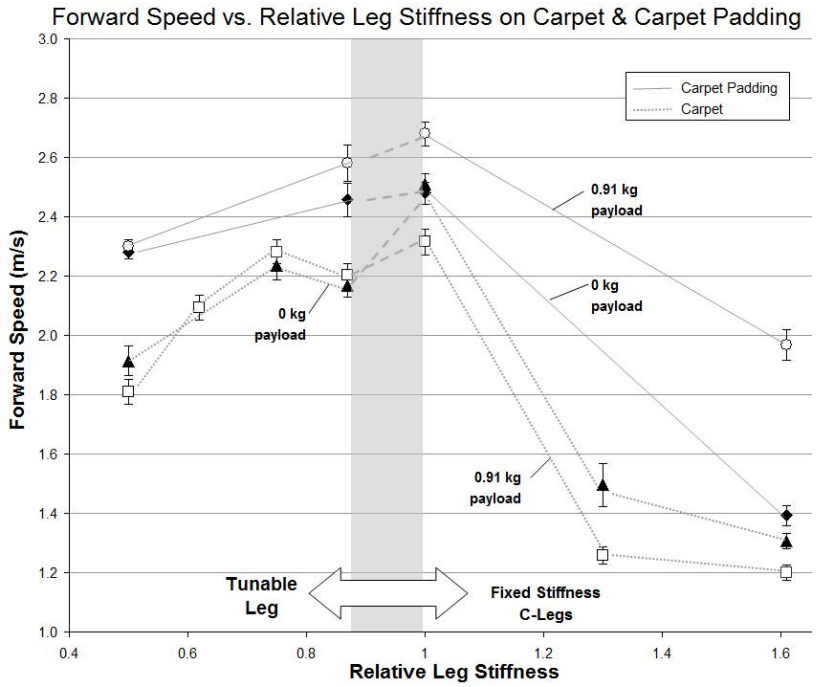


Figure 5.21: Data from the optimization experiments showing forward speed results from tunable leg and fixed stiffness leg optimizations on carpet and carpet padding.

### 5.1.8 Legs vs. Wheels

It is obvious that the value of a legged system emerges when the task at hand involves negotiating non-planar terrains and various surface conditions (i.e. gravel, sand, grass, pavement and so forth). These are conditions in which legged systems thrive and wheels struggle. However, in the following experiment we set aside these performance metrics, and asked the question, how do our compliant C-legs compare to wheels on flat terrain. For this experiment, six wheels (7 cm radius) were laser cut from 1/4" thick ABS (see Figure 5.24). Small teeth line the perimeter of each wheel to give the robot traction on the industrial grade carpet in our test arena. The Buehler Clock was adjusted (duty factor = 50%, stance phase = Pi rad) so that the wheels rotated at a constant rate. Ten results including specific resistance and forward speed where collected at the following rotation frequencies: 3 Hz, 4 Hz, 5

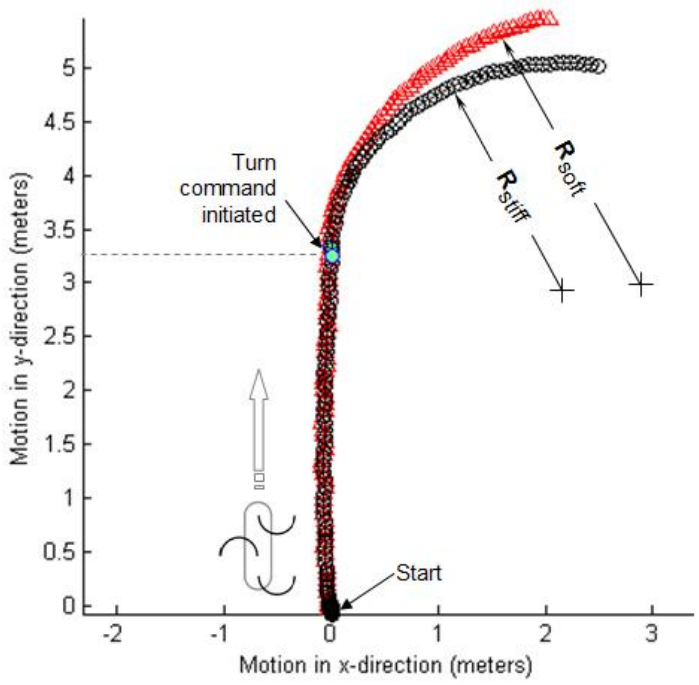


Figure 5.22: Shows the xy-position of the EduBot during turning experiments at a soft and stiff leg setting.

Hz, and 6 Hz.

Figure 5.25 shows that as speed increases specific resistance drops for wheeled and legged platforms. The top curve plots results collected from EduBot running at three different leg rotation frequencies. The bottom curve plots the results of the wheeled version of EduBot. Here we find that the leg results parallel the wheeled results; however, wheels are clearly more efficient on flat terrain.

### 5.1.9 Tunable Stiffness Legs and Obstacle Traversal

In another experiment, we explored the role of tunable legs in climbing over obstacles. In this particular experiment, two inch thick sheets of rigid foam home insulation were cut to 16 inch depths. This depth was chosen because it is 2 inches longer than the robot's body length and would force the entire robot to climb up before stepping

| Relative Leg Stiffness | Avg. Turning Radius (m) | Std. Dev. (m) | Lateral Leg Stiffness (N/m) |
|---|---|---|---|
| 0.5 ($R_{soft}$) | 4.88 | 0.28 | 463 |
| 0.87 ($R_{stiff}$) | 4.12 | 0.24 | 392 |

Figure 5.23: Specific resistance results when robot was run with a fixed gait for various leg stiffnesses and payloads.

down. In previous experiments we found that it was too easy for the robot to step over obstacles that were not deep enough. Two obstacles placed 10 feet apart on center with 10 feet of travel leading up to the first obstacle and 10 feet of travel following the last obstacle. The obstacle heights tested were 2 and 4 inches. Twenty trials were run at the softest and stiffest leg settings with the same fixed gait used earlier (w = 3 Hz, duty factor = 0.386, leg offset = -0.201 radians, stance sweep angle = 1.197 radians, kp = 0.233, kd = 0.032). The robot had no knowledge of the obstacles and therefore used the same gait for running and climbing. The results are shown in Figure 5.26 where for comparison purposes the results with no obstacle are also included. It should be noted that for the 4 inch obstacle results were only collected for the stiffest leg setting.

As one would expect we find that EduBot expends more energy to climb over the obstacles, which is given by the increase in specific resistance. The averages of the results don't suggest a significant difference in performance between the two leg stiffness settings climbing over the 2 inch obstacle. Though, if we assume the size of the error bars are an indication of stability, then the softer leg stiffness setting offered a quicker return to a stable gait following an encounter with an obstacle. The same experiments with the two obstacle heights were also conducted with wheels. At the two inch obstacle height (5.1 cm), the 7 cm radius wheels completed the course with an average specific resistance of 0.65 and a speed of 1.13 m/s. The results are

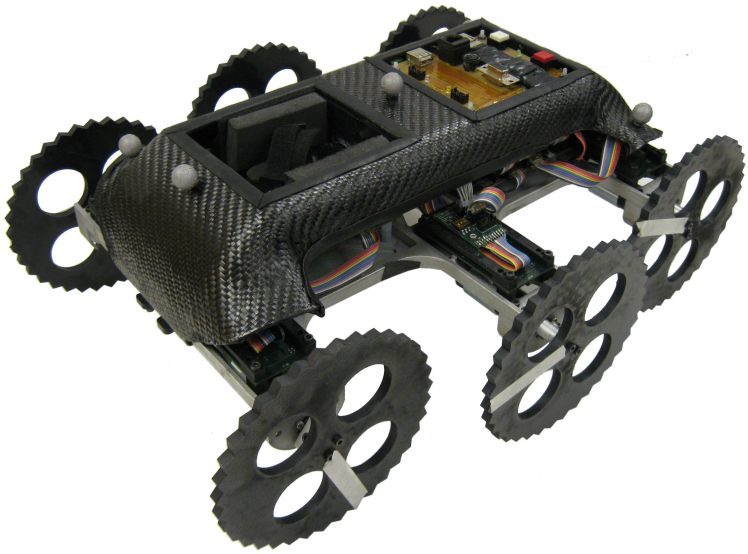

Figure 5.24: Picture of EduBot with 7 cm radius laser cut from 1/4" thick ABS.

worse compared to the same gait with no obstacle (see 3 Hz gait posted in Figure 5.25); however, they are better than the leg results. On the other hand, for the four inch obstacle, EduBot was unable to complete the course. The wheels demanded too much torque from the motors that the robot simply did not have enough battery power to climb over the obstacle. This highlights one of the advantages of legged locomotion on uneven terrain. A legged machine is more capable of climbing over obstacles because they can climb with a smaller moment arm. Wheeled platforms have a fixed radius that requires considerably more power from the robot to overcome tall obstacles.

### 5.1.10 Additional Tunable Leg Benefits

In this final section, we want to highlight some additional benefits of tunable legs aside from influencing speed and efficiency.

**Calibration**

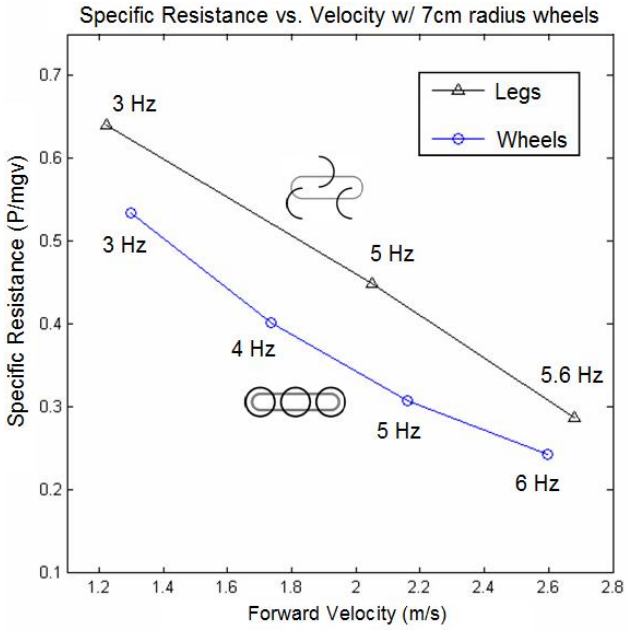


Figure 5.25: Comparison of specific resistance and forward velocity results for a legged and wheeled EduBot.

The ability to calibrate the legs to a desired stiffness is also important as it combats two problems: leg stiffness variability from manufacturing and stiffness softening. When a legs are created each one has a slightly different stiffness which requires a filtering process to group legs of similar stiffnesses. This requires one to produce many legs so that there are enough legs of a certain stiffness range to attach to the robot. A tunable leg on the other hand can accommodate variations in stiffness of the C-leg. This is also important as the legs soften at varying rates from cyclic loading.

**Improved Robot Survivability**

In this particular design, increasing leg stiffness also has the effect creating a splint over the C-leg. In the event that the C-leg should fracture, but not detach, the compliant slider can offer significant support to the leg at the stiffest setting. While the robot may not be able to run as fast or efficiently, it does offer a second

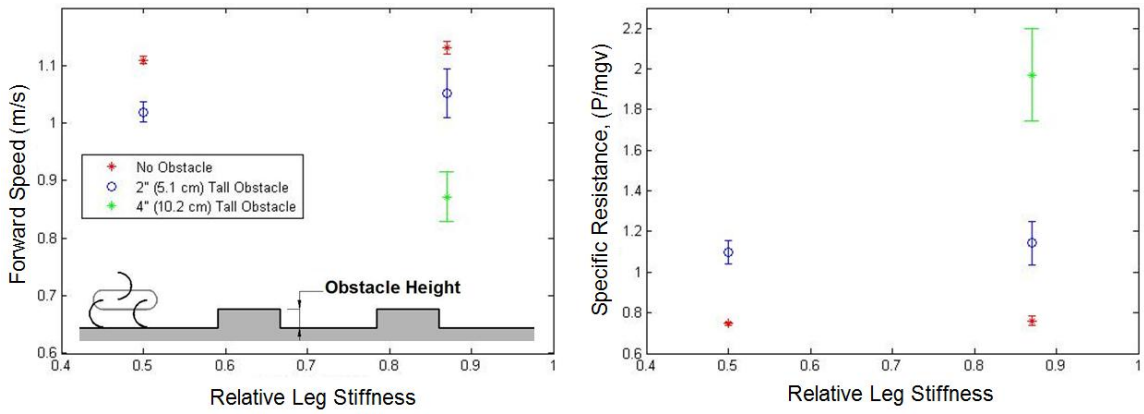


Figure 5.26: Obstacle traversal results for two different leg stiffnesses climbing over a 2 and 4 inch tall obstacles.

line of support to the legs so the robot can return to base.

**Leg Stiffness Differentiation**

The last item is a perceived or potential benefit of tunable stiffness legs. Simulation studies suggest that leg stiffness differentiation may be useful to control rolling behavior and improve stability in response to perturbations. In [16], simulation of EduBot locomotion demonstrated that maximum roll decreases as the middle legs are made stiffer. In another simulation, the authors concluded that running quadrupeds may respond faster to perturbations in ground height if hind leg stiffness is increased [47]. Additionally, if the payload shift to one side of the robot, or if the robot is runs transverse to a slope, leg differentiation may allow the robot to run more balanced.

# Chapter 6

# Conclusion

Since Raibert's work in 1980's, dynamic legged locomotion platforms continue to evolve and make impressive advances toward the goals of greater autonomy and robustness. Our goal throughout this work has been to explore, develop, and empirically evaluate robot legs capable of changing their leg stiffness when confronted with changes in speed, payload, and terrain. In pursuit of this goal, we have surveyed several mechanical stiffness tuning methods and have identified design principles and an effective strategy for developing tunable legs. In particular, we present a robust structure-controlled leg stiffness tuning method suitable for our dynamic running platform. We have shown that wfith a proper selection of materials and geometries, the proposed tunable leg can achieve a significant change in stiffness with relatively minor shape changes. Several materials were considered; however, we have found that composite materials offer the best combination of energy storage capacity, high yield strength, ease of manufacturing, and Youngs modulus control. These pieces have all come together to make what we believe is the first autonomous dynamic legged robot capable of automatic leg stiffness adjustment.

In addition to developing a robust tunable stiffness leg, we also report empirical results which offer insights into the role that passive tunable leg compliance has on efficiency and speed. When the results from thousands of running experiments were

compiled, we found that a leg stiffness near a RLS of 1 allowed the robot to run fast and efficiently. Increasing leg stiffness much beyond this point produced slower and energetically wasteful locomotion. Leg stiffnesses lower than a RLS of 1, converged to gaits that were slower, but nearly as efficient especially when compared to the results of the overly stiff legs. This suggests that a tunable leg with RLS range of one and lower will enable the robot to run efficiently for a range of speeds, payloads and terrains.

In spite of these successes, much work still needs to be done. A legged machine is a complicated system wherein the software, the controller, the actuators, and the natural dynamics of the mechanical system must all work in unison to deliver fast, stable, and efficient locomotion. With animals as a reference, there are clearly many more advances necessary before we can even begin to approach their speed and efficiency. We hope and anticipate that the knowledge gained during the research and development of the tunable C-leg will serve as a reference to expedite the development of future leg innovations.

# Appendix A

# Composite Leg Fabrication

The manufacture of composite C-legs is a multi-step process that produces a very springy and robust structure. The process that we have adopted has been outlined below.

**STEP 1: Mold creation and preparation**

The mold for Edubot C-legs is a 4.5" diameter aluminum tube. The surface of the mold must first be cleaned with acetone in order to remove any dirt, dust, oils, and so forth that may compromise the mold release. Once the surface has been cleaned, mold release can be applied. We have found Frekote (NC-55) by Loctite to be a very reliable product (Figure 2.2). Three coats should be applied in the following manner: apply one coat, wait 5 minutes, apply a second coast, wait five minutes, apply a third coat, and wait 30 minutes before applying composite plies. It should be noted that three coats are only necessary for the first use. Only one coat is necessary for each additional use of the mold.

**STEP 2: Cut Pre-preg into sheets**

The Edubot and RHex legs are fabricated using S2-6781 pre-preg fiberglass. S2 is a high strength (the S is for strength) fiberglass which means it can handle large strains before failure. Pre-preg means that the resin is already in the fabric and only needs to be heated to a specific temperature for a certain time to cure. Generally

the pre-preg composites come in rolls that must be kept at around -20°C to prevent the resin in the fabric from curing. A roll maintained at this temperature can last up to 1 (one) year in the freezer. Before using the roll, it should be removed from the freezer and allowed to thaw to room temperature which generally takes about 10-12 hours. If the roll is unwound before a full thaw you risk introducing cracks in the resin which may end up in the final part and create a weak spot.

Once thawed the pre-preg can be cut into smaller sheets, known as plies, (12"x23" in our case) as shown in Figure A.2. To make a leg that is both stiff in the sagittal plane and lateral direction, the plies must be cut at 0° and 45° to the direction of the weave. We have found that 6 plies (3 plies cut at 0° and 3 at 45°) offers the best compliance for Edubot legs.

**STEP 3: Laying Up**

Arrange the plies in a stack and alternate between 0° and 45° layers. Peel off one side of the plastic backing (Figure A.3). We typically remove the glossing side or the more flexible side first as the stiffer backing makes the ply easier to handle. Peeling of the glossy layer can be difficult and may require the use of a razor blade to grab a corner. It also helps to prop up the mold for easy rotation. This can be done be inserting a 2x4 through through the inside and placing the ends of the 2x4 on supports (Figure A.4). The layers should be wrapped around the mold one layer at a time by bending the tile at the middle and then pressing one half down followed by the other half (Figure A.5). It is important to apply a lot of pressure when pressing the layers to avoid creating wrinkles as they become voids and a source for delamination after curing. The edge of a small block of wax or wood is a useful tool for applying a considerable amount of pressure (Figure A.6).

**Step 4: Vacuum Bagging**

To prepare the mold for vacuum bagging first use a razor blade to even up the ends of the plies by trimming the excess (Figure A.7). The next step is to prepare perf layer which has a pattern of perforated holes. During the vacuum curing process

these holes allow excess resin to be absorbed into the breather layer. The perf layer should be cut to a size that is larger than needed (Figure A.8). The layer should be applied in the same manner as the plies (i.e. avoiding wrinkles) (Figure A.9). Cut off excess material and rub out any air bubbles (Figure A.10). Next take the vacuum bagging tape shown in Figure A.11, and wrap it around both ends of the mold (Figure A.12). Cut the breather layer to size so that it fits just inside the tape at the mold ends (Figure A.13). Lay the mold on top of the vacuum bag plastic and apply the vacuum bagging tape along the perimeter (Figure A.14). Peel back the paper cover on the tape and wrap the rest of the vacuum bagging material around the mold (Figure A.15). Be sure to place the loose half of the the vacuum connector between the breather layer and the vacuum bagging layer before fully sealing the mold. Use a razor blade to make a small incision at the through hole of the vacuum connector (Figure A.16). Connect the two half's of the vacuum connector together (Figure A.17), attach the vacuum hose (Figure A.18), and turn on the vacuum pump. Generally it is very difficult to apply the vacuum bagging layer without creating some wrinkles along the vacuum bagging tape. Thus it will be necessary to take advantage of the putty-like nature of the vacuum bagging tape and rub out the wrinkles to fully seal contents. Once the set-up has reached a full vacuum, disconnect the vacuum hose, feed it through the top of oven, insert the mold in the oven, reconnect the vacuum hose, and let it bake (Figure A.19). Baking times vary depending on the pre-preg resin used so be sure to read manufacturers instructions carefully.

**Step 5: Post Processing**

When the item has fully cooled after baking, the vacuum bagging materials can be removed (Figure A.20). The part can generally be removed from the mold by anchoring one end in a vice and pulling (Figure A.20). Once removed, the next step is to cut the composite tube into rings. For this tube diameter, a miter saw can be used (Figure A.22); however, for larger tube diameters, a vertical or horizontal band saw may be required. Next, the composite rings need to cut into a C-shape. A

template is useful for cutting C-shapes of consistent arc length (Figure A.23). For Edubot C-legs, the 188 degree template was laser cut out of ABS. The near final step involves drilling mounting holes at one end of the C-leg. A small jig was fabricated with a curved slot for the C-leg, and two through holes on the top for guiding the drill (Figure A.24). Once a tread has been glued on, and the fiberglass C-shape can be anchored to a leg mount to complete the fabrication of a composite C-leg as shown in Figure A.25.


Figure A.1: Mold release

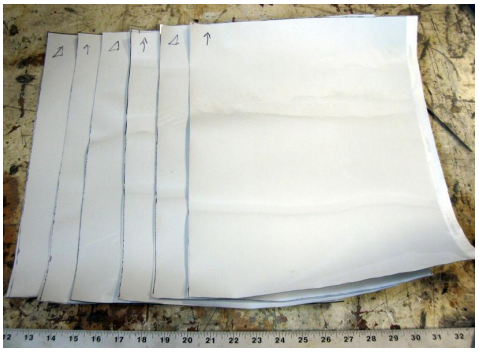

Figure A.2: Cut and arrange plies

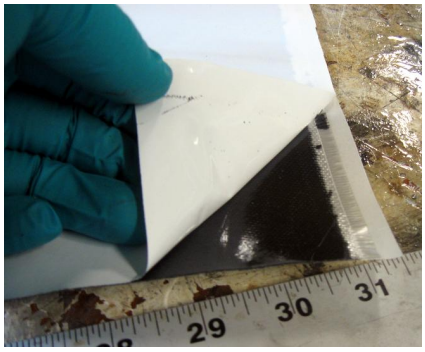


Figure A.3: Peel backing

Figure A.4: Prop mold up

Figure A.5: Apply Layer

Figure A.6: Apply pressure

Figure A.7: Trim ends with razor blade

Figure A.8: Cut peel ply layer

Figure A.9: Lay peel ply layer

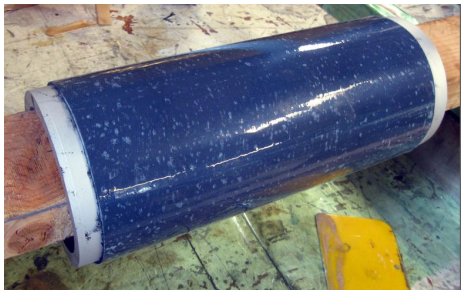

Figure A.10: Peel ply layer pressed onto layer

Figure A.11: Vacuum bagging tape

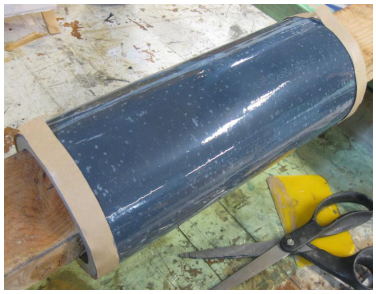

Figure A.12: Wrap tape around tube ends

Figure A.13: Cut breather layer to size

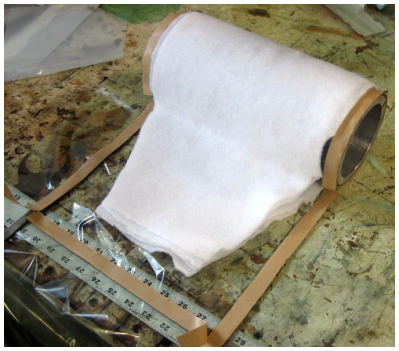

Figure A.14: Apply perimeter tape

Figure A.15: Peel paper off tape and wrap vacuum bag material around mold

Figure A.16: Cut hole for vacuum connection

Figure A.17: Connect two halves

Figure A.18: Connect vacuum hose

Figure A.19: Place in oven

Figure A.20: Remove vacuum bag material

Figure A.21: Pull off mold

Figure A.22: Cut into sections

Figure A.23: Cut into C-shape

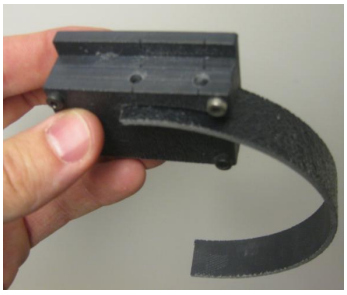

Figure A.24: Drill mounting holes

Figure A.25: Attach C-shape to leg Mount

# Appendix B

# Leg Stiffness Testing Apparatus

Measuring and recording leg stiffness is important for tracking leg stiffness softening and ensuring that each tripod is balance. One of the challenges though has been to determine an appropriate apparatus for measuring leg stiffness. Previous attempts constrained both ends of the C-shape and allowed only 1 DOF deflections. This load-deflection configuration approximated that of beam buckling conditions and not loading behaviour characteristic of RHex-like locomotion.

The leg stiffness measurement apparatus shown in Figure B.1, has 2 DOF. The leg hip is fixed to the *bottom rail*, which can travel up and down along the linear rods; however, gravity forces it to rest on the 1-axis *load cell*. The *top rail* can also move up and down and has a *linear guide* attached to the underside. The leg stiffness is measured by raising the top rail, attaching the leg to the bottom rail, and positioning the linear guide at one end of the top rail. The top rail is then lowered until the linear bearings on the top rail hit the aluminum shaft clamp stoppers. The static loading force can then be recorded and the process can be repeated for a new leg or stiffness setting.

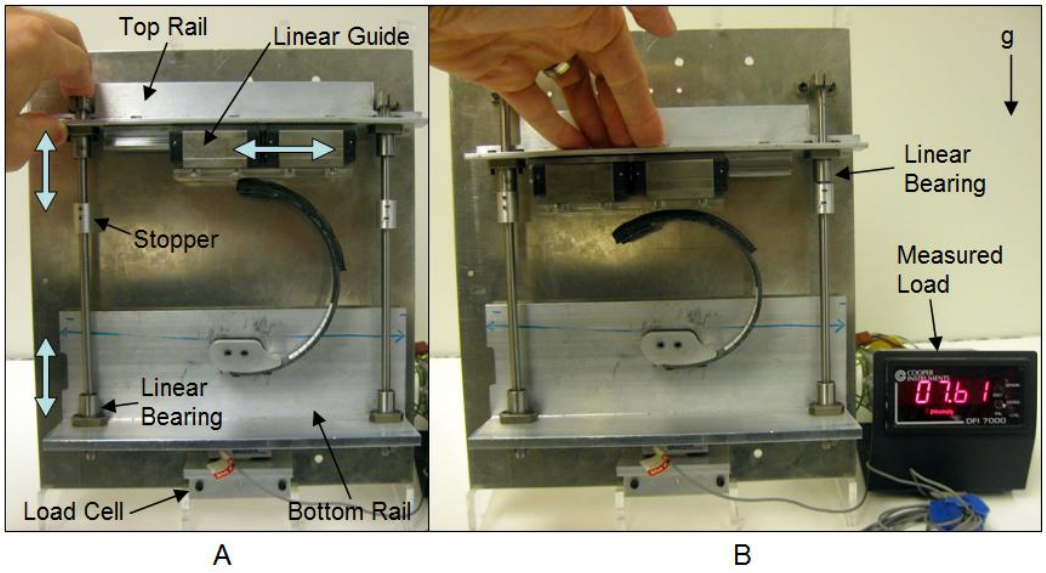


Figure B.1: Front view of the leg stiffness measurement apparatus. A) Leg is in the undeflected state where B) shows the leg in the deflected state with the corresponding load output.

# Appendix C

# Leg Stiffness Comparison

When comparing RHex performance to Edubot's performance, it is important to investigate a scaled comparison of the legs stiffnesses between both machines. A mismatch in leg stiffnesses may help explain differences in robot performance at the high speed gaits. The optimization experiments presented in Chapter 5 suggest legs that are too stiff converge to slower and less efficient gaits. Table C.1 presents the measured Young's modulus of the RHex and Edubot legs, which are made from two different epoxies in S2-6781 pre-preg fiberglass. The arc length is an estimation of the leg arc length measured from the hip to a typical touch down point.

For this exercise, we use the pseudo-rigid-body model to calculate the torsional spring constant for each leg and use this value as a means of comparing the stiffness of a RHex leg to an Edubot leg. As presented in Chapter 3, the torsional spring

| | Young's Modulus (GPa) | Width (mm) | Thickness (mm) | Leg Radius (cm) | *Arc Length (cm) | **Moment of Inertia (m^4) |
|---|---|---|---|---|---|---|
| **RHex Legs** | 25 | 24.5 | 3.15 | 8.34 | 16.7 | 6.381E-11 |
| **EduBot Legs** | 10 | 18 | 2.23 | 5.81 | 11.6 | 1.663E-11 |

* Calculated as 2 radian swept length

** Measured as $1/12bh^3$

Table C.1: Material and geometric properties of RHex and EduBot legs.

constant is calculated as

$$K_t = \rho K_\Theta \frac{EI_s}{l} \tag{C.1}$$

where $\rho = .749$, and $K_\Theta = 2.99$, which are determined from a look up table in [35] by first calculating

$$k_o = \frac{l}{R_i} \tag{C.2}$$

When the values in Table C.1 are inserted into Eqn. C.1 we find that $K_{t,RHex} =$ 21.4 N*m and $K_{t,EduBot} = 3.3$ N*m, which means RHex legs are roughly six times stiffer than EduBot legs. For a scaled comparison of the EduBot leg stiffness to RHex leg stiffness we rely on the relationship where

$$K_{leg} \propto M^{0.67} \tag{C.3}$$

where M is the robot mass [23]. The ratio of RHex's mass (8.2 kg) to Edubot's (3.3 kg) raised to the 0.67 power is 1.84, which means RHex's legs should be approximately 1.84 times stiffer than EduBot legs when scaled with mass. According to this approximation current RHex legs are approximately 3.5 stiffer than they need to be. Clearly this approxmation is subject to some error; however, the magnitude of the separation between the two leg stiffnesses is hard to ignore, and may explain why RHex was unable to run as fast and efficiently as Edubot.

# Bibliography


[1] M. Ahmadi and M. Buehler. The arl monopod ii running robot: Control and energetics. *IEEE ICRA*, 3:1689–1694, May 1999.

[2] R.M. Alexander. The mechanics of jumping by a dog (canis familiaris). *J. Zool. Lond.*, 173:549–573, 1974.

[3] R.M. Alexander. Walking and running. *American Scientist*, 72(4):348 – 354, 1984.

[4] R.M. Alexander. Three uses for springs in legged locomotion. *International Journal of Robotics Research*, 9(2):53–61, 1990.

[5] R.M. Alexander. *Principles of Animal Locomotion*. Princeton University Press, 2003.

[6] R. Altendorfer, N. Moore, H. Komsuoglu, M. Buehler, Jr. Brown H.B., D. McMordie, U. Saranli, R. Full, and D.E. Koditschek. Rhex: A biologically inspired hexapod runner. *Autonomous Robots*, 11(3):207–213, 2001.

[7] A. Arampatzis, G. Bruggemann, and V. Metzler. The effect of speed on leg stiffness and joint kinetics in human running. *Journal of Biomechanics*, 32:134–1353, 1999.

[8] M.F. Ashby. *Materials selection in mechanical design*. Butterworth-Heinemann, 2005.

[9] S. Beland. *High Performance Thermoplastic Resins and Their Composites*. Noyes Publications, 1991.

[10] A.A. Biewener. Muscle-tendon stresses and elastic energy storage during locomotion in the horse. *Comparative Biochemistry and Physiology Part B: Biochemistry and Molecular Biology*, 120(1):73 – 87, 1998.

[11] A.A. Biewener and T.J. Roberts. Muscle and tendon contributions to force, work, and elastic energy savings: a comparative perspective. *Exercise and Sport Sciences Reviews*, 28:99107, 2000.

[12] R. Blickhan and R.J. Full. Similarity in multilegged locomotion: Bouncing like a monopod. *Journal of Comparative Physiology*, 173(5):509–517, 1993.

[13] Y. Blum, S.W. Lipfert, and A. Seyfarth. Effective leg stiffness in running. *Journal of Biomechanics*, 42(14):2400–2405, 2009.

[14] M. Buehler, R. Battaglia, A. Cocosco, G. Hawker, J. Sarkis, and K. Yamazaki. Scout: a simple quadruped that walks, climbs, and runs. 2:1707–1712, May 1998.

[15] M. Buehler, U. Saranli, E. Papadopoulos, and D. Kodistchek. Dynamic locomotion with four and six-legged robots. In *International Symposium on Adaptive Motion of Animals and Machines*, Montreal, Canada, 2000.

[16] S. Burden, J. E. Clark, H. Weingarten, J .and Komsouglu, and D. E Koditschek. Heterogeneous leg stiffness and roll in dynamic running. In *IEEE International Conference of Robotics and Automation*, 2007.

[17] K. Byl. *Metastable Legged-Robot Locomotion*. PhD thesis, Massachusetts Institute of Technology, 2008.

[18] J. G. Cham. *On Stability and Performance in Open-loop Running*. PhD thesis, Stanford University, 2002.

[19] J. G. Cham, S. A. Bailey, and M. R. Cutkosky. Robust dynamic locomotion through feedforward-preflex interaction. In *ASME IMECE Proceedings*, Orlando, Flordia, 2000.

[20] Sachin Chitta, Mustafa Karabas, Kevin Galloway, and Vijay Kumar. Robotrikke: Design, modeling and experimentation with a robotic trikke. In *Proceedings of the ASME Design Engineering Technical Conference*, 2006.

[21] A.M. Dollar and R.D. Howe. Design and evaluation of a robust compliant grasper using shape deposition manufacturing. In *Proceedings of the ASME Design Engineering Technical Conference*, 2005.

[22] D. M. Dudek and R. J. Full. Passive mechanical properties of legs from running insects. *Journal of Experimental Biology*, 209:1502–1515, 2006.

[23] C. T. Farley, J. Glasheen, and T. A. McMahon. Running springs - speed and animal size. *Journal of Experimental Biology*, 185:71–86, 1993.

[24] R. Farley, C. T. Blickhan, J. Saito, and R.C. Taylor. Hopping frequency in humans: a test of how springs set stride frequency in bouncing gaits. *Journal of Applied Physiology*, 71:2127–2132, 1991.

[25] D.P. Ferris and C.T. Farley. Interaction of leg stiffness and surface stiffness during human hopping. In *American Physiological Society*, pages 15–22, 1997.

[26] D.P. Ferris, M. Louie, and C.T. Farley. Running in the real world: Adjusting leg stiffness for different surfaces. In *Proceedings of the Royal Society London*, volume 265, pages 989–993, 1998.

[27] R. J. Full and C. T. Farley. *Musculoskeletal dynamics in rhythmic systems: A comparative approach to legged locomotion*. Springer Verlag: New York, 2000.

[28] R. J. Full and M. S. Tu. Mechanics of a rapid running insect - 2-legged, 4-legged and 6-legged locomotion. *Journal of Experimental Biology*, 156(AR):215–231, 1991.

[29] G. Gabrielli and T.H. von Karman. What price speed? *Mechanical Engineering*, 72(10):775–781, 1950.

[30] K.C. Galloway, J.E. Clark, and D.E. Koditschek. Design of a multi-directional variable stiffness leg for dynamic runnings. In *ASME Int. Mech. Eng. Congress and Exposition*, 2007.

[31] K.C. Galloway, J.E. Clark, and D.E. Koditschek. Design of a tunable stiffness composite leg for dynamic locomotion. In *ASME IDETC*, 2009.

[32] P. Gregorio, M. Ahmadi, and M. Buehler. Design, control, and energetics of an electrically actuated legged robot. *Systems, Man, and Cybernetics, Part B: Cybernetics, IEEE Transactions on*, 27(4):626–634, Aug 1997.

[33] R. Ham, T. Sugar, B. Vanderborght, K. Hollander, and D. Lefeber. Compliant actuator designs. *IEEE Robotics and Automation Magazine*, 16(3):81–94, 2009.

[34] K.W. Hollander, T.G. Sugar, and D. Herring. Adjustable robotic tendon using a 'jack spring'tm. In *IEEE International Conference on Rehabilitation Robotics*, 2005.

[35] Larry L. Howell. *Compliant Mechanisms*. Wiley, New York, 2001.

[36] Larry L. Howell and Ashok Midha. Parametric deflection approximations for initially curved, large-deflection beams in compliant mechanisms. In *Proceedings of the ASME Design Engineering Technical Conference*, 1996.

[37] Jonathan Hurst. *The Role and Implementation of Compliance in Legged Locomotion*. PhD thesis, Carnegie Mellon University, 2008.

[38] W. Hurst, J. Chestnutt, and A. Rizzi. An actuator with physically variable stiffness for highly dynamic legged locomotion. In *Proceedings - IEEE International Conference on Robotics and Automation*, pages 4662–4667, 2004.

[39] S. Kawamura, T. Yamamoto, D. Ishida, T. Ogata, Y. Nakayama, O. Tabata, and S. Sugiyama. Development of passive elements with variable mechanical impedance for wearable robots. pages 248–253, 2002.

[40] R.F. Ker, R.M. Alexander, and M.B. Bennett. Why are mammalian tendons so thick? In *J. Zool. Lond.*, volume 216, page 309 324, 1988.

[41] R.F. Ker, M.B. Bennett, S.R. Bibby, R.C. Kester, and R.M. Alexander. The spring in the arch of the human foot. In *Nature*, volume 325, pages 147–149. Nature Publishing Group, 1987.

[42] S. Kuitunen, P.V. Komi, and H. Kyrolainen. Knee and ankle joint stiffness in sprint running. *Med Sci Sports Exerc.*, 34(1):166–73, 2002.

[43] S.M. Lee (Editor). *Composite Materials*, volume 2. VCH Publishers, Inc., 1990.

[44] P. Lin. *Proprioceptive Sensing for a Legged Robot*. PhD thesis, University of Michigan, 2005.

[45] T.A. McMahon. Mechanics of locomotion. *International Journal of Robotics Research*, 3(2):4–28, 1984.

[46] T.A. McMahon and G. C. Cheng. Mechanics of running: How does stiffness couple with speed? *Journal of Biomechanics*, 23(1):65–78, 1990.

[47] S. Meek, J. Kim, and M. Anderson. Stability of a trotting quaduped robot with passive, underactuated legs. In *IEEE International Conference on Robotics and Automation*, pages 347–351, 2008.

[48] R. Merz, Prinz. F. B., K. Ramaswami, M. Terk, and L. E. Weiss. Shape deposition manufacturing. In *Proceedings of the Solid Freeform Fabrication Symposium*, University of Texas at Austin, 1994.

[49] E. Z. Moore. Leg design and stair climbing control for the RHex robotic hexapod. Master's thesis, McGill University, Jan. 2002.

[50] E. Z. Moore, D. Campbell, F. Grimminger, and M. Buehler. Reliable stair climbing in the simple hexapod 'rhex'. In *Proceedings - IEEE International Conference on Robotics and Automation*, volume 3, pages 2222–2227, 2002.

[51] T. Morita and S. Sugano. Design and development of a new robotic joint using a mechanical impedance adjuster. In *IEEE International Conference on Robotics and Automation*, volume 3, pages 2469–2475, 1995.

[52] M. Okada, Y. Nakamura, and S. Hoshino. Design of active/passive hybrid compliance in the frequency domain-shaping dynamic compliance of humanoid shoulder mechanism. In *International Conference on Robotics and Automation*, volume 3, pages 2250–2257 vol.3, 2000.

[53] V.L. Orekhov. Design of a variable compliance leg using shape deposition manufacturing. 2007.

[54] D. Papdopoulos and M. Buehler. Stable running in a quadruped robot with compliant legs. In *Proc. of the IEEE International Conference on Robotics and Automation*, pages 444–449, 2000.

[55] B. Picasso, P. Priolo, C. Sitzia, and P. Diana. Stiffness reduction during fatigue in graphite/thermoplastic composite. *Proceedings of the American Society for Composites First Technical Conference*, pages 36–41, 1986.

[56] I. Poulakakis, E. Papadopoulos, and M. Buehler. On the stable passive dynamics of quadrupedal running. In *IEEE International Conference on Robotics and Automation*, volume 1, pages 1368–1373, Sept. 2003.

[57] M.H. Raibert. *Legged robots that balance*. MIT Press series in artificial intelligence. MIT Press, Cambridge, Mass., 1986.

[58] M.H. Raibert, B. Brown, M. Chepponis, J. Koechling, D. Dustman, K. Brennan, D. Barrett, C. Thompson, J. Herbert, W. Lee, and L. Borvansky. Dynamically stable legged locomotion. *Technical Report 1179 LL-6*, 1989.

[59] T.J. Roberts. The integrated function of muscles and tendons during locomotion. In *Comparative Biochemistry and Physiology part A*, volume 133, pages 1087–1099, 2002.

[60] J. Rummel, S. Lipfert, and A. Seyfarth. Knee joint stiffness for self-stable running. In *Journal of Biomechanics 40(S2) XXI ISB Congress, Poster Sessions, Poster 110*, page S590, 2007.

[61] J. Rummel and A. Seyfarth. Stable running with segmented legs. *International Journal of Robotics Research*, 27(8):919–934, 2008.

[62] U. Saranli, M. Buehler, and D.E. Koditschek. Rhex: A simple and highly mobile hexapod robot. *International Journal of Robotics Research*, 20(7):616–631, 2001.

[63] J. Schmitt, M. Garcia, R.C. Razo, P. Holmes, and R.J. Full. Dynamics and stability of legged locomotion in the horizontal plane: a test case using insects. *Biological Cybernetics*, 86(5):343–53, 2002.

[64] A Seyfarth, H. Geyer, M. Gunther, and R. Blickhan. A movement criterion for running. *Journal of Biomechanics*, 35(5):649 – 655, 2002.

[65] N.P. Suh. *The Principles of Design*. Oxford University Press, March 1990.

[66] O. Tabata, S. Konishi, P. Cusin, Y. Ito, F. Kawai, S. Hirai, and S. Kawamura. Microfabricated tunable stiffness device. *Proc. of the 13th Annual Int. Conf. On Micro Electro Mechanical Systems*, 1999.

[67] D. Tang, G. Zhang, and S. Dai. Design as integration of axiomatic design and design structure matrix. *Robotics and Computer-Integrated Manufacturing*, 25:610–619, 2009.

[68] R. Van Ham, M. Van Damme, B. Vanderborght, B. Verrelst, and D. Lefeber. Maccepa: The mechanically adjustable compliance and controllable equilibrium position actuator. In *Proceedings of CLAWAR*, pages 196–203, 2006.

[69] B. Vanderborght, B. Verrelst, R. Van Ham, M. Van Damme, D. Lefeber, B. Duran, and P. Beyl. Exploiting natural dynamics to reduce energy consumption by controlling the compliance of soft actuators. *Int. J. Rob. Res.*, 25(4):343–358, 2006.

[70] W. Wang, R. Loh, and E. Gu. Passive compliance versus active compliance in robot-based automated assembly systems. *Industrial Robot*, 25(1):48–57, 1998.

[71] J. Weingarten, R. Groff, and D.E. Koditschek. A framework for the coordination of legged robot gaits. In *IEEE International Conference of Robotics, Automation and Mechatronics, Singapore*, 2004.

[72] J. Weingarten, G. Lopes, M. Buehler, R. Groff, and D.E. Koditschek. Automated gait adaptation for legged robots. In *IEEE International Conference of Robotics and Automation*, 2004.

[73] D.E. Whitney. Physical limits to modularity. Technical report, MIT Engineering Systems Division, 2002.

[74] J. Yun Jun and J.E. Clark. Dynamic stability of variable stiffness running. In *International Conference on Robotics and Automation*. IEEE, 2009.

[75] Garth Zeglin. *The Bow Leg Hopping Robot*. PhD thesis, Carnegie Mellon University, 1999.

[76] Z. Zhang and H. Kimura. Rush: a simple and autonomous quadruped running robot. *Journal of Systems and Control Engineering*, 223(1):323–336, 2009.